1989

Fundamental studies of the extraction process in inductively coupled plasma mass spectrometry

Heoungbin Lim
Iowa State University

Order Number 9014923

Fundamental studies of the extraction process in inductively coupled plasma mass spectrometry

Lim, Heoungbin, Ph.D.

Iowa State University, 1989

U·M·I
300 N. Zeeb Rd.
Ann Arbor, MI 48106

Fundamental studies of the extraction process in inductively coupled plasma mass spectrometry

by

Heoungbin Lim

A Dissertation Submitted to the
Graduate Faculty in Partial Fulfillment of the
Requirements for the Degree of
DOCTOR OF PHILOSOPHY

Department: Chemistry
Major: Analytical Chemistry

Approved:

Signature was redacted for privacy.

In Charge of Major Work

Signature was redacted for privacy.

For the Major Department

Signature was redacted for privacy.

For the Graduate College

Iowa State University
Ames, Iowa

1989

TABLE OF CONTENTS

GENERAL INTRODUCTION

Reed designed a plasma torch which could sustain a spheroidal plasma using tangential gas flow in 1961 (1). Since that time, the inductively coupled plasma (ICP) has evolved as an important analytical tool. Annular ICPs were developed in 1968 by Greenfield et al. (2) and in 1969 by Dickinson and Fassel (3).

One of the most prominent characteristics of an annular ICP is the formation of a central, cooler channel. An annular, toroidal shape implies that the central channel of the plasma is relatively cool compared to the surrounding zones, which causes an inward radial flow of the plasma and the formation of a vortex ring and the central channel.

The formation of the central channel in the ICP provides important advantages for atomic emission spectroscopy (AES). Because the central tunnel is long, narrow, and sharply bounded, the ICP exhibits little self-absorption, a relatively long-residence time, and effective vaporization, atomization, and ionization. These characteristics provide excellent detectability and sensitivity in ICP-AES.

Atomic fluorescence spectrometry (AFS) with the ICP, high resolution ICP spectrometry (HRS-ICP), and especially mass spectrometry with the ICP (ICP-MS) were developed later as complementary techniques to ICP-AES. For ICP-AFS, a laser (4), a hollow cathode lamp (HCL) (5-7), or the ICP itself (8,9) have been used as an excitation source. The techniques employed to achieve high resolution detection of the ICP emission lines include echelle and grating spectroscopy (10-12), Fabry-Perot interferometry (13,14), and Fourier transform spectroscopy (FTS)

(15,16). High resolution ICP spectrometry is quite useful for elemental analysis using the isotopic shift effect. For the determination of radioactive elements, this method is free from instrumental contamination, unlike mass spectrometry.

A vacuum ultraviolet inductively coupled plasma (VUV-ICP) allows the extension of ICP-AES to the determination of nonmetals and metalloids in aqueous and gaseous samples (17). Therefore, VUV-ICP-AES can be coupled with gas chromatography (GC) and liquid chromatography (LC) for the determination of the halogens.

One of the prominent complementary ICP techniques is ICP-MS, which was pioneered by Houk et al. (18). Because almost all the sample flows through the central tunnel in the ICP, the analyte can be efficiently collected and transported into a mass spectrometer. In addition, the ICP is an excellent ion source for mass spectrometry due to its high temperature (approximately 7000 K). Therefore, the combination of the remarkable characteristics of the ICP with the excellent selectivity and sensitivity of mass spectrometry provides a powerful analytical capability for elemental and isotopic analysis. In fact, the detection limits of ICP-MS are often a factor of 10^3 better than those of ICP-AES. There are numerous reviews and general studies on ICP-MS (19-21), including a recent review by Houk and Thompson (22).

The scope of application of ICP-MS is very wide. The capabilities of ICP-MS for estimating isotope ratios can be used for isotope dilution for elemental analysis, isotope labelling for nutritional and biological study, and isotope ratio determinations for geological analysis.

Elemental analysis is another major area of application of ICP-MS, which has a decided advantage for heavy elements. The ICP-MS spectrum for a heavy element consists of only a few peaks whereas an ICP-AES spectrum generally has many spectral lines.

However, there are clearly several areas in which ICP-MS performance needs improvement. One of the difficulties for ICP-MS is long-term drift, which is typically 2% of relative standard deviation (RSD) per hour and is worse than in ICP-AES. Matrix interferences in ICP-MS are also worse than in ICP-AES. The main reason for matrix effects is not entirely clear yet, but the matrix effect may be caused by the interaction of the plasma with the extraction device (Figure 1) of the ICP-MS instrument, for example, the space charge effect (23). There is also evidence that the interaction of the ICP with the interface affects the ICP-MS spectrum. For instance, Crain and co-workers reported that the instability of the ICP generated by the interaction produced the discrete frequency noise in ICP-MS signals (24).

Consequently, the study of the ICP-MS interface becomes one of the main topics to improve the analytical performance of ICP-MS.

Sampling method in ICP-MS

The sampling interface and the ICP generally used for ICP-MS are shown in Figure 1. The early fundamental study of ICP-MS concentrated on the boundary layer sampling and continuum sampling. In general, the boundary layer sampling was performed with a blunt cone tip. At this time the stagnant layer of gas formed between the orifice and the

flowing plasma, and served as a barrier to gas penetration (Figure 2a). During this extraction process, atoms and/or ions from the ICP collided with species in the cool, stagnant boundary layer. Therefore, ion-neutral recombination, ion-electron recombination, metal oxide formation, and other reactions were expected in the boundary layer (25).

If the orifice diameter of the sampler cone is large enough (> 70 μm), the particles from the plasma are directly extracted by puncturing the boundary layer and a white, funnel-like gas stream forms between the plasma and the orifice. The plasma actually forms a secondary discharge to the orifice (Figure 2b). This secondary discharge, also called a "pinch", is an efficient excitation source for AES, but causes erosion of the sampling orifice and high photon background for the electron multiplier detector of the mass spectrometer (25,26). This secondary discharge as an emission source is discussed in Section V. The secondary discharge can be attenuated by employing a center tap load coil in the ICP, so that it is not a severe problem in ICP-MS any more (26). Salt deposition and oxide ion formation are less severe with a large sampling orifice. Such an orifice can also be made with relatively thick metal near the tip, so it is resistant to erosion or expansion.

Supersonic jet in ICP-MS

Because the pressure difference between the ICP (atmospheric pressure) and the MS (high vacuum), two cones are used for the interface of ICP-MS, as shown in Figure 1. When the ICP expands through a small

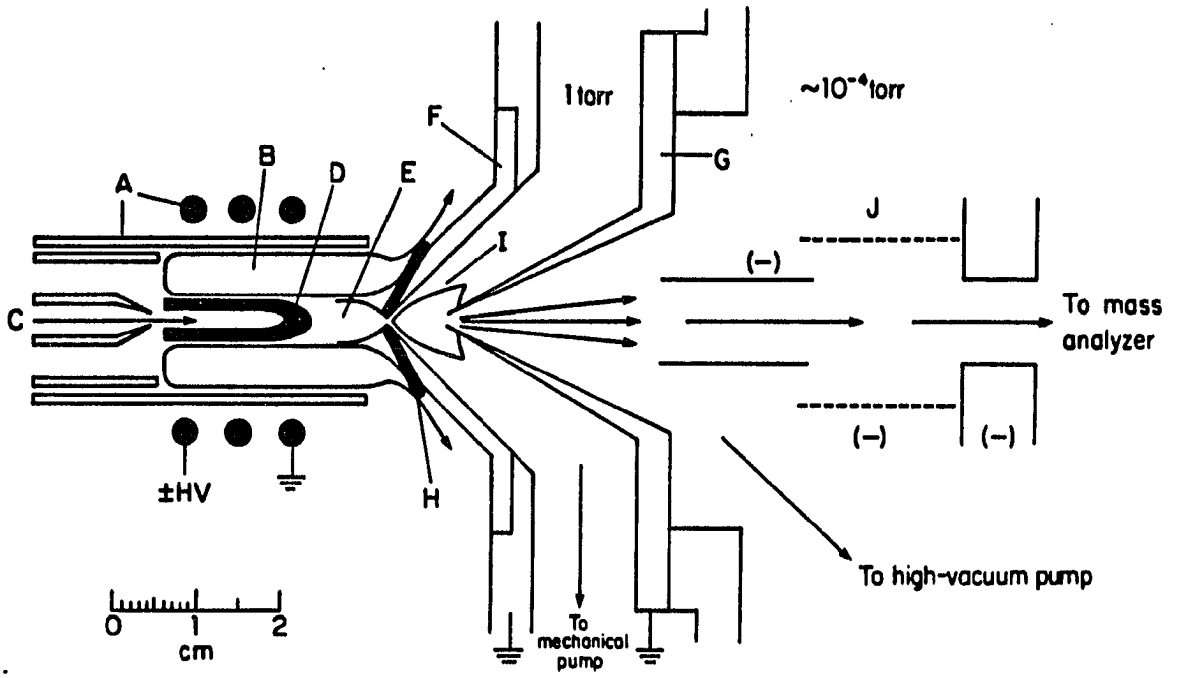

Figure 1. ICP and sampling interface. (A) torch and load coil (HV = high voltage), (B) induction region of ICP, (C) solution aerosol being injected into axial channel, (D) initial radiation zone, (E) normal analytical zone, (F) sampler cone with orifice in the tip, (G) skimmer cone, (H) boundary layer of ICP gas deflected outside sampling orifice, (I) expanding jet of gas sampled from ICP, and (J) ion lens elements. Reproduced from reference (20) with permission

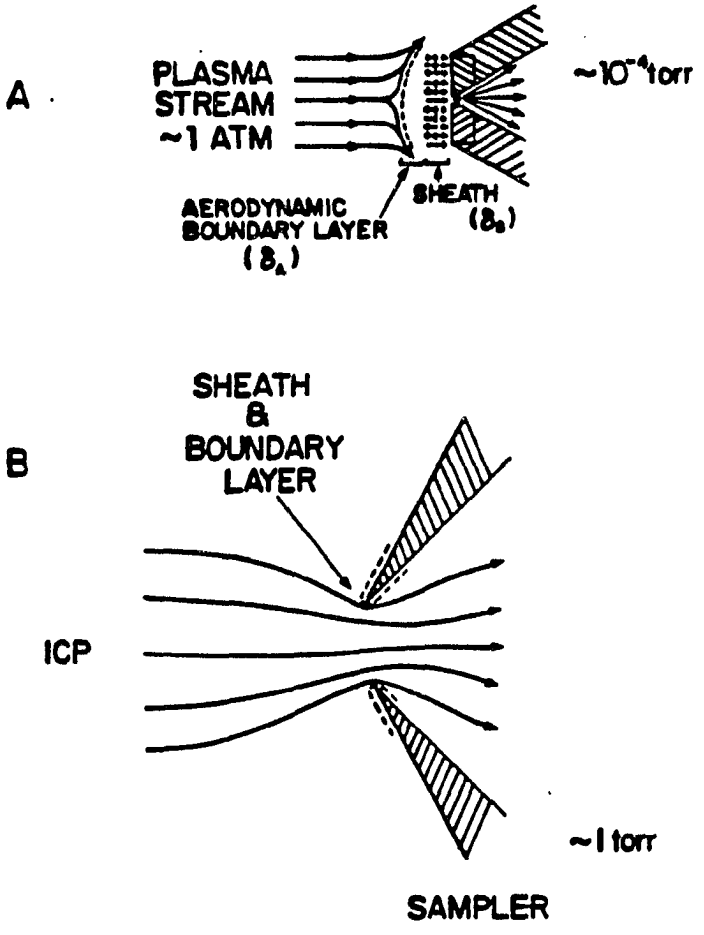

Figure 2. Sampling devices for ICP-MS: (A) pinhole-size orifice (diam. ~50 μm). Ions are sampled from the sheath and boundary layer. (B) continuum flow sampler (diameter ~1 mm). The gas flows directly through the orifice; the boundary layer and sheath are present only around the edge of the orifice. Reproduced from reference (22) with permission

sampling orifice of the first cone, sampler cone from Figure 1, two kinds of beam expansions may occur, depending on the orifice diameter (D) and the mean free path of gas molecules in the ICP (λ_o). If D << λ_o, gas molecules in the vicinity of the sampling orifice can pass into the vacuum chamber without colliding with other gas particles. Under this effusive expansion condition, the internal energy states of the gas are not influenced by the presence of the hole. On the other hand, if D >> λ_o, there will be many collisions as the gas flows through the orifice, and the expansion is supersonic. The supersonic molecular beam has been well-studied in gas dynamics (27-30). The application of the supersonic beam to analytical spectroscopy is discussed in the several references (31-34).

The most prominent phenomena of a supersonic jet are the cooling effect and the velocity narrowing effect. In the expansion, the collisions in and downstream of the orifice convert random atomic or molecular motion into directed mass flow along the beam axis, and this conversion causes the temperature to decrease. Because the gas cools, the velocity distribution in the supersonic expansion becomes very narrow compared to the effusive expansion.

Since a large sampling orifice is commonly used in ICP-MS today, the expansion beam in the first chamber is supersonic. Douglas and French described the properties of free jet expansions and molecular beam skimming applied to the sampling of an ICP for mass spectrometry (35).

Two equations are contemplated, which can be useful to understand the extraction process of ICP-MS. Assuming the expansion is isentropic,

the temperature or pressure of the supersonic jet can be calculated using the following equation:

$$T/T_o = (P/P_o)^{(\gamma-1)/\gamma} \quad (1)$$

where T : Temperature of expansion jet

T_o : Temperature of reservoir

P : Pressure of expansion jet

P_o : Pressure of reservoir

γ : Heat capacity ratio = C_p/C_v (For the Ar gas, $\gamma = 5/3$).

Because the position of the second cone, the skimmer, is related to the location of Mach disk, the following empirical equation is useful as well (36).

$$X_m = 0.67D(P_o/P_1)^{1/2} \quad (2)$$

where X_m is the location of the Mach disk and P_1 is the background pressure. Since all parameters in the above equation are measured experimentally, the distance downstream of the Mach disk can be calculated. The skimmer in ICP-MS is positioned inside the Mach disk (Figure 1).

Diagnostic study for ICP

For fundamental study of the ICP, various temperatures, electron number densities, and number densities of analyte and argon species have

generally been considered. Spectroscopic measurements have commonly been used to estimate these temperatures. Popular methods for the fundamental study of the ICP are described in several references (37,38).

Ionization temperature (T_{ion}) may be determined from the measurements of the relative intensities of atom and ion lines of a suitable species and the knowledge of the electron density, n_e, via the Saha equation (39-41), provided the species available have sufficiently intense atomic and ionic lines. As an alternate method, ICP-MS can be employed to measure T_{ion} in the ICP (42,43).

The temperature governing the energy population of atomic levels is defined as excitation temperature (T_{exc}). In thermal equilibrium, the population density of a atomic level follows a Boltzmann distribution, so the observed emission intensity of a transition from a upper level to a lower level is a function of the transition probability, excitation energy and T_{exc} (40,44-46). The relative intensities of two or more lines are generally used for the measurement of T_{exc}. However, inaccuracies in the transition probabilities often cause large errors in the excitation temperature associated with this method.

Similarly, the rotational temperature (T_{rot}) which is often regarded as the gas kinetic temperature because of the fast exchange between rotational and kinetic energy in molecules, can be estimated by measuring the emission intensities of the rotational lines emitted from a diatomic molecule (46-50). The Doppler temperature (T_{Dopp}) is defined as the temperature that corresponds to the kinetic motion of species. The estimation of T_{Dopp} requires the precise evaluation of spectral line

widths and a deconvolution procedure for other sources of line broadening.

The Langmuir probe method has been extensively examined for estimating T_e and n_e, since the theoretical basis for the interpretation of probe characteristics was first developed (51-53). T_e can be calculated from the slope of a plot of logarithm of absolute electron current versus applied voltage from the electron retarding field region of the probe characteristic curve. The probe characteristic contains the information of electron density in the plasma as well, because the probe current is a function of probe voltage, electron temperature and electron density.

The Stark broadening method is an effective way to measure the electron density (54-57). The Hamiltonian for the Stark effect, which is the interaction of an emitting atom with a static electric field generated by the surrounding ions and electrons, is just the product of electric field and distance of charge, i.e., the electric-dipole interaction. Therefore, the spectral lines from the plasma are broadened due to this interaction, called Stark broadening. The H_β line (486.1 nm) is generally used because the Stark broadening is unusually dominant for hydrogen lines. Although the H_β Stark method is considered to be more reliable than other methods, it still requires extraction of the Doppler and instrumental broadening from the measured line profile.

EXPLANATION FOR DISSERTATION

The focus of this dissertation will be the analytical and fundamental study of the jet and secondary discharge formed during the extraction process in ICP-MS. The alternate format is used in this dissertation. In the next section, the design of an optical cell to sample the ICP, the formation of a supersonic jet, and the analytical study of the jet as an emission source are described. In Section II, T_{rot} and T_{Dopp} are estimated by the measurement of OH rotational line intensities and linewidths with high resolution spectrometry, respectively. The electrical probe method is discussed to measure the potential, T_e, and n_e in the jet in Sections III and IV. The application of the secondary discharge as an emission source is the main topic in Section V. In particular, the matrix effects in the jet and secondary discharge are emphasized in this dissertation.

SECTION I. ATOMIC EMISSION SPECTROMETRY WITH A REDUCED PRESSURE AFTERGLOW EXTRACTED FROM AN INDUCTIVELY COUPLED PLASMA

INTRODUCTION

The inductively coupled plasma (ICP) has proven to be an excellent excitation source for elemental analysis of solutions by atomic emission spectrometry (AES) (1,2). One reason for the success of the ICP is that volatilization and atomization interferences are minimal because the analyte is efficiently atomized in the high-temperature, atmospheric-pressure environment. It seems that such an environment is essential for proper dissociation of analytes from sample particles such as those generated by solution nebulization. In a conventional ICP the analyte atoms then continue through the axial channel where they are excited and ionized at atmospheric pressure. In some ways, the observation of ICP emission at reduced pressure might offer potential advantages in that line widths should be sharper than from an atmospheric pressure source. The same experimental techniques for sampling the ICP for mass spectrometry (MS) should also be useful for AES at reduced pressures (3,4). In fact, in ICP-MS the initial extraction process is often accompanied by emission of visible radiation from inside the first vacuum chamber (5). In addition to potential analytical applications, the observation of emission spectra from such an afterglow could also provide fundamental information about processes occurring during the extraction step, which would be useful for further improvements in ICP-MS. In this section it is reported for the first time that the results of initial investigations indicate the feasibility of using an analytical ICP at atmospheric pressure for atomization while observing

atomic emission spectra at reduced pressure as the analyte species are extracted into a vacuum chamber.

EXPERIMENTAL

A scale diagram of the ICP, extraction system, and afterglow chamber is shown in Figure 1. Instrumental components and typical operating parameters are listed in Table I. These conditions were used for all the experiments described below unless otherwise indicated.

ICP instrumentation

A continuous-flow ultrasonic nebulizer with aerosol desolvation was used (6-8). The ICP was operated horizontally only because such a plasma was already available in our laboratory; the conventional vertical arrangement would serve as well. The load coil for the ICP was grounded at its downstream end to the shielding box to minimize arcing between plasma and sampling orifice (4,9).

Afterglow chamber

A flat sampling disk (rather than the cone typically used in ICP-MS) was used because it was considered desirable to be able to collect radiation from as close to the actual orifice as possible. Although the sampling disk was flat, the orifice was large enough for continuum gas flow through the boundary layer between the orifice and the plasma (3,5). The sampling disk had a knife-edged surface to seal it to the copper cooling flange. The orifice became discolored but did not erode or expand over a period of at least 1 month. The cooling flange was also grounded to the shielding box. A quartz cylinder served as the chamber wall so that observations could be made in the ultraviolet.

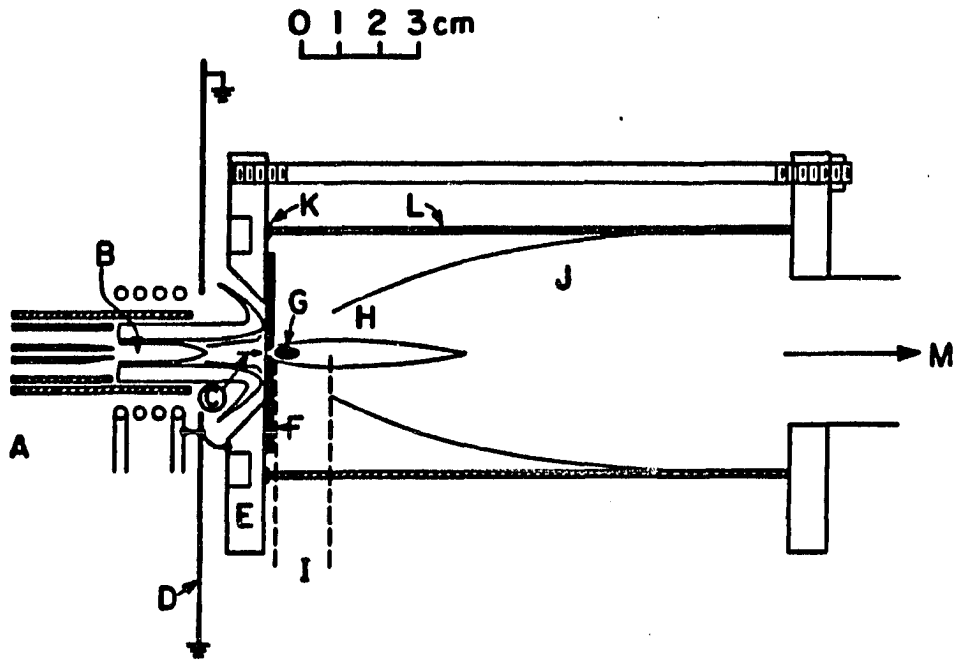

Figure 1. ICP and afterglow apparatus: (A) ICP torch and load coil, (B) initial radiation zone of ICP, (C) normal analytical zone of ICP, (D) copper shielding box, (E) copper flange with water cooling jacket, (F) stainless steel disk with sampling orifice, (G) supersonic jet, dark "zone of silence" inside red barrel shock and Mach disk, (H) intense red emission downstream from supersonic jet, (I) region viewed by monochromator (dotted lines), (J) diffuse red emission, (K) Viton gaskets, (L) quartz tube, (M) flange to vacuum tubing and rotary pump

Table I. Instrumental facilities

component	operating conditions, materials, or dimensions
nebulizer power supply: Model UNPS-1 Plasma Therm, Inc. (now RF Plasma products)	transducer frequency 1.36 MHz forward power 43 W reflected power 1 W
nebulizer assembly, spray chamber, desolvation apparatus: Ames Laboratory construction (6,7)	transducer and desolvation chamber ice water cooled desolvation temperature 80 °C solution uptake rate 3.2 mL min^{-1}
ICP generator: Type HFP2500D with impedance-matching network Plasma Therm, Inc.	forward power 1.1 kW reflected power 5 W frequency 27.12 MHz
ICP torch: Ames Laboratory construction (8)	argon flow rates: outer gas 14 L min^{-1} aerosol gas 0.6 L min^{-1} auxiliary gas used only during ignition
extraction system	0.56 mm diameter circular orifice in stainless steel disk orifice centered on ICP 20 mm from top of load coil
pressure measurement: Convection Series 275 gauge Granville-Phillips	chamber pressure 0.7 torr while sampling ICP
vacuum pump: Model 1374 Sargent-Welch	pumping speed 8 L s^{-1} at pump
monochromator: Model 82000 Jarrell-Ash Division (now Thermo Jarrell-Ash)	Ebert mount focal length 0.5 m grating 1160 grooves mm^{-1}, blazed at 250 nm entrance and exit slits 10 mm high x 25 μm wide (fixed)
photomultiplier: Model R955 Hammamatzu	bias voltage -850 V
electrometer: Model 601 Keithley Instruments	spectra plotted on x-y recorder

The quartz tube was sealed to the cooling and pumping flanges by Viton gaskets.

Optics and detection

A quartz lens (5cm diameter, f/2) was used to form a focused image (magnification 0.6) of the afterglow on the entrance slit of the spectrometer. The section of the afterglow viewed is shown in Figure 1; note that the ICP itself was not observed. The dispersion of the monochromator used was not adequate measure line widths in these initial experiments. Spectra were collected in a darkened room; otherwise, radiation from the fluorescent lights was significant relative to the dark current and background from the afterglow. Careful grounding of the detection electronics and recorder was necessary to alleviate rf interference.

Solution

Standard solutions were prepared volumetrically by dilution of aliquots of commercial stock solutions (Fisher Scientific). The solvent was distilled deionized water.

RESULTS AND DISCUSSION

Afterglow structure

The physical appearance of the afterglow is depicted in Figure 1. The sampling disk itself glowed red hot with a pale blue glow along its outer edge. The barrel shock, "zone of silence (10)", and Mach disk of the supersonic jet were clearly visible just behind the orifice. Outside the boundaries of the jet a red glow filled the chamber, the glow being most intense near the center. The radiation collected in this study was spatially integrated over the afterglow regions both inside the jet and downstream from it. Deposition of material on the sampling orifice or inside the chamber walls was not observed, although highly concentrated solutions were not analyzed in this study.

Spectral characteristics

The background spectrum emitted by the afterglow is shown in Figure 2. The numbers listed on the intensity scales for these and subsequent spectra are in the same units. The most prominent features in the background were the two OH bands in the ultraviolet, several weak lines around 330-430 nm, and numerous strong lines from Ar I in the red. The afterglow emitted many fewer Ar I lines in the region 330-600 nm than the normal analytical zone (11) of a typical ICP (12). The intensities of the red Ar I lines relative to each other were very similar to those seen previously from an atmospheric pressure Ar afterglow (13) or an ICP (14). These transitions terminate in the first four excited states of

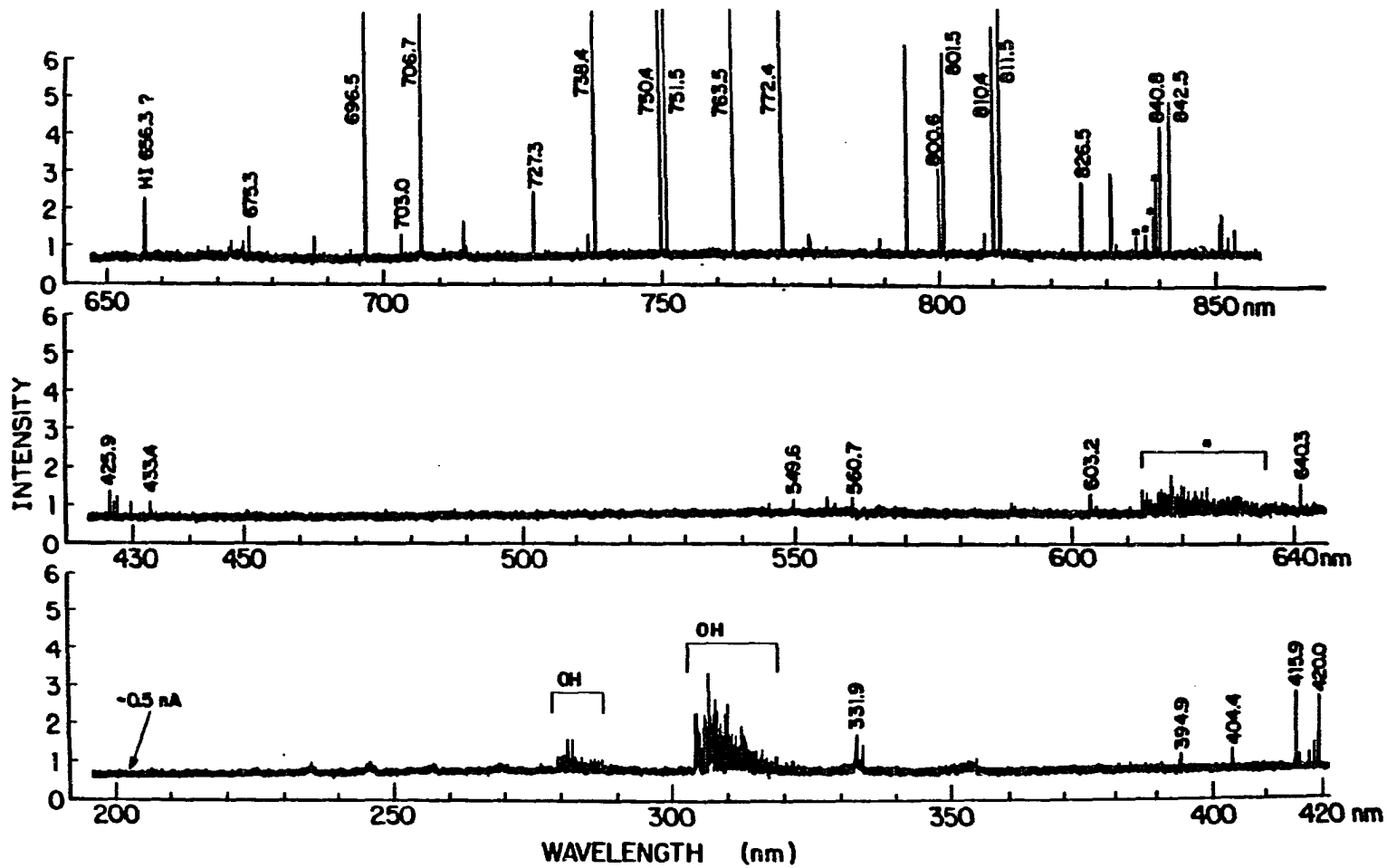

Figure 2. Background spectra emitted from afterglow during nebulization of de-ionized H_2O. Wavelengths listed represent Ar I lines. Asterisks denote second-order features. Some of the red Ar I lines are deliberately off-scale so weaker features can be seen

Ar I, two of which are metastable ($^3P_2$, $^3P_0$) and two of which ($^3P_1$, $^1P_1$) decay radiatively to the ground state. Observation of the red lines proves the existence of metastable Ar atoms in the afterglow; these species have been implicated to play a significant role in energy transfer and excitation in various Ar plasmas.

The line around 650 nm in Figure 2 is tentatively identified as the H_α transition (656.3 nm). If this assignment is correct, it is very interesting that this line should be seen but not H_β (486.1 nm) and the other lines of the Balmer series (15), which are prominent from the ICP (12). Weak bands from NO were also observed in the region 200-250 nm. Their intensities decreased strongly as the sampling orifice was moved closer to the torch end, indicating that they likely originated from air entrained into the plasma. Naturally, the NO bands interfered with analyte emission, so operating conditions were adjusted to minimize them. Lines from the stainless steel used to construct the sampler (e.g., Fe and Cr) were not observed in the background. In the absence of a line or band, the background level and standard deviation of the background were the same as the dark current and dark current noise of the photomultiplier. The background was considerably lower (by factors of 2-40, depending on wavelength) than that typically seen from an ICP (12). Use of a cooled photomultiplier with pulse counting detection could yield a lower background than seen in this work. The low emission background should facilitate observation of atomic fluorescence or simultaneous multielement atomic absorption (16) from the afterglow as well.

Spectra were observed from various analyte elements (e.g., Fe, La, and Na); examples for Ca, Mg, Zn, Cd and Mn with only a few lines are shown in Figures 3 and 4. In general, ion lines were much more prominent than neutral atom lines. As shown in Table II, ratios of ion to atom line intensities from the afterglow were similar to those seen for the same lines from the normal analytical zone of a typical ICP. Even the alkali metals emitted only very weak neutral atom lines, indicating that either these elements were present as ions or the excited states of the neutral atoms were not populated in the afterglow region viewed. If ion-electron recombination was extensive during the extraction process, neutral atom lines should have been significant because the recombination process would populate emitting levels of the neutral (17, 18). These observations tentatively support the contention of Douglas that recombination of analyte ions with electrons is not rapid during the ion extraction process for ICP-MS (19). The reader should note that the intensities for neutral atom lines were not far above those corresponding to the detection limits (e.g., Ca I 422.7 nm in Figure 3 and Zn I 213.8 nm in Figure 4), so comparisons involving neutral atom lines are only approximate.

Although the background emitted by the afterglow was much smaller than that emitted by an ICP, so were the analyte line intensities. To compare further the afterglow spectra with those emitted by an ICP, the line intensities for various elements were normalized to those for the strongest line seen (Ca II 393.4 nm) and compared to analogous ratios for a typical ICP. For each ratio the intensities were also adjusted to

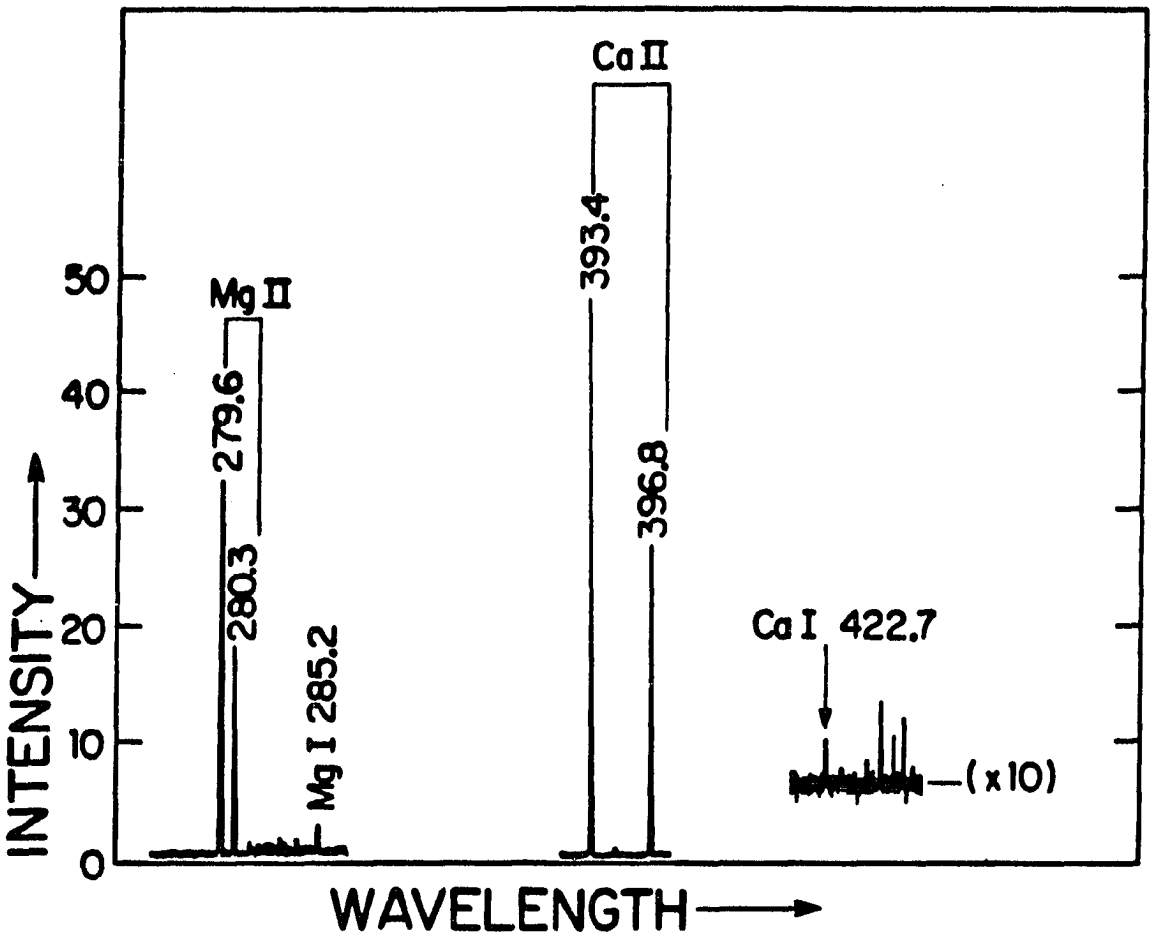

Figure 3. Spectra from Ca and Mg at 10 mg L^{-1}. Note that vertical scale is less sensitive than for Figures 2 and 4

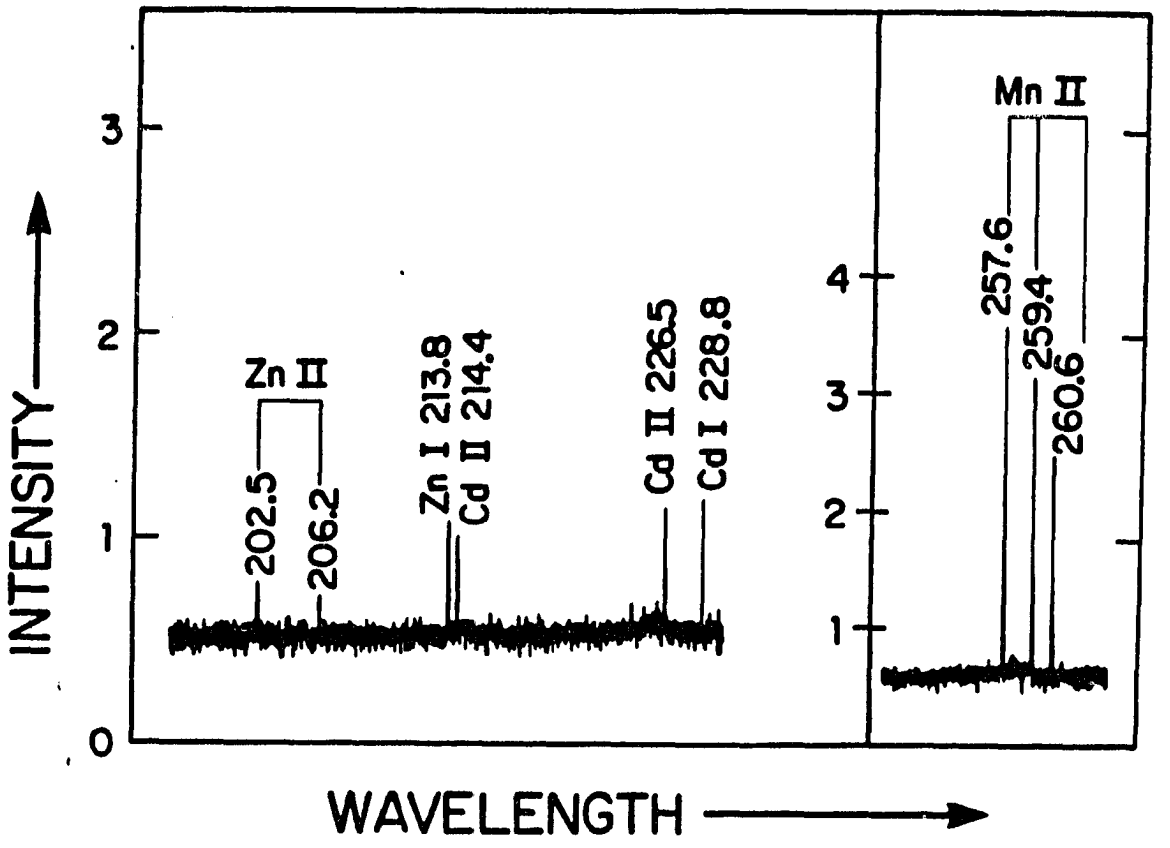

Figure 4. Spectra from Zn (40 mg L^{-1}), and Mn (10 mg L^{-1}). Note different vertical scales

Table II. Ion/atom line ratios for afterglow compared to those for ICP

line pair, nm	intensity ratio[a]	
	from afterglow	from ICP[b]
Ca II 393.4/Ca I 422.7	120	62
Mg II 279.6/Mg I 285.2	14	10
Zn II 202.2/Zn I 213.9	0.44	0.26
Zn II 206.2/Zn I 213.9	0.34	0.21
Cd II 226.5/Cd I 228.8	0.84	0.86
Cd II 214.4/Cd I 228.8	0.73	0.74

[a]Net intensities used throughout.

[b]Reference 12. The normal analytical zone was observed in this work.

Table III. Line intensities normalized to Ca ion emission

line, nm	net intensity relative to Ca II 393.4 nm, %	
	from afterglow	from ICP[a]
Mg II 279.6	67	81
Mg II 280.3	37	41
Mg I 285.2	4.6	7.8
Zn II 202.6	0.14	0.17
Zn I 213.9	0.34	0.66
Cd II 226.5	0.35	0.94
Cd I 228.8	0.41	1.1
Mn II 257.6	6.2	5.0

[a]Reference 12. The normal analytical zone was observed in this work.

correspond to the same solution concentration (in mg L^{-1}) of the various elements. The resulting data are shown in Table III. As was the case for ion/atom line ratios, the normalized analyte signals from the afterglow were similar to those from a typical ICP, with the relative intensities for Zn I and the Cd lines being perhaps a bit less from the afterglow.

Detection limits were best for elements with relatively few strong ion lines such as Ca (50 μg L^{-1}), Mg (70), and Mn (100). Obviously, detection limits for elements with more complex spectra or elements without strong ion lines were poorer, as indicated for Zn and Cd in Figure 4. Calibration curves for Ca II and Mg II were linear (correlation coefficients = 0.9994-0.9999) up to 10-20 mg L^{-1}. At higher concentrations the curves drooped gradually toward the horizontal axis, which could be due to self-absorption of the resonance lines observed. Band emission from analyte molecules such as MO or MOH (M = Ca, Mg, and Ce) could not be seen above the background noise when 100mg L^{-1} solutions of these elements were introduced into the plasma.

Effects of operating conditions

The analytical performance of ICP-MS instruments is sensitive to operating parameters chosen for the ICP, particularly aerosol gas flow rate (4,20). The effects of aerosol gas flow rate and forward power on the net intensities from the afterglow are depicted in Figures 5 and 6. The different lines of a particular element varied with power and aerosol gas flow rate in a similar fashion. The Cd, Zn, and Mg lines (Figure 5) were somewhat more sensitive to power than the other lines

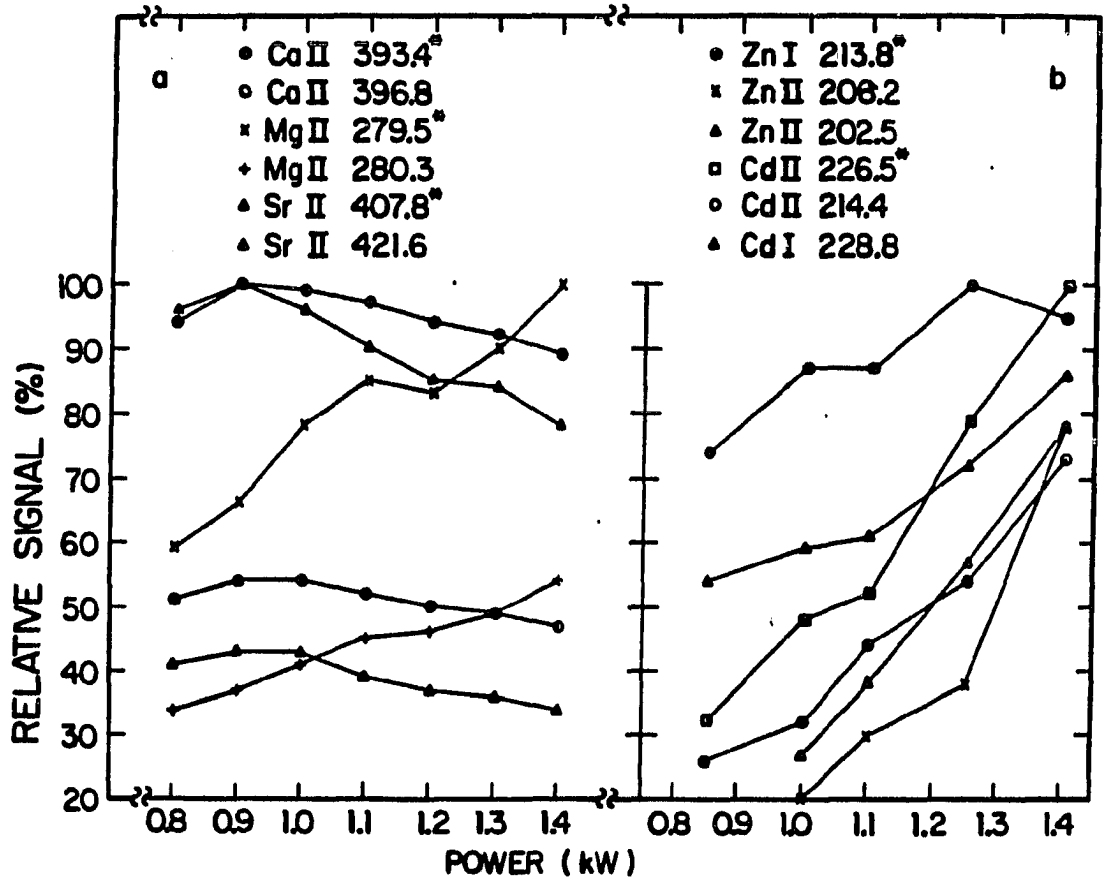

Figure 5. Dependence of net line intensity on forward power. The intensities for the various lines are normalized to that for the most intense line of each element (denoted by asterisk)

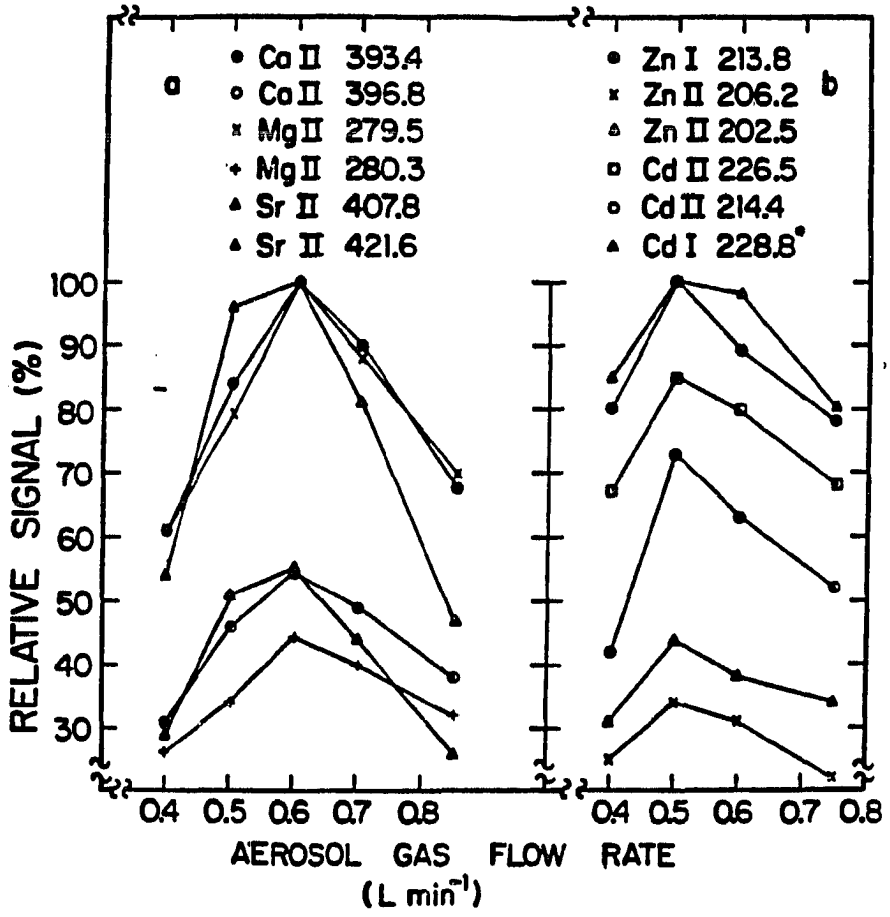

Figure 6. Dependence of net line intensity on aerosol gas flow rate: same normalization and legend as Figure 5, except that the Cd intensities were normalized to Cd I 228.8 nm

and increased continuously over the range of power studied. Significantly better signals for Cd II and Zn II could be obtained at higher power than for the conditions used to obtain the spectra in Figure 4. As aerosol gas flow rate changed (Figure 6), the Cd and Zn lines peaked at slightly lower flow rate than the Ca, Mg, and Sr lines. The shape of the plots in Figure 6 was roughly similar to those seen for ICP-MS (20). The background level and background noise did not change appreciably as power and aerosol gas flow rate changed.

Effects of Na on analyte line intensities

One of the most useful features of the ICP as an emission source is that the total solute concentration can vary over quite a wide range without greatly affecting the analyte response under typical multielement operating conditions (21,22). With ICP-MS at present the general consensus is that these interference effects are more severe than usually seen in ICP-AES (23) and that their underlying causes are complex. The results of a similar study with afterglow emission and Na as an interferent are shown in Figure 7. Blanks containing only Na in the indicated concentrations were also analyzed to verify the absence of significant Ca or Mg in the stock NaCl solution. Suppression of analyte intensity with increasing Na concentration was seen for all the lines studied; no enhancements were observed. Both lines for Ca II and Mg II were suppressed to a similar extent; the suppression of the Mg I line was slightly less extensive than for Mg II. The extent of suppression was similar to that seen by Bear and Fassel when a similar nebulizer was used with conventional ICP-AES (6) and less than when a similar

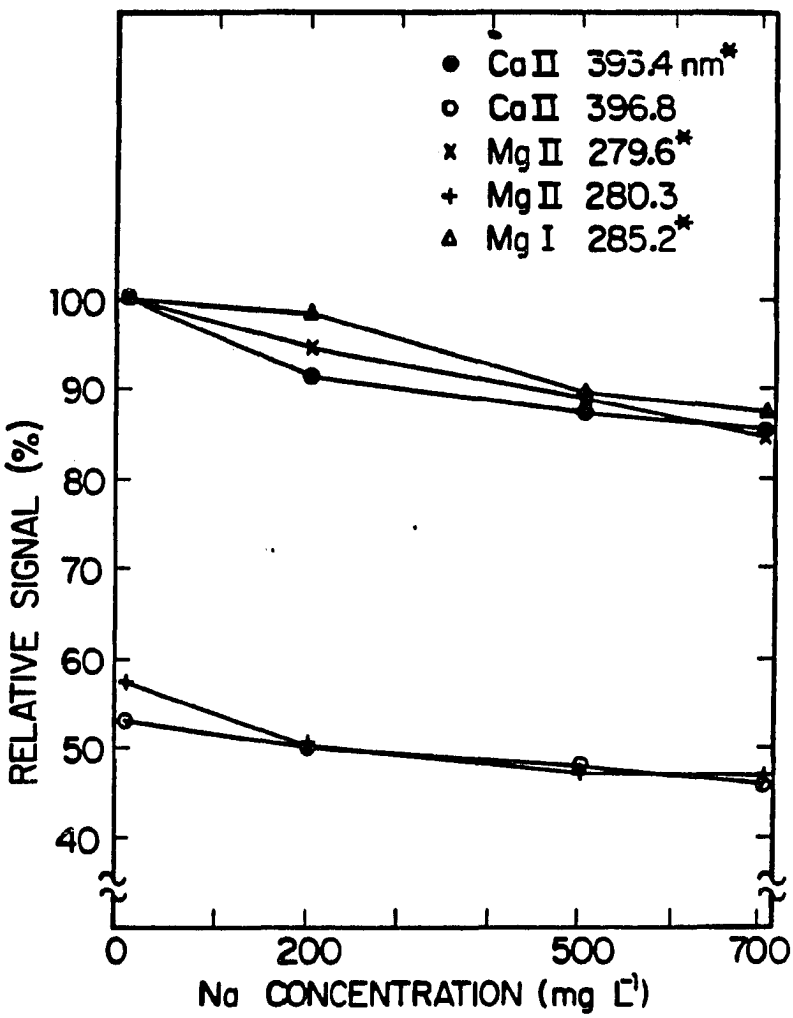

Figure 7. Dependence of net line intensity on Na concentration, Ca and Mg at 10 mg L^{-1}: Ca II 396.8 normalized to Ca II 393.4 nm and Mg II 280.3 normalized to Mg II 279.6 nm

nebulizer and plasma operating conditions were used for ICP-MS (23). The Ca and Mg signals from the original standard (i.e., that without Na) recovered completely after the series of Na standards had been analyzed. Thus, the observed signal suppression was not caused by orifice plugging, which was negligible for the interferent concentrations used during these experiments.

CONCLUSION

Numerous interesting experiments are suggested by the present work. Use of a high-resolution monochromator (24) for line-width measurements would determine if the lines emitted by the afterglow are sharper than those from the ICP. If so, interferences caused by overlapping spectral lines could be less severe than for ICP emission provided, of course, that the spectrometer bandwidth is sufficiently narrow. Incorporation of a secondary excitation source (e.g., microwave or rf antenna for emission or laser for fluorescence) inside the afterglow chamber should enhance line intensities and improve detection limits. The afterglow is physically separate from the ICP so that some isolation and separate control of atomization processes (in the ICP) and excitation processes (in the afterglow) may be possible (25). Measurement of various temperatures and particle number densities in the jet and afterglow on a spatially resolved basis would permit basic characterization of the conditions and processes occurring therein. With this information the analytical performance of either the afterglow or of ICP-MS could be improved.

LITERATURE CITED

1. Fassel, V. A. Science (Washington, D. C.) 1978, 202. 183-191.
2. Barnes, R. M. CRC Crit. Rev. Anal. Chem. 1978, 7, 203-296.
3. Date, A. R.; Gray, A. L. Analyst (London) 1983, 108, 1033-1050.
4. Olivares, J. A.; Houk, R. S. Anal. Chem. 1985, 57, 2674-2679.
5. Houk, R. S.; Fassel, V. A.; Svec, H. J. Dynamic Mass Spectrom. 1981, 6, 234-251.
6. Bear, B. R.; Fassel, V. A. Spectrochim. Acta, Part B 1986, in press.
7. Olson, K. W.; Haas, W. J., Jr.; Fassel, V. A. Anal. Chem. 1974, 46, 75-80.
8. Scott, R. H.; Fassel, V. A.; Kniseley, R. N.; Nixon, D. E. Anal. Chem. 1974, 46, 75-80.
9. Douglas, D. J.; French, J. B. Spectrochim. Acta, Part B 1986, 41B, 197-204.
10. Beijerinck, H. C. W.; Van Gerwen, R. J. F.; Kerstel, E. R. T.; Martens, J. F. M.; Van Vliembergen, E. J. W.; Smits, M. R. Th.; Kaashoek, G. H. Chem. Phys. 1985, 96, 153-173.
11. Koirtyohann, S. R.; Jones, J. S.; Yates, D. A. Anal. Chem. 1980, 52, 1965-1966.
12. Winge, R. K.; Fassel, V. A.; Peterson, V. J.; Floyd, M. A. Inductively Coupled Plasma-Atomic Emission Spectroscopy. An Atlas of Spectral Information; Elsevier: Amsterdam, The Netherlands, 1985; Appendix A.

13. Rice, G. W.; D'Silva, A. P.; Fassel, V. A. Anal. Chim. Acta 1984, 166, 27-38.

14. Blades, M. W.; Hieftje, G. M. Spectrochim. Acta, Part B 1982, 37B, 191-197.

15. Herzberg, G. Atomic Spectra and Atomic Structure; Dover: New York, 1944; p 24.

16. Harnly, J. M. Anal. Chem. 1986, 58, 933A-943A.

17. Larson, G. F.; Fassel, V. A. Appl. Spectrosc. 1979, 33, 592-599.

18. Eljoundi, A.; Batal, A.; Mermet, J. B. Spectochim. Acta, Part B 1985, 40B, 1007-1011.

19. Douglas, D. J. Short Course on Inductively Coupled Plasma Mass Spectrometry; Winter Conference on Plasma Spectrochemistry: Kona, HI, 1986.

20. Horlick, G.; Tan, S. H.; Vaughan, M. A.; Rose, C. A. Spectrochim. Acta, Part B 1985, 40B, 1555-1572.

21. Larson, G. F.; Fassel, V. A.; Scott, R. H.; Kniseley, R. N. Anal. Chem. 1975, 47, 238-243.

22. Blades, M. W.; Horlick, G. Spectrochim. Acta, Part B 1981, 36B, 881-900.

23. Olivares, J. A.; Houk, R. S. Anal. Chem. 1986, 58, 20-25.

24. Edelson, M. C.; Dekalb, E. L.; Winge, R. K.; Fassel, V. A. Spectrochim. Acta, Part B 1986, 41B, 475-486.

25. Allen, G. M.; Coleman, D. G. Anal. Chem. 1984, 56, 2981-2983.

SECTION II. SOME FUNDAMENTAL CHARACTERISTICS OF A REDUCED PRESSURE AFTERGLOW EXTRACTED FROM AN INDUCTIVELY COUPLED PLASMA

INTRODUCTION

Inductively coupled plasma-mass spectrometry (ICP-MS) has developed into a very useful technique for elemental and isotopic analysis (1-4). Understanding the ion extraction step is crucial in order to improve the analytical utility of ICP-MS; fundamental information about the processes occurring and the conditions prevailing during the sampling of an ICP would also be valuable for this end. It should be possible to obtain information about temperatures and collisional events occurring during extraction from optical spectra of atoms, ions and molecules after they have traveled through the sampling orifice. These studies could also lead to a new, analytically useful source of free atoms, where the analyte is vaporized and atomized in the atmospheric pressure ICP while spectra are observed from a region at low pressure with a low spectral background. For instance, Whitten et al. recently showed that the hyperfine structure of the Na D lines could be resolved by using Doppler free high resolution spectroscopy in a supersonic jet extracted from a flame (5).

A previous section described initial studies of emission spectra from a low pressure plasma extracted from an ICP (6). The present work reports more detailed studies of conditions in the emitting region of the extracted plasma including measurements of temperatures and spectral linewidths.

EXPERIMENTAL

Appearance and structure of extracted plasma

The inductively coupled plasma torch, the sampling apparatus and the supersonic jet are shown in Figure 1. The gas in the axial channel of a conventional Ar ICP flows through a circular sampling orifice into an evacuated chamber. The chamber walls are transparent so the extracted plasma can be observed visually.

The physical appearance of the extracted plasma seen inside the vacuum chamber is also depicted in Figure 1. The dark "zone of silence" was clearly evident. The zone of silence was surrounded by a bright red emitting layer, which was assumed to represent the barrel shock and Mach disk. The positions, shapes, and dimensions of these regions were approximately as predicted by theoretical descriptions of a supersonic expansion through a large sampling orifice (7-9). Downstream from and outside these shock waves, a red afterglow persisted for some distance.

Instrumentation and operating conditions

The optical arrangements used for the three experiments described herein are shown in Figures 2 and 3. Instrumental components and operating conditions are given in Table I. The extracted plasma was generated with the same device described previously (6), except that a vertical, 40 MHz plasma was used in the present work.

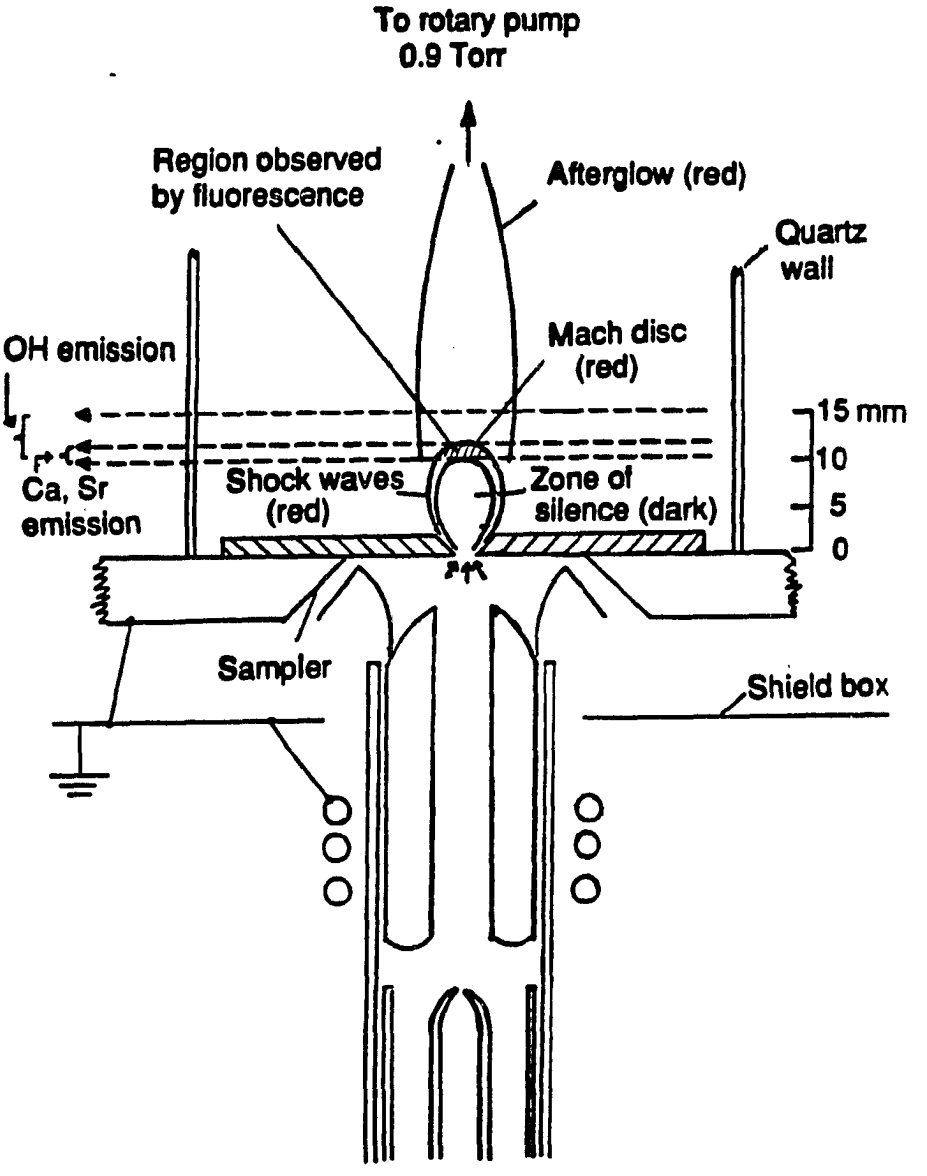

Figure 1. Inductively coupled plasma torch, sampling apparatus and supersonic jet showing zone of silence, Mach disk, shock waves, and afterglow. The regions observed in the three experiments are also shown

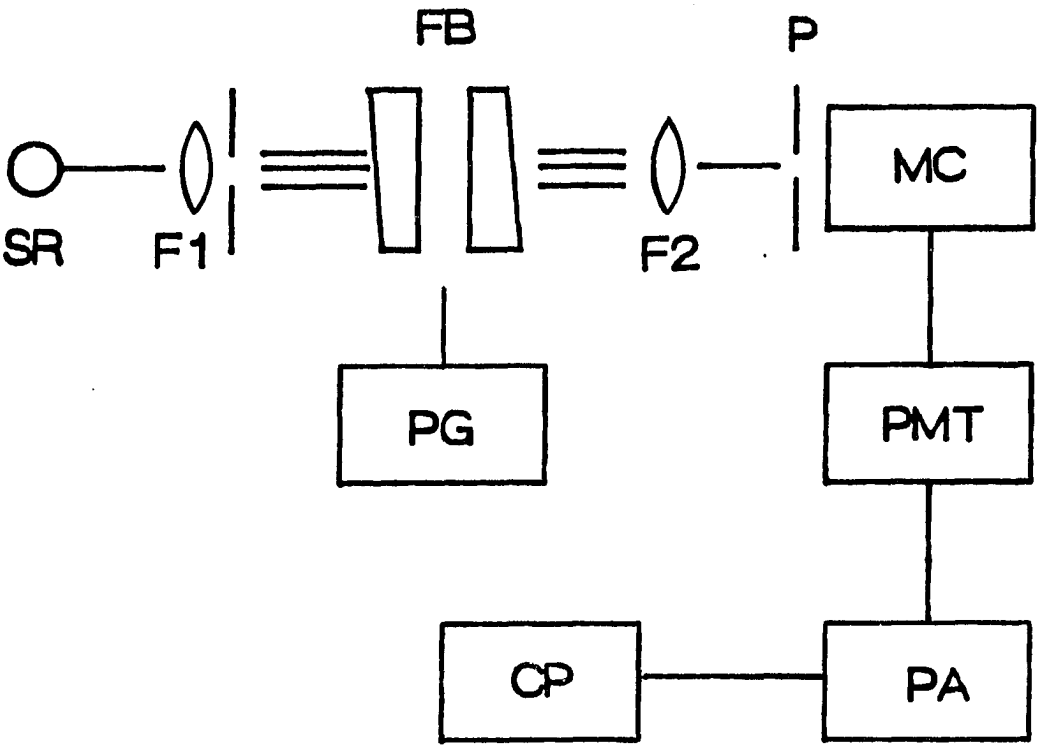

Figure 2. Top view of optical apparatus for emission studies: SR, source; F1,F2, lenses; A, aperture (2 mm inside diameter); P, pinhole (200 μm diameter); FB, Fabry-Perot interferometer; MC, monochromator; PMT, photomultiplier tube; PA, picoammeter; CP, computer. The interferometer and apertures were removed for the OH measurements

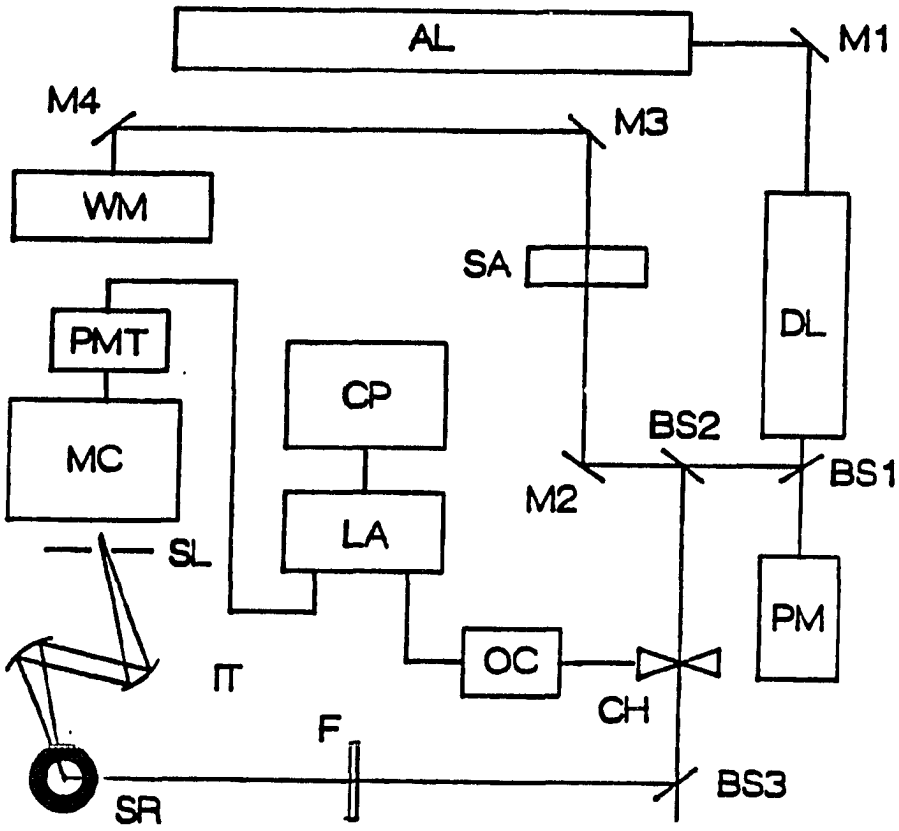

Figure 3. Apparatus for laser induced fluorescence studies. AL, argon ion pump laser; M, mirrors; DL, ring dye laser; BS, beam splitters; PM, power meter; SA, spectrum analyzer; WM, wavemeter; CH, chopper; OC, optical chopper controller; LA, lock-in amplifier; CP, controlling computer; F, neutral density filter; SR, source (top view); IT, image transfer system; SL, tangential image slit; MC, monochromator; PMT, photomultiplier

Table I. Instrumental components

Component Description/Manufacturer	Operating Conditions
ICP generator:	
Type HFP 25000 with AMNPS-1 impedance matching network RF Plasma Products, Inc. Kresson, NJ load coil grounded at downstream end nearest sampling orifice. see Figure 1	forward power 1.0 kW reflected power <10 W frequency 40 MHz
plasma torch: Ames Laboratory design (10) outer tube extended 35 mm beyond tip of aerosol injector	argon flow rates (L min^{-1}) outer 18 aerosol 1.2 auxiliary 10
nebulizer: concentric pneumatic Type C Meinhard Associates	solution uptake rate 0.6 mL min^{-1}
extraction system: (6) see Figure 1	flat stainless steel disk orifice diam. 0.53 mm
sampling position	orifice centered on ICP 27 mm above top of load coil (~8 mm from tip of initial radiation zone (11) when Y introduced at ~1000 mg L^{-1})
pressure measurement: thermocouple gauge Model 601 Varian	operating pressure 0.9 torr while sampling ICP
vacuum pump: rotary vane pump Model D30 Leybold-Heraeus	pumping speed: 13 L s^{-1} at pump

Table I. (continued)

Component Description/Manufacturer	Operating Conditions
monochromator: Model HR-320 Instruments SA, Inc.	Czerny-Turner configuration focal length 0.32 m holographic grating ruled at 2400 grooves mm^{-1} blazed at 546 nm slit widths: 10 μm for OH spectra 250 μm for interferometry 100 μm for fluorescence
photomultiplier: Model 9804QA Thorn EMI Gencom	bias voltage - 850V
picoammeter: Model 485 Keithley Instruments	
computer: Hewlett-Packard Vectra 20 Mbyte hard disk MS-DOS V.3.1 operating system Ames Laboratory software	
<u>fluorescence Experiments (Figure 3)</u>	
same monochromator, detector, and picoammeter	
argon ion laser: Innova 90-5 Coherent	output power 4.6 W all lines

Table I. (continued)

Component Description/Manufacturer	Operating Conditions
ring dye laser: Model 699-21 Coherent	output power 70 mW @589 nm Rhodamine 6G dye scan range 25 GHz line width <20 MHz
power meter: Model 365 Scientech	
beam splitters: Newport Corp.	
wavemeter: Model WA-20 Vis Burleigh	
spectrum analyzer: Model SA-200-Sx Burleigh	
lock-in amplifier: SR-510 Stanford Instruments	chopping frequency 400 Hz sensitivity 2 mV pre-time const. 300 ms post-time const. 0.1 s
Fabry-Perot Interferometer: Model R-150 Burleigh Instruments, Inc.	free spectral range 44 pm in the vicinity of 400 nm coated to pass 400 to 490 nm

Rotational temperature (T_{rot}) measurements

The rotational temperature, T_{rot}, was determined by measuring the intense OH band components (305-325 nm) emitted directly from the Mach disk and afterglow (6). The aperture, pinhole and Fabry - Perot interferometer were removed for this experiment. The monochromator was used in second order to disperse the lines adequately, and a quartz filter (Type UG5, Schott Optical Glass) was used to block first order visible light at 610-650 nm, which would interfere with the OH band in second order. Distilled de-ionized water was nebulized for this experiment.

The intensities of the OH lines listed in Table II were measured. The detector response was considered uniform for this whole set of lines. As shown in Figure 1, the region observed was approximately 5mm high and included both the bright Mach disk (~2 mm) and the adjacent section of the less luminous afterglow (~3 mm). Naturally, the measured intensities and the resulting temperatures were weighted averages of the actual values in the various regions observed. The line intensities and transition probabilities were used to generate a Boltzmann plot (12-15), the slope of which was equivalent to $-1/kT_{rot}$ (k = Boltzmann constant). The quantity T_{rot} is generally considered a measure of the gas kinetic temperature (13).

For comparative purposes, the same intensities of the OH lines were measured from the ICP (i.e., the extraction apparatus was removed). The observation position was 25 mm above the load coil, which corresponded roughly to the center of the normal analytical zone (11) for the extended torch and plasma conditions used.

Table II. OH lines and transition probabilities used for T_{rot} measurements (12); g = statistical weight, A = Einstein coefficient for spontaneous emission, ν = frequency

wavelength (nm)	designation	excitation energy (cm^{-1})	gAν value (rel. units)
308.40	$R_2 1$	32542	2.7
307.70	$R_2 3$	32778	9.0
307.44	$R_2 4$	32947	13.0
307.11	$R_2 14$	36393	54.1
307.30	$R_2 15$	36903	58.0
308.90	$R_2 20$	39847	69.9

Linewidth measurements for Ca II and Sr II emission

As shown in Figure 2, a Fabry - Perot interferometer was used with the grating monochromator to provide high spectral resolution. Because of the apertures in the optical path, the field of view for the Ca II and Sr II measurements was narrower than for the OH measurements. Thus, the expansion was viewed primarily through the Mach disk (Figure 1). Both the aperture and pinhole attenuated the light levels by a factor of ca. 400, hence, concentrated analyte solutions (1000 mg L^{-1} of Ca and of Sr) and strong lines (Ca II 393.4 nm and Sr II 407.7 nm) were used to provide sufficient emission intensities.

The Doppler contribution to the observed linewidth was determined by the following procedure. The instrumental contribution β_i to the measured full width at half maximum was determined first. The hyperfine structure of the Hg line at ca. 435.8 nm from a low pressure Hg arc lamp was measured using the Fabry - Perot interferometer. The free spectral range of the interferometer was 44 pm, the finesse was approximately 40, and the resolving power was 400,000. The full width at half maximum (FWHM) of a hyperfine component of the Hg line at 435.80 nm was measured to be 1.1 pm (16). The intrinsic width of this hyperfine Hg component was determined to be 0.4 pm by measuring the spectrum of this lamp with the high resolution, Fourier transform spectrometer at Los Alamos National Laboratory (17). Assuming Gaussian lineshapes, β_i was then determined from the formula:

$$\beta_i = (1.1^2 - 0.4^2)^{1/2} = 1.0 \text{ pm} \qquad (1)$$

Line profiles were then measured for the Ca and Sr lines emitted from the Mach disk region (Figure 1). Any spurious noise spikes were

removed, and the line profiles were smoothed by an Savitsky - Golay procedure. The intensities were normalized and the Voigt "a" parameters were calculated. The FWHMs of the Gaussian components (β_g) of these lines were then calculated (18). The a parameter was 0.2 for both lines. The Doppler width (β_{Dopp}) (19) and Doppler temperature (T_{Dopp}) were then calculated from the following equations:

$$\beta_{Dopp} = (\beta_g^2 - \beta_i^2)^{1/2} \quad (2)$$

$$\Delta\lambda_{Dopp} = 7.16 \times 10^{-7} \lambda_o \sqrt{T_{Dopp} / M} \quad (3)$$

where $\Delta\lambda_{Dopp}$ = Doppler width in frequency units (s^{-1}), λ_o = frequency at line center (s^{-1}) and M = relative atomic weight of the emitting element. As with T_{rot}, T_{Dopp} is generally considered to be a measure of the gas kinetic temperature.

The solution concentrations of Ca and Sr were varied to look for possible self-absorption effects (6,20). The analyte signal varied linearly with concentration up to the highest concentration studied (1000 mg L^{-1}), therefore there was no evidence of self-absorption in this experiment. As with the OH measurements, the same Ca II and Sr II lines were also observed from the normal analytical zone (25 mm above the load coil) of the ICP.

The regions observed in the optical experiments described below are shown in Figure 1. Note that the Mach disk and/or the downstream afterglow, where collisions have perturbed the free flow of the supersonic jet, were observed. The emission was spatially integrated

over the width and depth of the region observed, whereas the fluorescence observations were spatially resolved as described later.

Fluorescence measurements

The apparatus for this experiment is shown in Figure 3. The continuous wave ring dye laser was operated in single frequency mode and was pumped with all lines of an argon ion laser. Half the dye laser output was transmitted through a beam splitter (BS1) to a power meter. Forty-five percent of the original output of the dye laser was directed to a wavemeter to measure the wavelength of the laser beam. The remainder (5%) of the dye laser output was passed through a mechanical chopper. The modulation frequency was monitored by a fast response phototransistor internal to the chopper, the output of which was used as the reference input for a lock-in amplifier. The laser beam was attenuated by one or more neutral density filters before entering the vacuum chamber. Without the filters, the laser power reaching the cell was approximately 4 mW. The measured fluorescence line width was the same when various filters were used, which indicated that power broadening was negligible.

Fluorescence was observed from the Mach disk (Figure 1) along an optical axis perpendicular to the laser beam. Two mirrors (both of focal length 500 mm and 50 mm diameter; aluminum coated with MgF_2, Melles Griot, Irvine CA) were used in an over-and-under configuration to focus the fluorescence on to the entrance slit of the monochromator (21,22). An external slit placed at the tangential image of the mirror system transmitted only radiation from the spatial region illuminated by

the laser beam. The entrance slit of the monochromator was at the sagittal image of the mirror system and passed only a vertical slice of the radiation coming through the external slit. Thus, a rectangular spatial zone, centered at the Mach disk (Figure 1), was observed.

Non-resonance fluorescence involving the two Na D lines was monitored. The laser wavelength was scanned across the line at 588.995 nm while the monochromator transmitted the line at 589.592 nm. The concentration of sodium in solution was 200 mg L^{-1}.

The Na D lines were chosen for study because of their high fluorescence quantum efficiencies and also because their wavelengths were within the tuning range of the laser. Deduction of T_{Dopp} from the measured linewidths was complicated by hyperfine effects. The upper levels of the D lines had small splittings that were not observable in the present experiment. However, the ground state was known to be split by ca. 2 pm (1.8 GHz) (5), which was significant compared to the expected Doppler widths. Each Na D line was actually a doublet (23) with an intensity ratio of 5:3; each component of the doublet was broadened independently.

The contribution of this hyperfine structure to the measured linewidth for Na was determined in the following way. A Voigt profile was generated for each component at the same value of T_{Dopp}. The a parameter was estimated to be 0.2. The two profiles were spaced 1.8 GHz apart, and their relative intensities were adjusted to conform to the expected 5/3 ratio. The two profiles were then added together to yield a composite line profile. The value of T_{Dopp} used in these computations was then adjusted until the calculated line profile matched the measured

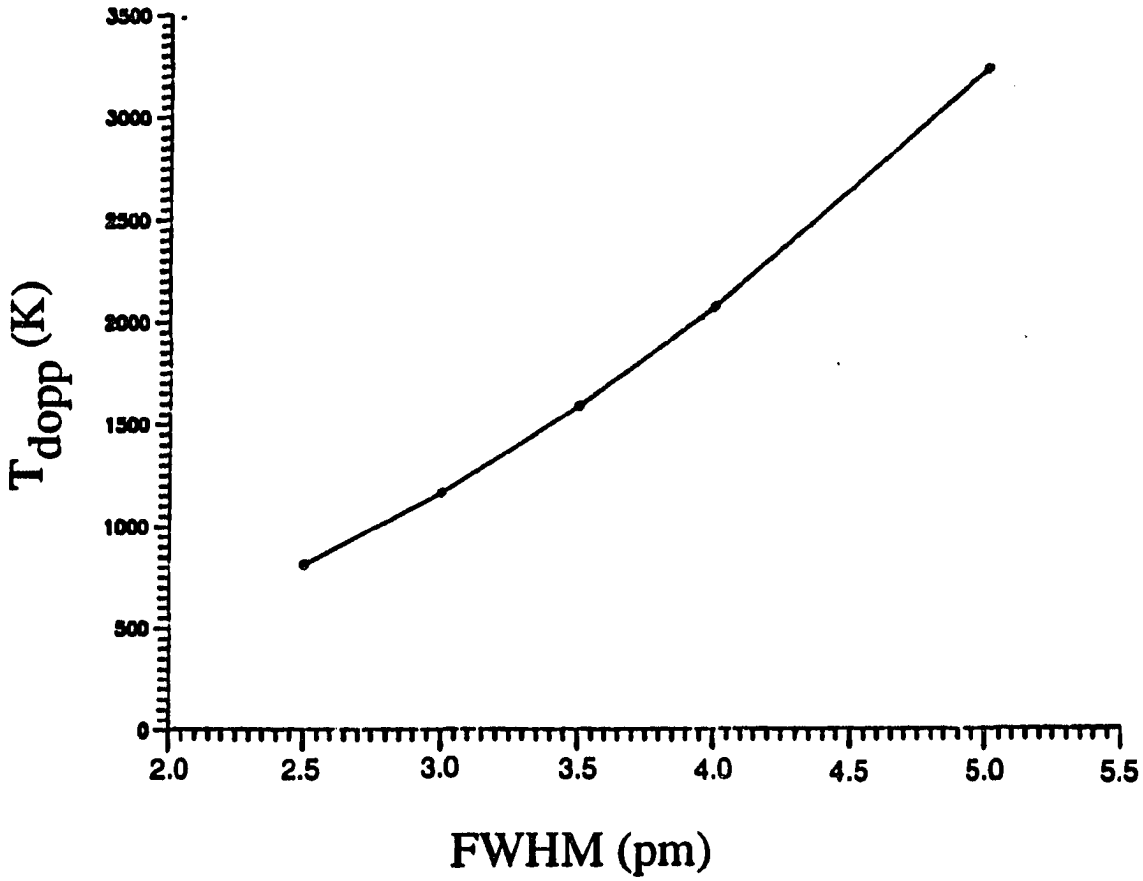

Figure 4. Calculated values of FWHM of Na D line, including broadening due to hyperfine structure, for various Doppler temperatures

line profile. The calculated FWHM of the composite line profile is shown for various T_{Dopp} values in Figure 4. The width of the laser output (<20 MHz) was considered to be negligible compared with that of the observed fluorescence.

RESULTS AND DISCUSSION

T_{rot} measurements

A spectrum of the OH band from the Mach disk and afterglow is shown in Figure 5. The Boltzmann plots are shown in Figure 6. In both instances the Boltzmann plots yielded reasonably straight lines without the curvature recently reported for OH measurements in ICPs (24). For the ICP, T_{rot} was determined to be 3800 $\pm$400 K, which was in good agreement with the value of 3900 K measured by Kawaguchi et al. (12). For the Mach disk and afterglow, T_{rot} was determined to be 2400 $\pm$300 K. As shown in Figure 5, the line with the highest excitation energy ($R_2$20) was not very intense from this latter source, hence the scatter for these two points in the Boltzmann plot (Figure 6). The uncertainties represent one standard deviation as determined from regression analysis of the data shown in the Boltzmann plots.

T_{Dopp} measurements

Some typical emission spectra obtained with the interferometer apparatus are shown in Figure 7. These spectra have not been smoothed, nor have the noise spikes been removed. As shown for Ca II 393.4 nm, the lines from the Mach disk were much weaker than those from the ICP. The Ca II line from the Mach disk was narrower than that from the ICP by a factor of approximately two. The Sr II line was narrower than the Ca II line, as expected because of the larger atomic mass of Sr (Equation 3).

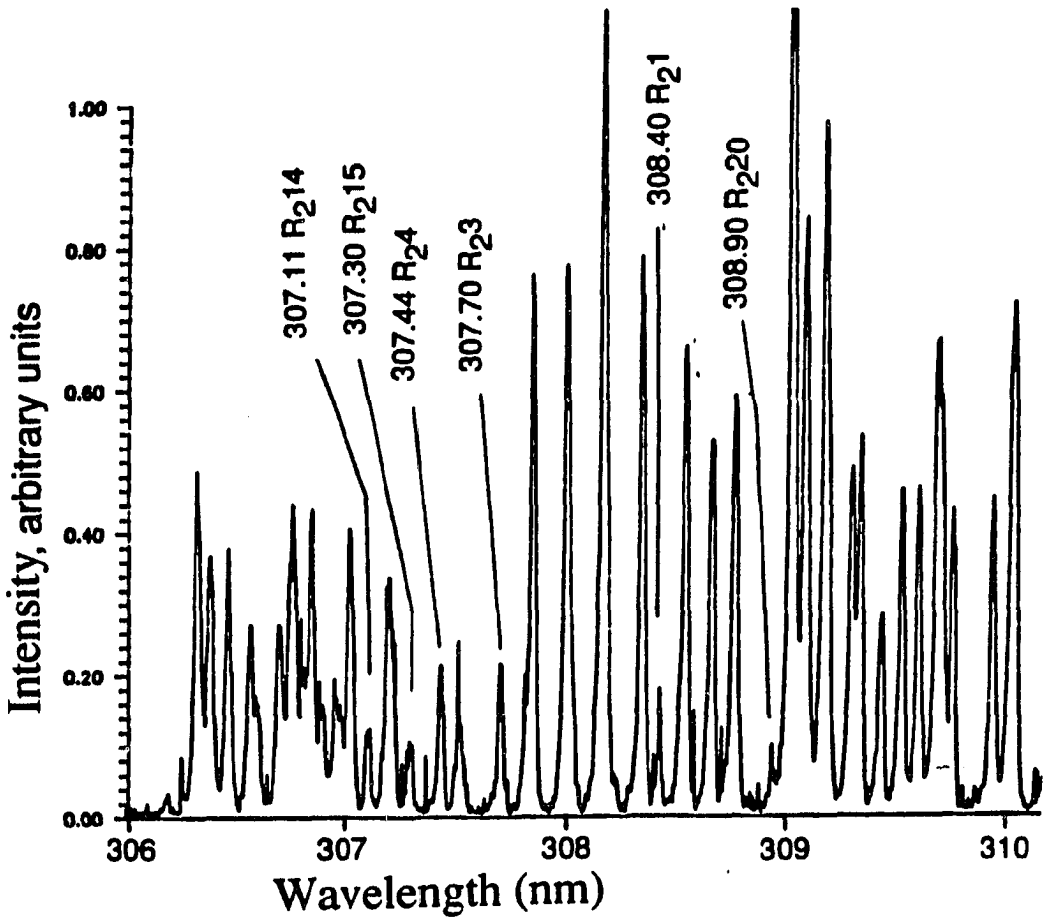

Figure 5. Partial spectrum of OH band obtained from Mach disk and afterglow. The lines used to determine T_{rot} (Table II and Figure 6) are identified

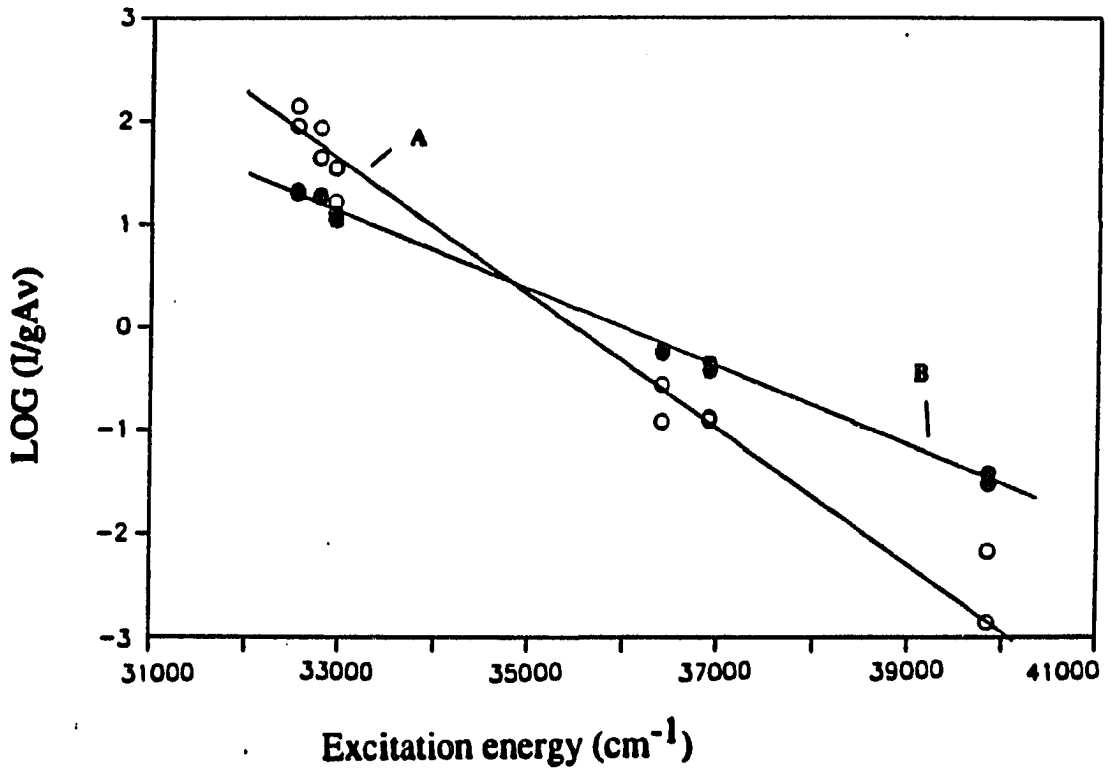

Figure 6. Boltzmann plots obtained from OH line measurements from A, the Mach disk and afterglow and B, from the ICP. Duplicate measurements are shown for each line and each source

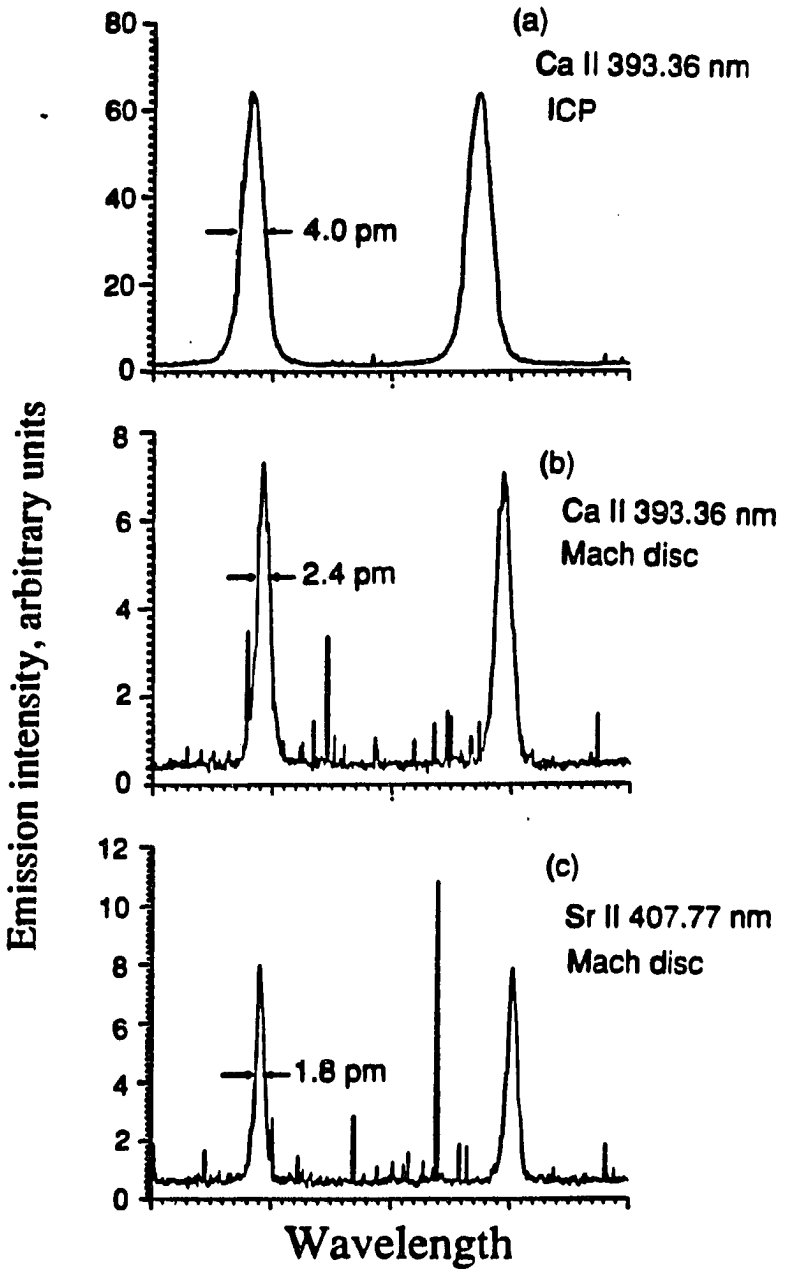

Figure 7. Spectra obtained with high resolution apparatus (Figure 2) for Ca and Sr ion lines emitted from Mach disk. The analyte concentration was 20 mg L^{-1} in (a), 1000 mg L^{-1} in (b) and (c). The spectra are plotted on the same wavelength scale. The units on the intensity scales are consistent. Two scans of each line are shown, i.e., the other components of these doublet lines are removed by the monochromator

Table III. Measured widths of emission lines and Doppler temperatures

Source	Ca II 393.4 nm Linewidths (FWHM, pm) Total	Doppler	T_{Dopp} (K)	Sr II 407.7 nm Linewidths (FWHM, pm) Total	Doppler	T_{Dopp} (K)
ICP	4.0	3.4	5900	3.6	2.4	5900
	4.1	3.5	6100	(3.2)[a]	(2.5)[a]	
	4.0	3.3	5700			
	(4.1)[a]	(3.5)[a]				
MACH	2.4	2.1	2200	1.8	1.6	2800
DISK			± 200[b]			± 200[b]

[a]Values in parentheses were reported by Boumans and Vrakking (25).

[b]Uncertainties in T_{dop} correspond to a ±0.1 pm uncertainty in Doppler width.

The results for linewidth and T_{Dopp} measurements are presented in Table III. Triplicate results are shown for Ca II from the ICP to illustrate the typical reproducibility of these measurements. The Doppler widths observed from the ICP agreed closely with those reported by Boumans and Vrakking (25). The T_{Dopp} values observed from the ICP (ca. 6000 K) were higher than those found in the previous studies of Human and Scott (4900-5400 K) (20) but were consistent with more recent measurements by Faires et al. (26). The T_{Dopp} values from the ICP were also substantially higher than T_{rot} values (ca. 3800 K), as has been noted in several other studies (13). The T_{Dopp} values from the Mach disk were substantially lower than those from the ICP. For the Mach disk, the magnitude of the T_{Dopp} values (2200-2800 K) was similar to the T_{rot} values measured from the OH spectrum.

An excitation scan of Na fluorescence from the Mach disk is shown by the solid line in Figure 8. The FWHM of the line was 4.2 pm, which corresponded to a T_{Dopp} of 2300 K (Figure 4). For the same line emitted by the ICP, Boumans and Vrakking measured a width of 10.3 pm (25). Thus, the Na D line observed by fluorescence from the afterglow was substantially narrower than the same line emitted by the ICP, as was also observed for the Ca II and Sr II emission lines described previously. Simulated profiles for this Na I line at two temperatures (2100 and 2600 K) are also shown in Figure 8. The measured line profile lies inside the two simulated ones, indicating the uncertainty in T_{Dopp} to be of the order of $\pm$200 K.

Three different techniques were used to study the Mach disk region.

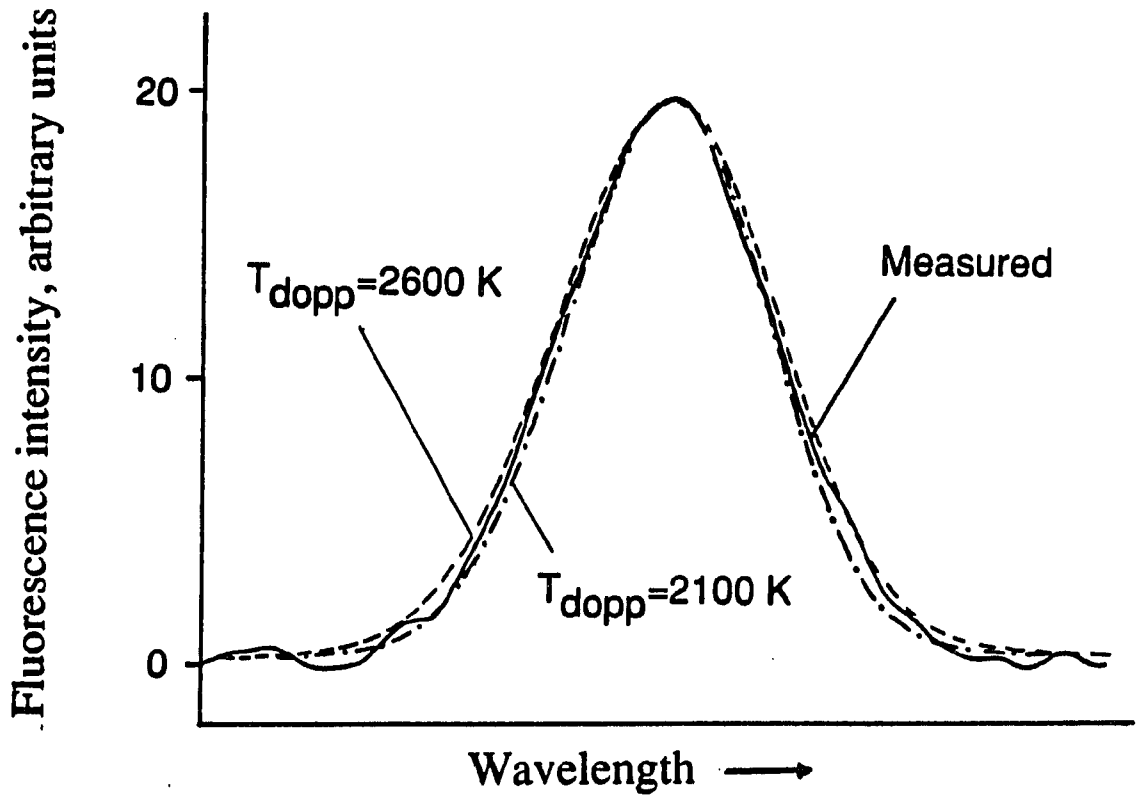

Figure 8. Na fluorescence line at 589.592 nm. Solid curve: measured line profile from Mach disk. Dotted curves: calculated line profiles at two values of T_{Dopp} (see Experimental section)

Each yielded gas kinetic temperatures close to 2200 K. A definitive statement on the existence of local thermodynamic equilibrium in the Mach disk requires additional measurements of excitation temperatures, electron temperatures, etc. The temperature values for the Mach disk are substantially greater than those expected inside the zone of silence (Figure 1). The equations describing free jet expansions indicate that the gas kinetic temperature should drop from ca. 5000 K in the ICP to 100 K or less after the gas has expanded into the vacuum system by a distance of 8-10 orifice diameters (9). The measured temperatures of 2200 K in the Mach disk clearly indicate that the species are re-heated by collisions therein, as predicted. These processes are apparently both rapid and efficient, as the atoms have already re-heated to approximately half the source temperature after travelling only 1-2 mm through the shock waves. Previous measurements of gas kinetic temperatures in a partially ionized jet extracted from an argon plasma also showed a rapid heating effect in the Mach disk region (27). Collisions in the Mach disk probably also populate excited states, with subsequent emission.

Visual observations

Some further deductions about conditions in the extracted gas are possible from the visual observations depicted in Figure 9. Two different positions of the laser are shown. Yellow fluorescence from Na atoms was strongest from the Mach disk and shock waves and was easily visible throughout the cell except from the zone of silence. The zone

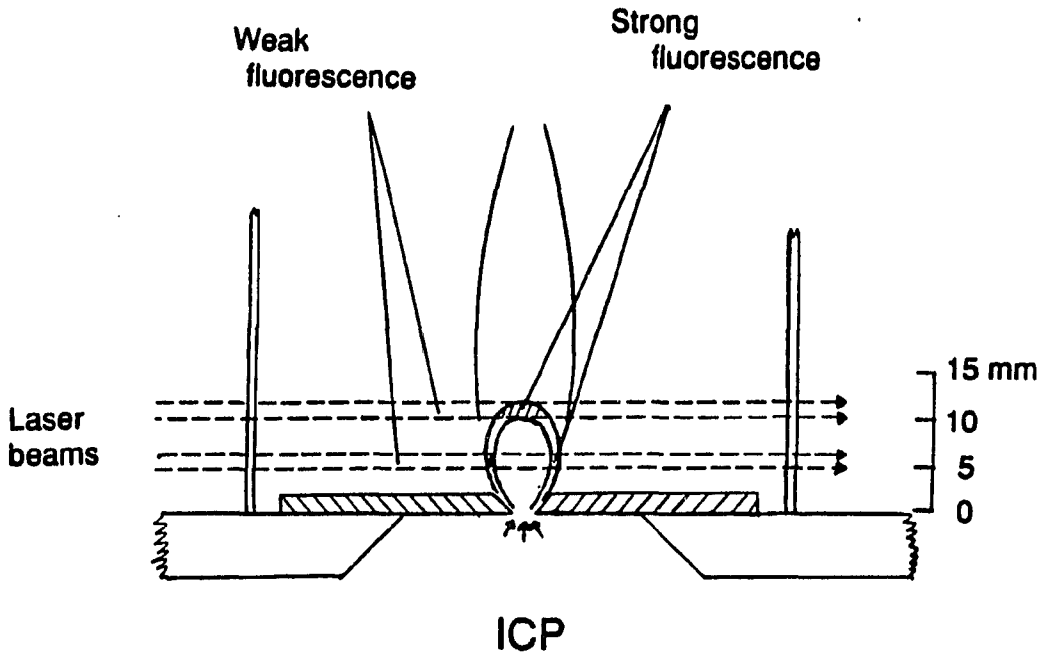

Figure 9. Visual appearance of fluorescence from either Na I or Ba II lines from Mach disk and shock waves. See text for discussion

of silence was also fairly dark and was much less luminous than either the Mach disk, barrel shock or afterglow. The volume of the ellipsoidal zone of silence was estimated to be approximately 0.25 cm^3 from the dimensions shown in Figure 9. This value was smaller than that of the whole cell by a factor of about 1000. Despite the much larger volume of the cell, Na I fluorescence was easily visible along the laser path between the cell wall and the barrel shock region, where the Na particle density was expected to be approximately three orders of magnitude smaller than within the zone of silence. The comparative lack of fluorescence from the zone of silence indicated that very few neutral Na atoms were present there.

This observation can be understood from the following considerations. In the ICP, 99% or more of the Na was ionized (2). Thus, the Na in the gas flowing into the sampling orifice was mostly Na^+. Inside the supersonic jet, there was apparently little recombination of Na^+ with electrons (9). The Na ions survived the extraction process as such, so that there were few neutral Na atoms and little fluorescence from Na I lines inside the zone of silence. As the extracted species reached the shock waves and Mach disk, the collisions that occurred induced some ion-electron recombination, forming neutral Na atoms, which could be observed.

The results of some initial experiments involving ionic fluorescence are pertinent here. Figure 9 also depicts the visual appearance of the system when the laser was tuned to the Ba II lines at either 585.368 nm or 614.172 nm. Barium was present in solution at 1000 mg L^{-1}. Blue anti-stokes fluorescence could be readily seen from the

shock waves and Mach disk but not from the zone of silence. The lower levels for these Ba II transitions were excited states 0.6-0.7 eV above the lowest level of Ba^+ (28). The lack of fluorescence from excited levels of Ba^+ indicated that these states were not populated inside the zone of silence. Apparently, excited levels of Ba^+ were deactivated early in the extraction. These levels were not re-populated until the Ba ions experienced collisions again in the shock waves and Mach disk. Thus, the zone of silence was relatively dark; the bulk of the emitted light emitted from the shock waves, Mach disk, and the afterglow downstream. The laser could not be used to study Ba II lines involving the ground state (e.g., 455.403 and 493.409 nm), which should be observable in the zone of silence. Study of these lines is therefore an objective for future research.

LITERATURE CITED

1. Houk, R. S.; Thompson, J. J. Mass Spectrom. Reviews 1988, 7, 425.
2. Houk, R. S. Anal. Chem. 1986, 58, 97A.
3. Gray, A. L. Spectrochim. Acta, Part B 1985, 40, 1525.
4. Date, A. R.; Gray, A. L. Application of Inductively Coupled Plasma Mass Spectrometry; Blackie and Sons Ltd.: London, 1988.
5. Whitten, W. B.; Koutny, L. B.; Nolan, T. G.; Ramsey, J. M. Anal. Chem. 1987, 59, 2203.
6. Houk, R. S.; Lim, H. B. Anal. Chem. 1986, 58, 3244.
7. Beijerinck, H. C. W.; Van Gerwen, R. S. F.; Kerstel, E. R. T.; Martens, J. F. M.; Van Vliembergen, E. J. W.; Smits, M. R. Th.; Kaashach, G. H. Chem. Phys. 1985, 96, 153.
8. Campargue, R. J. Phys. Chem. 1984, 88, 4466.
9. Douglas, D. J.; French, J. B. J. Anal. At. Spectrom. 1988, 3, in press.
10. Scott, R. H.; Fassel, V. A.; Kniseley, R. N.; Nixon, D. E. Anal. Chem. 1974, 46, 75.
11. Koirtyohann, S. R.; Jones, J. S.; Yates, D. A. Anal. Chem. 1980, 52, 1965.
12. Kawaguchi, H.; Ito, T.; Mizuike, A. Spectrochim. Acta, Part B 1981, 36B, 615.
13. Hasegawa, T.; Haraguchi, H. In Inductively Coupled Plasmas in Analytycal Atomic Spectrometry; Montaser, A.; Golightly, D. W. Ed.; VCH: New York, 1987; Chapter 8.

14. Schram, D. C.; Raaymakers, I. J. M. M.; Schenkelaars, H. J. W.; Boumans, P. W. J. M. Spectrochim. Acta, Part B 1983, 38B, 1545.

15. Walker, Z.; Blades, M. W. Spectrochim. Acta, Part B 1986, 41B, 761.

16. Rank, D. H.; Skarinko, F.; Eastman, D. P.; Saksena, G. D.; McCubbin, T. K., Jr.; Wiggins, T. A., J. Opt. Soc. Am. 1960, 50, 1045.

17. Palmer, B. A.; Hof, D. Chemical and Laser Sciences Division, Los Alamos National Laboratory, Los Alamos, NM 87545, private communication, 1988.

18. Kielkopf, J. F. J. Opt. Soc. Am. 1973, 63, 987.

19. Alder, J. F.; Bombelka, R. M.; Kirkbright, G. F. Spectrochim. Acta, Part B 1980, 35B, 163.

20. Human, H. G. C.; Scott, R. H. Spectrochim. Acta, Part B 1976, 31B, 459.

21. Salomon, S. G.; Holcombe, J. A. Anal. Chem. 1978, 50, 1714.

22. Carney, K. P.; Goldberg, J. M. Anal. Chem. 1986, 58, 3108.

23. Kuhn, H. G. Atomic Spectra, 2nd edition; Academic: New York, 1969; p. 347.

24. Raeymakkers, B.; Broekart, J. A. C.; Lewis, F. Spectrochim. Acta, Part B 1988, 43, 941.

25. Boumans, P. W. J. M.; Vrakking, J. J. A. M. Spectrochim. Acta, Part B 1986, 41B, 1235.

26. Faires, L. M.; Palmer, B. A.; Engleman, B., Jr.; and Niemczyk, T. M. Spectrochim. Acta, Part B 1984, 39B, 819.

27. Fraser, R. B.; Robben, F.; Talbot, L. Phys. Fluids 1971, 14, 2317.

28. Meggers, W. F.; Corliss, C. H.; Scribner, B. F. Table of Spectral Line Intensities; Part I - arranged by Elements; NBS Monograph 145; U. S. Department of Commerce: Washington, DC, 1975

SECTION III. LANGMUIR PROBE MEASUREMENTS OF POTENTIAL INSIDE A SUPERSONIC JET EXTRACTED FROM AN INDUCTIVELY COUPLED PLASMA

INTRODUCTION

ICP-MS has proven to be a valuable technique for elemental and isotopic analysis (1,2). The extraction process is crucial to ICP-MS. Fundamental characterization of conditions in the gas extracted from the ICP and study of processes occurring during extraction could provide basic information to improve the fundamental understanding and analytical performance of ICP-MS. The potential in the ICP and the interaction of the ICP with the sampling orifice is important because the strength of any discharge between the two influences the mass spectra, the orifice lifetime, and the ion kinetic energies. A floating Langmuir probe can be inserted into the plasma to estimate the plasma potential (3-5). Langmuir probes should also be valuable for characterizing the supersonic jet inside the first stage of the vacuum chamber (6-8). These measurements should actually be easier in the jet than in the plasma because a) the probe does not get as hot in the jet, b) the sampling orifice shields RF interference from the probe and measuring circuit, and c) cooling or recombination of electrons as they approach the probe are often less significant in low-pressure plasmas (9-11).

Probe measurements also provide information that complements that obtained from measurements of ion kinetic energies, which influence the transmission and focal properties of the ion lens used to conduct ions from the skimmer to the mass analyzer (4,12-15). In particular, the dependence of ion energy on ion mass has been attributed to the juxtaposition of two effects. Entrainment of ions in the argon flowing

through the orifice results in their acceleration to the speed of argon in the free jet. If all species move at the same velocity, the kinetic energy is proportional to mass. A plot of ion kinetic energy as a function of mass should yield a straight line that passes through the origin. However, such a line generally intersects the vertical axis at a potential value of a few eV. This offset potential could be caused by penetration of the potential from the plasma through the orifice into the jet. A positive potential therein would repel positive ions and displace the ion kinetic energies to more positive values than would be predicted from aerodynamic effects of the expansion alone (13).

The present work reports the results of floating Langmuir probe measurements inside the supersonic jet. The relation of these measurements to ICP-MS is described.

EXPERIMENTAL

ICP and sampling chamber

The ICP used in this study has been described (15). The generator frequency was 27 MHz, the plasma was operated horizontally, and the load coil was grounded and shielded as shown in Figure 1. A continuous flow ultrasonic nebulizer was used, and the resulting aerosol was desolvated before it was introduced into the ICP (16,17). This nebulizer was visually estimated to produce aerosol at an efficiency of ~5%, i.e., two to five times the efficiency of a typical pneumatic nebulizer. Standard operating conditions are listed in Table 1 of Reference (15).

The sampling chamber (Figure 1) resembled that used previously for optical studies of the plasma extracted from the ICP (7,8). The chamber was machined from a copper cube. Viewing windows, a side port leading to a rotary mechanical pump (pumping speed 10 L s^{-1}), and an end port with a centered electrical feedthrough for the probe were provided. The pressure in the chamber was 2 torr during sampling of the ICP.

The sampler was a nickel disk with a circular orifice (0.73 mm diam.) drilled into its center. The sampler was screwed to a water-cooled copper flange that was mounted on the sampling chamber. A flat sampler was used (rather than the conventional cone typical in ICP-MS) so that the jet and probe could be viewed optically. As shown in Figure 1, the sampler was grounded. Note that no skimmer was present.

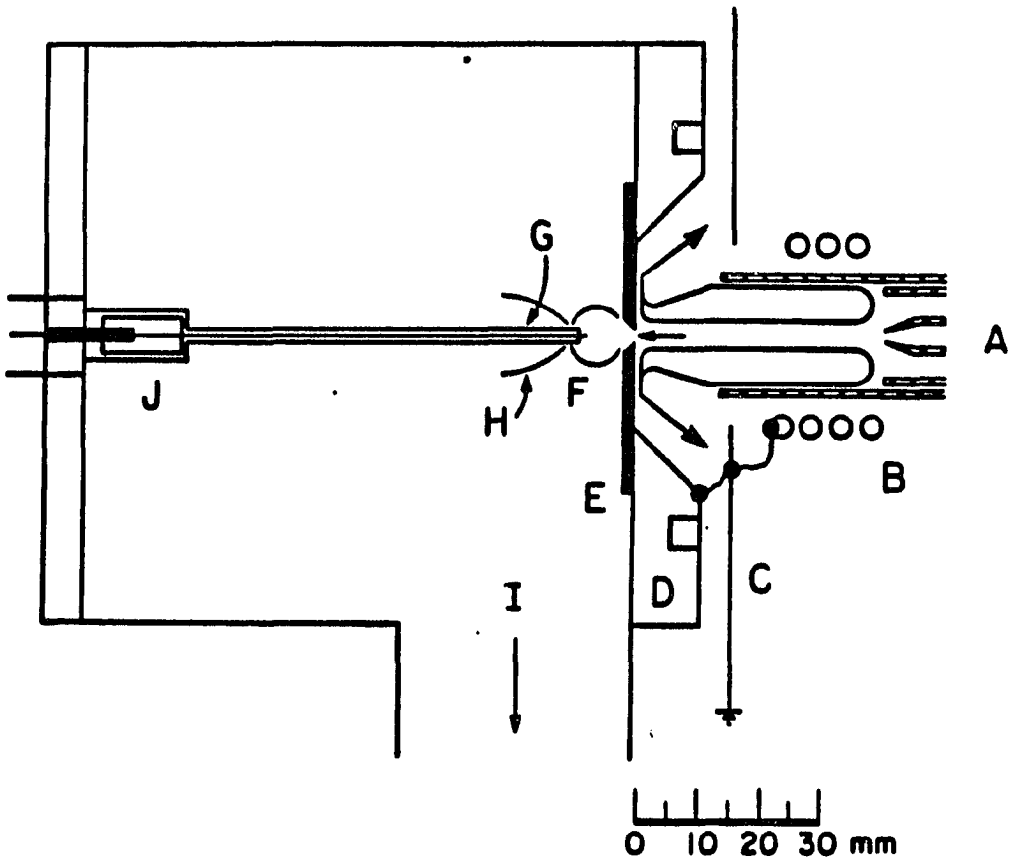

Figure 1. Experimental apparatus. A: ICP and torch, B: load coil, C: copper shielding box, D: water-cooled copper flange, E: nickel sampler with circular orifice in center, F: supersonic jet, G: Langmuir probe in alumina sleeve, H: shock wave generated by probe, I: line to rotary vacuum pump, J: stand-off and electrical feedthrough

Langmuir probe

The supersonic jet and probe are shown in Figure 1. The probe was a solid tungsten rod with a diameter of 0.7 mm. A hollow alumina sleeve covered most of the probe so that only a 1.1 mm long section of the probe tip was exposed. The probe tip was stationary and was positioned on center inside the Mach disk of the supersonic jet 8 mm from the sampling orifice, i.e., at roughly the same distance from the sampler as a skimmer would be for an ICP-MS experiment. It was not necessary to swing the probe to prevent it from melting, as was done in previous experiments in the ICP (4,5). The alumina sleeve did get very hot (i.e., it glowed orange-red) because it was exposed to the shock wave where collisions reheated the extracted gas to ~2200 K (6,8). The probe tip also got hot by conduction from the sleeve. The probe gradually became pitted and its edges became rounded after exposure for ~30 hours, after which time a fresh probe was used. The probe was held on center and was connected to the feedthrough by a brass stand-off that was sheathed with a Macor sleeve.

The probe output was connected via a coaxial cable (~1.5 m long) to an X-Y recorder (Model 2000, Houston Instruments, input impedance 1 MΩ) and digital voltmeter (Model 177, Keithley Instruments, input impedance 10 MΩ). The signal at both recorder and voltmeter was zero and the noise was negligible if a) the plasma was on but the cable was disconnected from the probe, or b) the torch was placed near the sampler (as shown in Figure 1) with power to the load coil but no plasma present (i.e., the Tesla coil was not used to start the plasma). The lack of signal in these two experiments indicated that the voltages observed

subsequently with the plasma present were not simply due to RF interference. At the beginning of a day's experiments, when the plasma was first positioned close to the sampler, a brief "warm-up" period of 1-2 min was necessary for the probe voltage to stabilize.

Optical and MS instrumentation and solutions

Optical emission from the Mach disk region (with the probe present) was observed in one experiment described below. The monochromator (focal length 0.5 m) and detector for this study have been described (7). A fiber optic cable (~2 m long) with imaging optics was used to conduct light from the Mach disk to the monochromator.

The results of one experiment using this same plasma with an ICP-MS device are also reported. The instrument and the method for measuring ion kinetic energies have been described (15).

Unless otherwise stated, deionized distilled water was nebulized for the experiments described below. Matrix solutions were prepared by diluting stock solutions of $LiNO_3$, $NaNO_3$, KNO_3, RbCl, and $CsNO_3$ with 1% HNO_3 in deionized distilled water.

RESULTS AND DISCUSSION

Effect of sampling position

The plasma was ignited while it was separated from the sampler, as is customary in our laboratory. The plasma was then translated axially toward the sampler. This positioning process was generally done as quickly as possible to minimize exposure of the sampler to arcing. For illustrative purposes, Figure 2 shows the variation in probe signal with sampling position as the plasma was translated gradually in 10 mm increments toward the sampler. The plasma was kept centered on the sampler at each position. The potential in the jet (hereafter simply called the potential) increases as the plasma moves closer to the sampler. A secondary discharge between the plasma and sampling orifice can be both seen and heard at these positions. The potential is of positive polarity and can get very high indeed, up to ~+160 V at an axial position of 32 mm. The high, noisy potential at these positions is one reason why it is difficult to do ICP-MS under conditions that yield a strong secondary discharge. The shock waves are visibly erratic and pulsing at these sampling positions.

If the plasma is moved closer to the sampler by another 10 mm, the potential drops precipitously to 10 V or less. This range of sampling positions (12-22 mm from the load coil) corresponds roughly to that found useful for ICP-MS with this particular plasma (15). The secondary discharge is neither visible nor audible, and the visible emission from the shock waves is much steadier at these closer sampling positions.

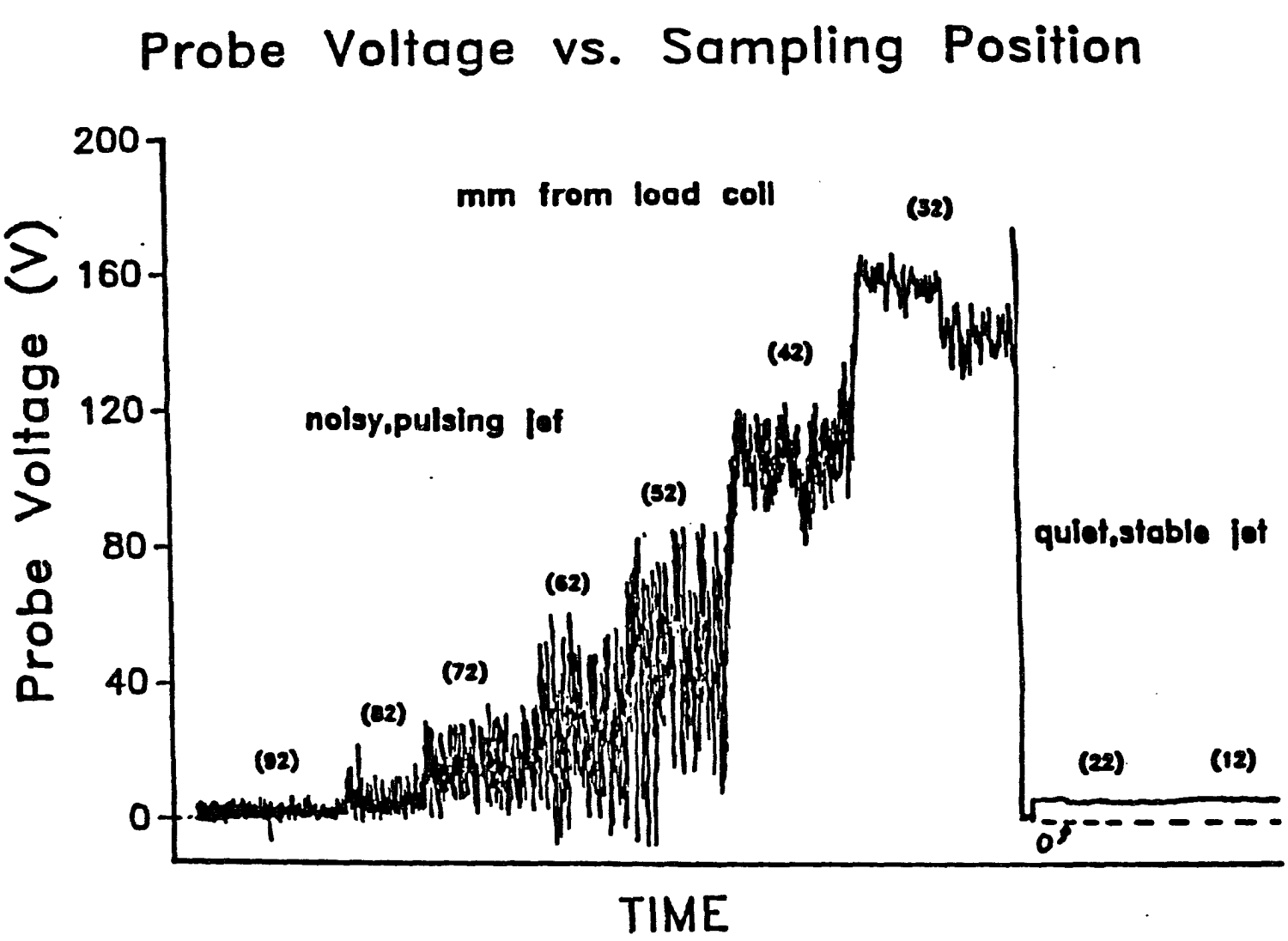

Figure 2. Probe voltage as plasma is translated closer to sampler. Sampling positions are indicated in parentheses in mm from downstream turn of load coil

Presumably, when the plasma is too far from the sampler, the interaction between the plasma and the sampler is unstable. Perhaps air entrainment cools the plasma and causes formation of cool boundary layers at the sampler that prevent the plasma from "shorting" properly through a space-charge sheath to the grounded sampling orifice.

To further contrast the behavior of the sampling system under a strong discharge to that with a weak discharge, spectral scans across a strong ion line emitted from the Mach disk were performed. The results are shown in Figure 3. The upper trace shows that a weak discharge yielded a significant Sr II line, as usually seen from inside the sampling chamber in optical studies (7,8). In contrast, the lower trace in Figure 3 indicates that axial positions corresponding to a strong discharge and high potential yielded much less emission from the same Sr II line. The lack of Sr II emission when the discharge was strong agrees with the general observation, made here and elsewhere, that it is more difficult to detect analyte ions in ICP-MS when the discharge is intense. In contrast, a strong discharge actually intensifies ion line emission from the gas in the plasma outside the orifice (18). The reasons for the apparent lack of excited Sr ions in the Mach disk when the discharge is strong may also include a) the low density of Sr^+ in the ICP at a position 42 mm from the coil, and b) the low temperature of both the ICP and the Mach disk at this sampling position.

In any Langmuir probe experiment, it is advisable to evaluate whether the probe perturbs the plasma being studied. Insertion of the probe into the jet did not cause formation of a visible shock wave around the probe tip (Figure 1) or any other visible disruption of the

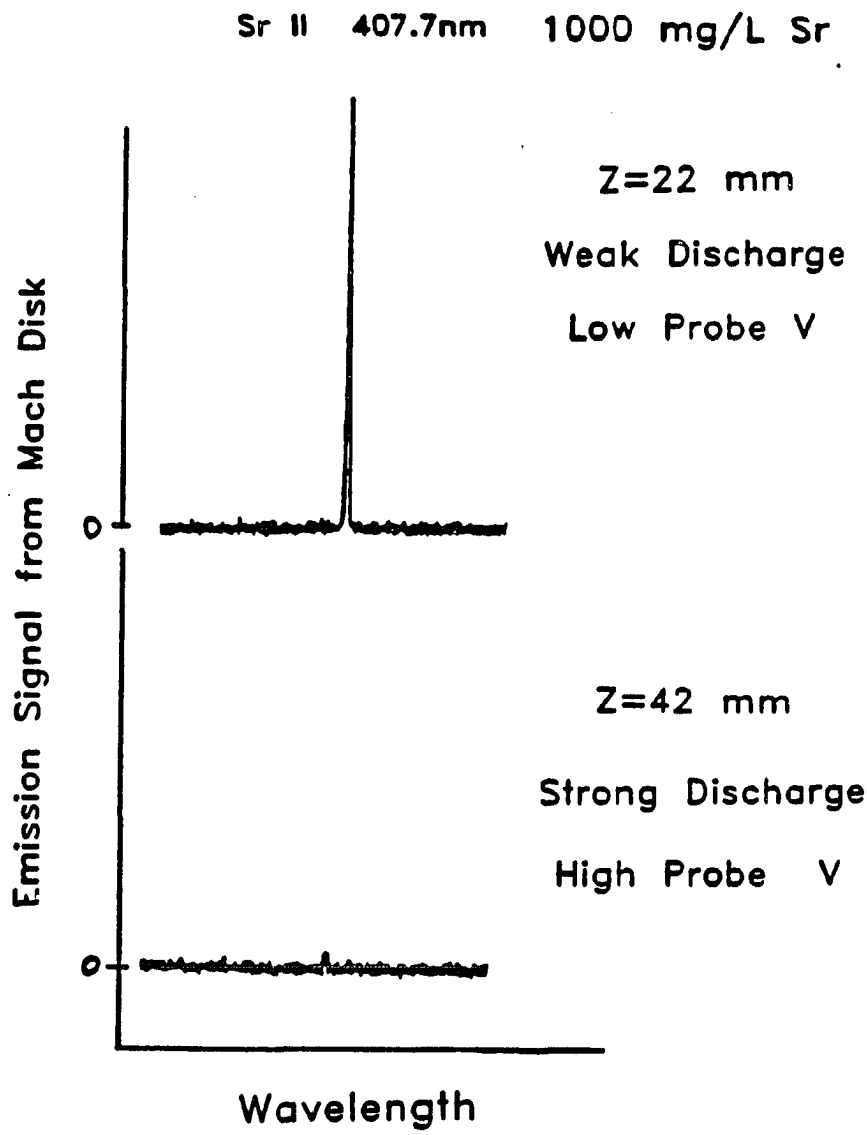

Figure 3. Emission spectra of Sr II 407.7 mm from Mach disk region of extracted plasma. Top: sampling position = 22 mm; bottom: sampling position = 42 mm. Both plots are on same scale. Strontium concentration was 1000 ppm

supersonic jet. At a sampling position of 32 mm, where the discharge was strongest and the potential was highest, the current drawn by the probe and recorder was approximately 160 V/10^6 Ω ~ 0.16 mA. The total current flow through the orifice was estimated to be roughly 500 mA based on the gas flow rate through the orifice (~10^{21} atoms s^{-1}) (6,19), the total atom density in the ICP (~10^{18} atoms cm^{-3}), and the total ion and electron density in the ICP (~10^{15} ions cm^{-3} or electrons cm^{-3}). This estimate of total current through the orifice is much greater than even the maximum value of probe current. Thus, the probe did not perturb the jet by draining too many charge carriers from it.

Effect of plasma operating parameters

All subsequent experiments were done at a sampling position of 22 mm from the load coil (as depicted in Figure 1) so that the discharge was not severe and the potential not too high. First, the forward power to the load coil was varied at constant aerosol gas flow rate (Figure 4). The amplitude and the noise of the potential shown in this figure are typical. Potential increased as power decreased. A similar trend was seen as power was varied at other aerosol gas flow rates at sampling positions where the discharge was not severe.

Next, aerosol gas flow rate was varied at constant power. Typical results are shown in Table 1. In general, the potential increased as aerosol gas flow rate increased. The observed trends in potential with aerosol gas flow rate and power followed those seen in measurements of potential in the plasma and ion kinetic energy with this type of load coil on various ICP-MS instruments for which the load coil geometry is

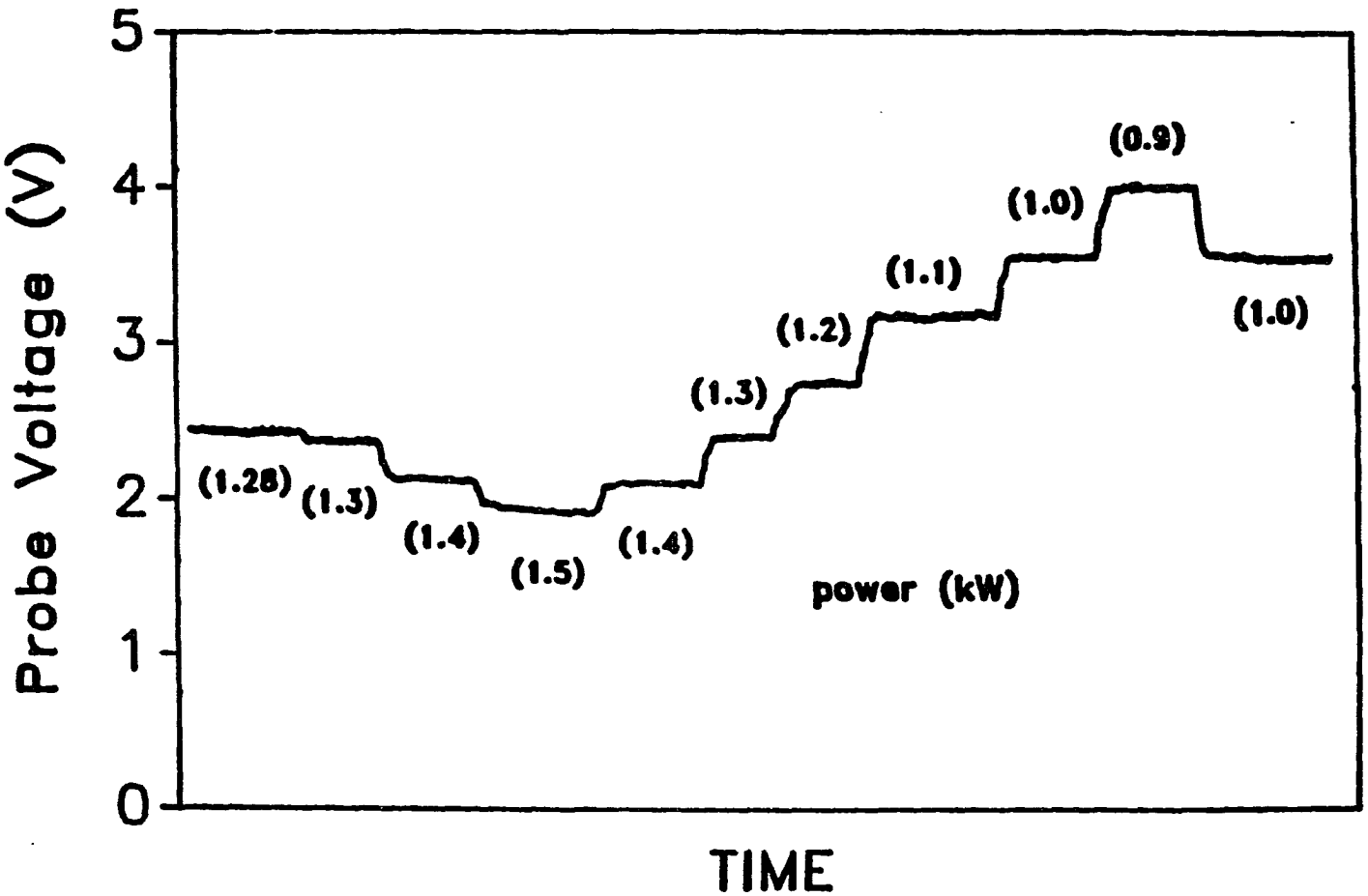

Figure 4. Probe voltage at various forward powers, indicated in parentheses in kW. Aerosol gas flow rate = 0.6 L min^{-1}

Table 1. Probe potential at various aerosol gas flow rates

Aerosol gas flow rate (L min^{-1})	Probe potential (V) at indicated forward power	
	1.1 kW	1.35 kW
0.35	2.88 ±0.02[a]	2.16 ±0.02
0.40	--	2.21
0.50	3.10	2.33
0.60	--	2.55 ±0.03
0.65	3.33 ±0.03	--
0.70	--	2.63
0.76	3.58	2.93 ±0.05
0.90	3.83 ±0.04	--

[a]Uncertainties indicate peak-to-peak noise on measured potentials.

such that a weak secondary discharge is thought to persist (4,12,14,15,19).

Comparison of jet potential with ion kinetic energies

It is also interesting to compare the trend of jet potential with aerosol gas flow rate (Table 1) to the trends seen when ion kinetic energy was measured (by ICP-MS) as a function of mass at various aerosol gas flow rates. The ion kinetic energy results are shown in Figure 5. For low aerosol gas flow rates (below 1.03 L min^{-1}), the ion energy increases with on mass. The reproducibility of each of these measured energies is typically $\pm$0.2 V (15). The shapes of these curves are much like those reported by Fulford and Douglas. In particular, kinetic energies for ions in the middle of the mass range, such as In^+, tend to be a little below a line connecting the energies of the lightest and heaviest ions (13). In the present work, as aerosol gas flow rate increases, the intercepts of these curves with the vertical axis also increase. This trend would be expected a) if these non-zero intercepts were caused by the presence of a positive potential in the jet that accelerates ions to higher energies than they would get just from the expansion alone (13), and b) if the magnitude of the potential increased with aerosol gas flow rate.

The intercept for the lowest curve in Figure 5 (aerosol gas flow rate = 0.73 L min^{-1}) is approximately 5.5 V. These ion energies are the "maximum" values or "cut-off" values measured from the foot of a plot of ion signal versus retarding potential (12,15); this is the customary method of determining ion energy in our laboratory. These values thus

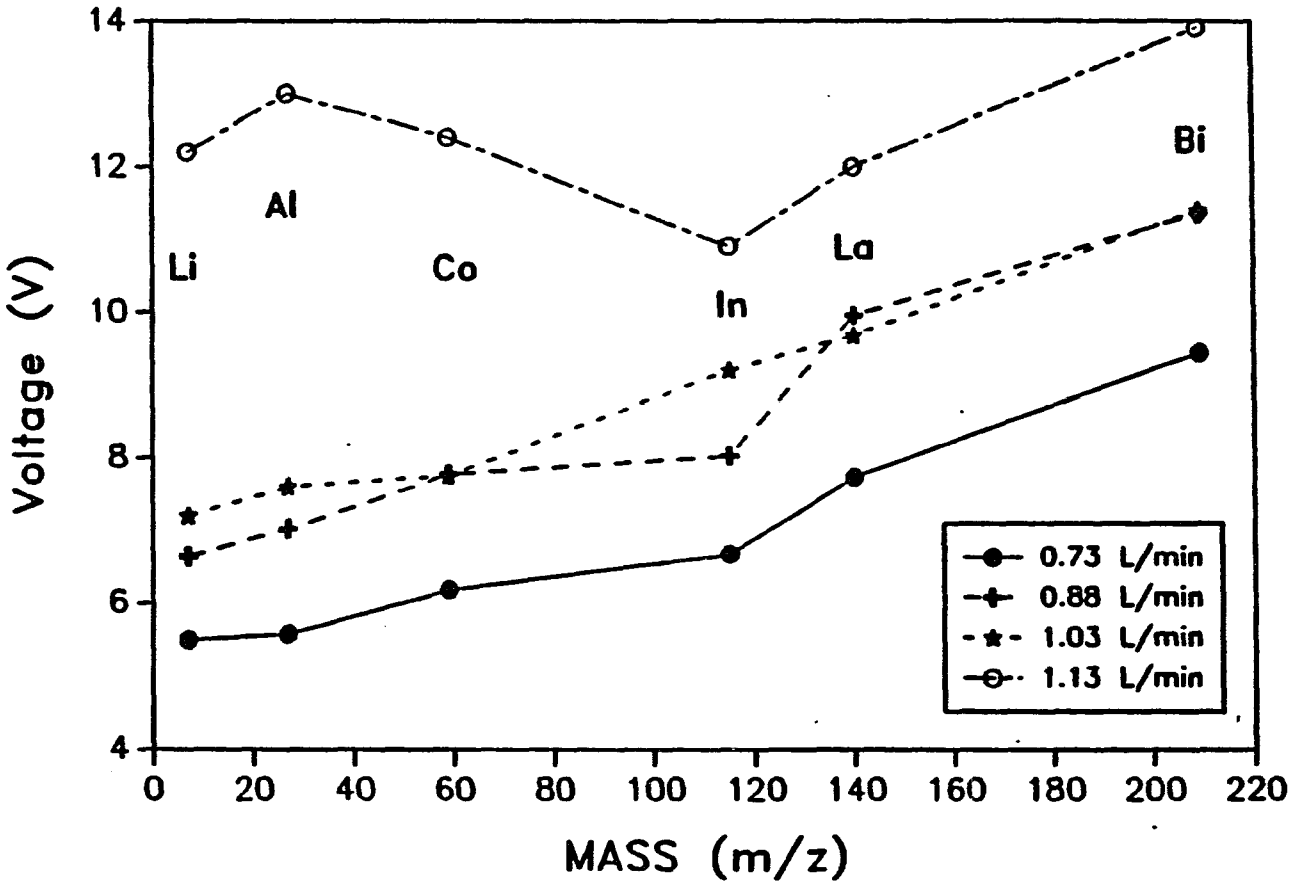

Figure 5. Maximum or "cut-off" ion energy for a range of elements. Power = 1.45 kW. Aerosol gas flow rates are shown in legend

represent the mean energy plus half of the spread or distribution of energies, which is generally several eV. The mean or most probable energies would be roughly half of the values shown in Figure 5. Thus, a plot of mean or most probable energies as a function of mass would intercept the axis at roughly 5.5/2 = 2.7 V, i.e., about half the intercept shown for the maximum values in Figure 5. This value is close to the corresponding jet potential of 2.8 eV measured with the Langmuir probe for similar power and aerosol gas flow rate. Thus, both the sign and the magnitude of the potential measured in this experiment are in reasonable agreement with the intercept potential determined from ion energy measurements. The intercept values of ion energies cannot be compared with measured potentials in the jet much more closely than this for various reasons. The samplers used in the two experiments differed in geometry (i.e., a flat plate versus a cone) and in orifice diameter (0.73 versus 0.94 mm), and ion energy measurements in ICP-MS are only approximate anyway because the use of ion lenses can influence the measured ion energy distribution.

The upper curve in Figure 5 shows ion energy results for a relatively high value of aerosol gas flow rate, which causes a high plasma potential. The ion energies are higher for all the elements than was the case at lower aerosol gas flow rate. The smooth dependence of ion energy with mass is no longer apparent relative to the point-to-point variability in the data.

The observations described in this section are consistent with the potential measured in the jet being caused mainly by a weak residual potential in the plasma. Some of this potential is coupled into the jet

by the charge carriers flowing through the orifice. The plasma potential and the jet potential increase as aerosol gas flow rate increases and as power decreases. The uncertainty values shown in Table 1 and the potential plots in Figure 4 indicate that, for conditions corresponding to a weak discharge, changing a plasma parameter that caused the potential to increase generally also induced an increase in the noise on the potential. This increase in noise with magnitude of the jet potential was seen throughout the present work. If the potential does influence the ion kinetic energy, the transmission characteristics of the ion optics and thus the intensity of the ion beam would also become less stable as the fluctuations in potential increase. This increase in noise in the potential in the jet could represent another limitation to using too strong a residual discharge in ICP-MS, in addition to excessive doubly charged ions and metal ions from erosion of the sampling orifice, high ion energies, etc.

Effect of matrix elements

The effects of high concentrations of matrix elements on potential were also studied. The alkali metals were chosen as matrix elements because they all should be ionized almost completely in the ICP (20). Figure 6 shows the general behavior observed and also illustrates how the experiments were performed. First, the potential was monitored for a blank solution (left part of curves). Then, the solution was changed to one containing the matrix element; the central sections of the curves show the jet potential with matrix element present. Finally, the matrix solution was replaced by the blank (right sections of curves). At

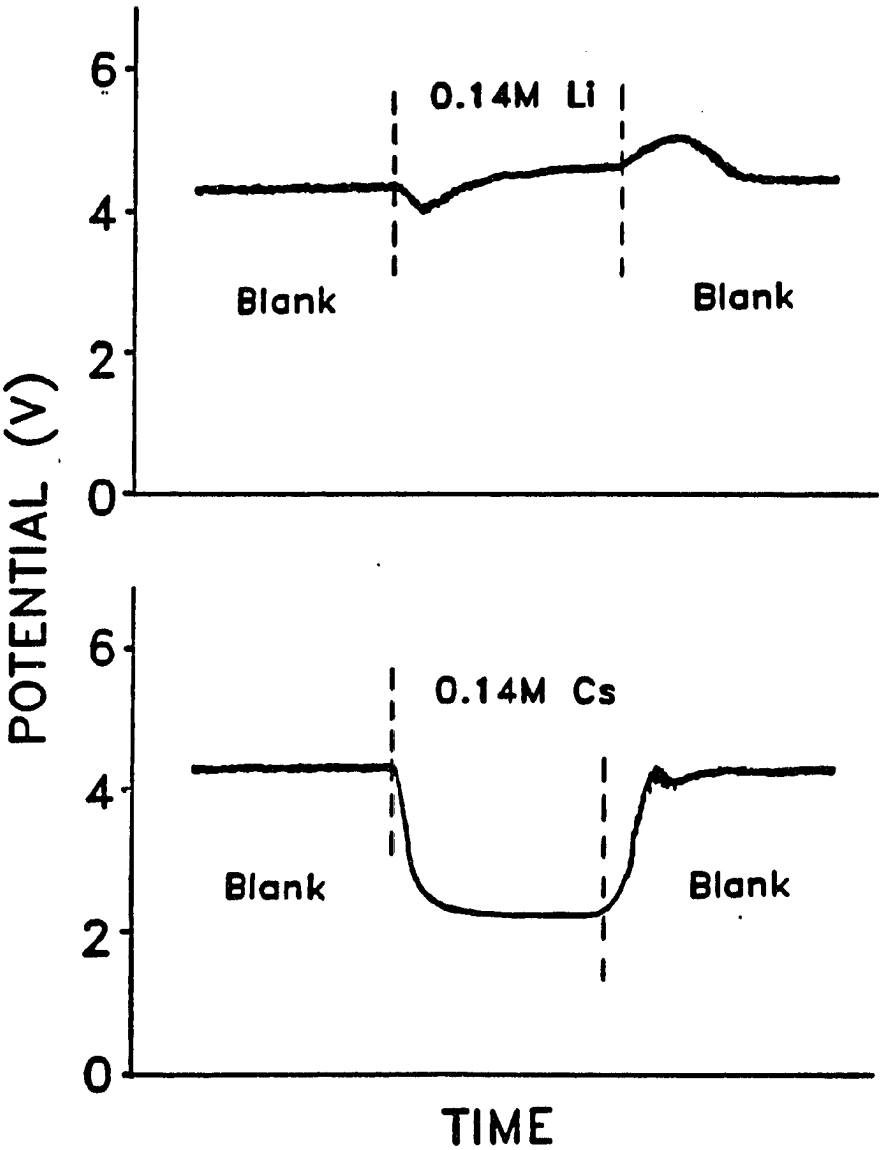

Figure 6. Matrix effects induced on probe potential by Li (top) and Cs (bottom), each at 0.14 M. Dotted lines indicate times when solution was changed

times, a "hump" in the potential was observed after each change of solutions, as indicated in Figure 6. These "humps" were more pronounced and more persistent when the change in potential with matrix present was greatest. Eventually, steady signals were observed, and these represent the potential values reported below. After the blank solution was re-introduced, the potential generally recovered to within $\pm$0.2 V of its original value. Thus, introduction of the matrix element did not permanently change the apparatus, i.e., the sampling orifice did not plug and the probe did not become coated with matrix salt. This observation agreed with the findings of Douglas and Kerr that alkali metals did not plug the orifice severely at concentrations of 0.1% or so (21).

A more comprehensive summary of the influence of matrix elements on the jet potential is shown in Figure 7. A histogram format is used. The various matrix solutions are at equimolar concentrations. As above, the blank was nebulized first (first open rectangle), then the indicated matrix element (checkered rectangle).

Inspection of Figure 7 indicates the following trends. Lithium and sodium induced small changes in potential that were in either a positive or negative direction. Potassium always caused a substantial decrease in potential. The heavier matrix elements (Rb and Cs) induced a greater decrease in potential than did K. The extent of the matrix effect was greatest at low power and high aerosol gas flow rate, which represented the type of conditions where matrix effects in ICP-MS often tend to be greatest as well (22,23). This dependence of matrix effect on plasma parameters is illustrated in more detail for a Cs matrix in Figure 8.

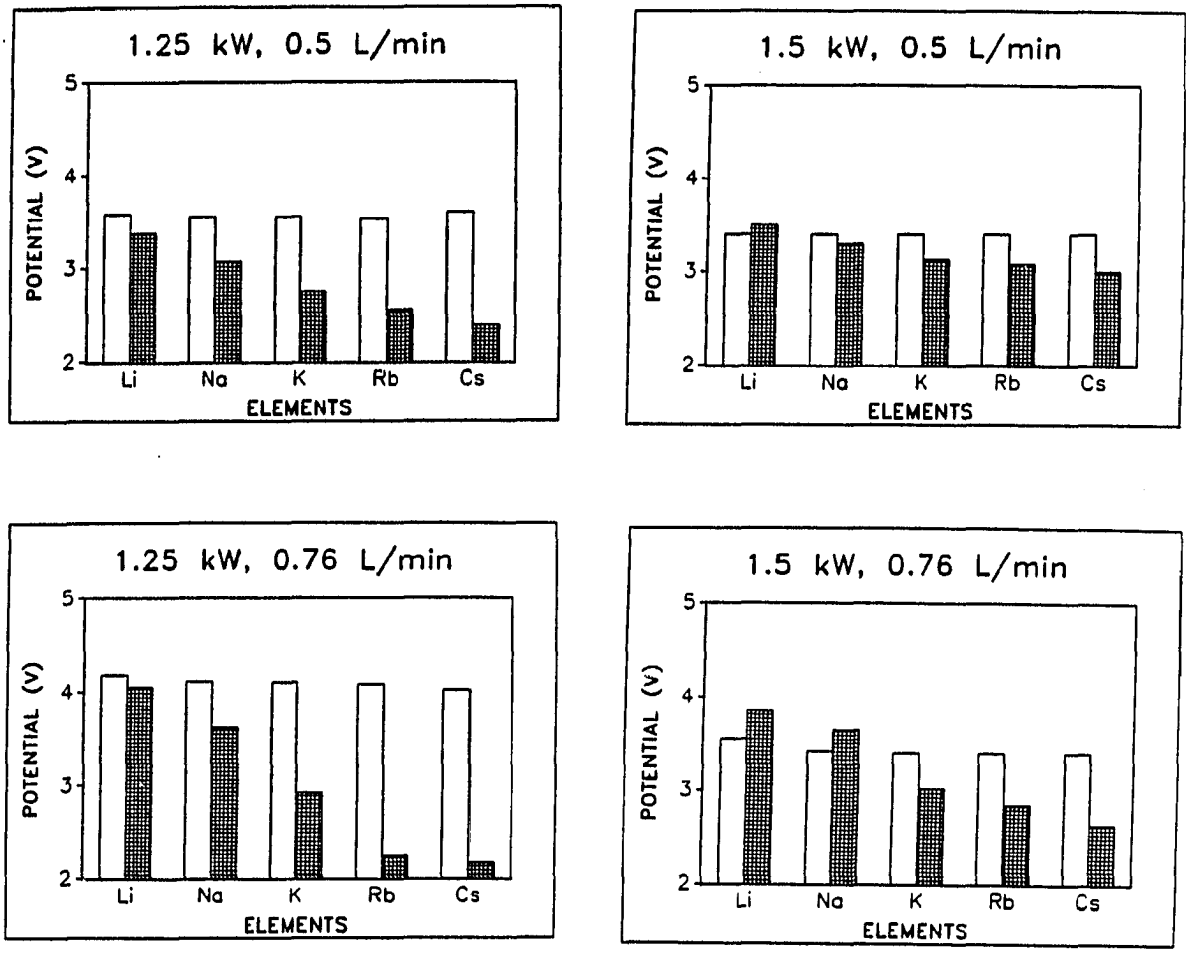

Figure 7. Histograms showing effect of various matrix elements (each at 0.14 M) on probe potential. Open rectangles represent the potential from the blank solution, checkered rectangles indicate the potential from each matrix element

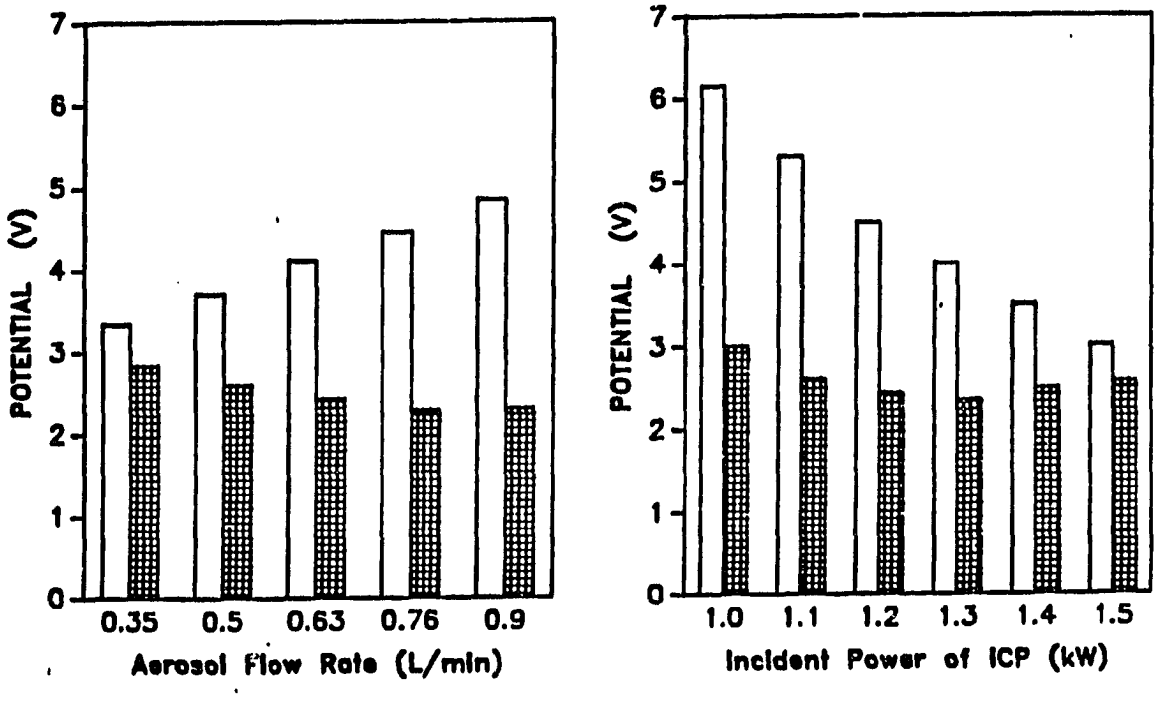

Figure 8. Effect of Cs (0.14 M) on probe potential at various values of power and aerosol gas flow rate. Open rectangles: potential from blank; checkered rectangles: potential from matrix solution. Left frame: power = 1.25 kW. Right frame: aerosol gas flow rate = 0.76 L min^{-1}

Note that lower power and higher aerosol gas flow yielded a higher potential from the blank solution and a more extensive drop in potential when Cs was added.

In the previous experiments concerning matrix effects, each matrix solution was 0.14 M. This molar concentration was chosen because it corresponded to 1000 mg L^{-1} Li. The concentration of matrix element was also varied for Li and Cs; representative results are shown in Figure 9. Lithium at any concentration between 200 to 1000 mg L^{-1} induced a small positive change in potential relative to the potential observed from the blank solution. The potential decreased when Cs was added, and the magnitude of the potential drop increased as the concentration of Cs increased. In Figure 9, the blank potential in the top frame was ~4.3 V; in the bottom frame, it was somewhat lower (~3.8 V). The effect of Li on potential was slightly positive in Figure 9 and slightly negative in the comparable experiment in the bottom left frame of Figure 7. These small differences simply reflect the fact that the various experiments were performed on different days. The plasma conditions were not exactly reproducible and the probe and sampler aged from day-to-day.

It is possible that the changes in potential observed for the different matrices are indeed related to matrix effects in ICP-MS. However, it is also possible that these phenomena are largely an artifact of the probe measurement method. In particular, if the mass of the ions in the jet changes greatly when a matrix is added, the mobilities of positive charge carriers in the jet changes. A floating

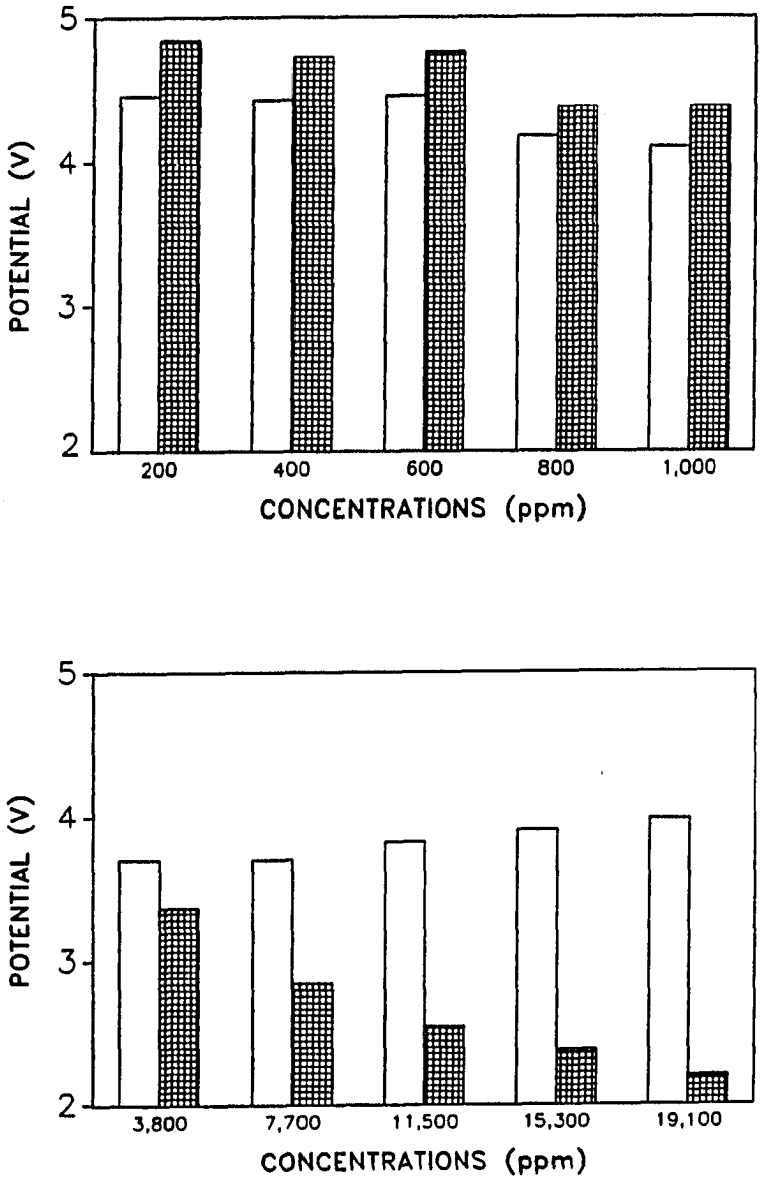

Figure 9. Matrix effects induced by Li (top) and Cs (bottom) at various concentrations. Power = 1.25 kW, aerosol gas flow rate = 0.76 L min^{-1}. Open rectangles: potential from blank; checkered rectangles: potential from matrix solution at indicated concentrations

Langmuir probe assumes a potential that is negative with respect to the surrounding plasma so that the electron current and ion current reaching the probe are equal. The magnitude of this floating potential does depend on ion mass (9). Suppose addition of a concentrated Cs solution causes heavy Cs ions to supplement or replace Ar^+, O^+, and other normal background ions in the jet near the probe. With Cs present, the potential then floats to a less positive (i.e., more negative) value that attracts the less mobile Cs^+ more strongly so that they can reach the probe at a rate that cancels the electron current. The apparent potential at the probe could depend on concentration and mass of matrix element just from this effect rather than from a real change in potential in the jet. The negative change in potential in the presence of heavy matrix elements disagrees with ion energy measurements reported with this same plasma, which showed no change in ion energy in the presence of 0.05 M Na and K and a 0.5 V increase when U was present (15). Fulford and Douglas also report little change in ion energy in the presence of a matrix for a system with little or no secondary discharge (13). Further measurements of matrix effects on ion energy and potential (in both the plasma and the jet) with matched conical samplers for both experiments are desirable to clarify this matter.

LITERATURE CITED

1. Houk, R. S.; Thompson, J. J. Mass. Spectrom. Rev. 1988, 7, 425.
2. Date, A. R.; Gray, A. L. Application of Inductively Coupled Plasma Mass Spectrometry; Blackie and Sons Ltd.: London, 1988.
3. Douglas, D. J.; French, J. B. Spectrochim. Acta, Part B 1986, 41B, 197.
4. Gray, A. L.; Houk, R. S.; Williams, J. G. J. Anal. At. Spectrom. 1987, 2, 13
5. Houk, R. S.; Schoer, J. K.; Crain, J. S. J. Anal. At. Spectrom. 1987, 2, 283.
6. Douglas, D. J.; French, J. B. J. Anal. At. Spectrom. 1988, 3, 743.
7. Houk, R. S.; Lim, H. B. Anal. Chem. 1986, 58, 3244.
8. Lim, H. B.; Houk, R. S.; Edelson, M. C.; Carney, K. P. J. Anal. At. Spectrom. in press (1989).
9. Clements, R. M.; Smy, P. R. Smy, J. Phys. D: Appl. Phys. 1974, 7, 551.
10. Smy, P. R. Adv. Phys. 1976, 5, 517.
11. Swift, J. D.; Schwar, M. J. R. Electrical Probes for Plasma Diagnostics; Iliffe Books: London, 1969.
12. Olivares, J. A.; Houk, R. S. Appl. Spectrosc. 1985, 39, 1070.
13. Fulford, J. E.; Douglas, D. J. Appl. Spectrosc. 1986, 40, 971.
14. Gray, A. L.; Williams, J. G. J. Anal. At. Spectrom. 1987, 2, 599.
15. Crain, J. S.; Houk, R. S.; Smith, F. G. Spectrochim. Acta, Part B 1988, 43B, 1355.

16. Olson, K. W.; Haas, W. J., Jr.; Fassel, V. A. Anal. Chem. 1977, 49, 632.

17. Bear, B. R.; Fassel, V. A. Spectrochim. Acta, Part B 1986, 41B, 1089.

18. Houk, R. S.; LaFreniere, B. R.; Lim, H. B.; Fassel, V. A. Fassel, Appl. Spectrosc. 1987, 41, 391.

19. Olivares, J. A.; Houk, R. S. Anal. Chem., 1985, 57, 2674.

20. Houk, R. S. Anal. Chem. 1986, 58, 97A.

21. Douglas, D. J.; Kerr, L. A. J. Anal. At. Spectrom. 1988, 3, 749.

22. Tan, S. H.; Horlick, G. J. Anal. At. Spectrom. 1987, 2, 745.

23. Thompson, J. J.; Houk, R. S. Appl. Spectrosc. 1987, 41, 801.

SECTION IV. LANGMUIR PROBE MEASUREMENT OF ELECTRON TEMPERATURE IN A SUPERSONIC JET EXTRACTED FROM AN INDUCTIVELY COUPLED PLASMA

INTRODUCTION

ICP-MS has become an important technique for elemental and isotopic analysis (1-3). The process of extracting ions from the plasma into the mass spectrometer is crucial in ICP-MS. Fundamental characterization of the extraction process could perhaps lead to improvements in the analytical capabilities of ICP-MS. Previous basic studies of the extraction process include characterization and/or elimination of the electrical discharge between the plasma and the sampler (4-6), optical measurements on the extracted gas (7-10), and studies of gas dynamics (11) and orifice plugging (12).

Langmuir probes are simple, versatile tools in plasma diagnostics. They have been shown to be useful for measuring T_e, n_e, and potentials in the plasma (4-6,13) and in the jet (14). The present work extends the Langmuir probe method to measurement of T_e, n_e, and V_f inside the supersonic jet. The effects of plasma parameters (e.g, power and aerosol gas flow rate), nebulized water and matrix elements, and the secondary discharge on these quantities are discussed.

EXPERIMENTAL

Apparatus

The extraction chamber and the probe have been described (14). Standard operating conditions are listed in Table 1 of reference (14). An ultrasonic nebulizer with aerosol desolvation was used to introduce sample (15,16). In cases where a "dry plasma" was desired, the nebulizer and spray chamber were bypassed, and the "aerosol" gas was added directly to the base of the torch to prevent loading the gas with water vapor. The forward power and aerosol gas flow rate were varied from 0.9 kW to 1.6 kW and 0.4 L min^{-1} to 0.9 L min^{-1}, respectively.

The sampling orifice (0.76 mm diam.) was located on center, 22 mm downstream from the load coil. The probe tip (1 mm long x 0.38 mm radius) was centered on the zone of silence of the supersonic jet 4 mm downstream from the sampling orifice. The grounded sampling orifice served as a reference electrode, as required for a single probe measurement. As in the previous work (14), the grounded sampling chamber shielded the probe from RF interference from the ICP. A special circuit (13) was not necessary to remove RF interference from the probe signal.

For the T_e measurement, the probe output was connected in series via a coaxial cable to a floating ammeter (John Fluke MFG Co., Inc., internal impedance 5 Ω) and a voltage supply (Lambda model LPD-424A-FM). A voltmeter (Soar ME-550, internal impedance 11 MΩ) was used to measure the applied potential relative to ground at the output positions of the voltage supply and the ammeter. The magnitude of the voltage

drop across the ammeter was only about 50 mV when the measured current was ~10 mA at an applied voltage of 6 V. Thus, the error in the estimated applied voltage due to the impedance of the ammeter was considered negligible.

The data collection device for the potential measurements with a floating probe was described in reference 14. Matrix solutions were prepared with 1% HNO_3 in deionized distilled distilled water.

Probe measurements in supersonic jet

The evaluation of various plasma properties using a Langmuir probe is described in numerous references (13,17-25). In general, probe measurements have been performed under two conditions: a tenuous plasma with a small probe, and a dense plasma with a large probe. The criteria for these conditions can be determined by the ratio of probe radius (r_p) to Debye length (λ_D). For example, $r_p/\lambda_D >> 1$ for a dense plasma and $r_p/\lambda_D < 1$ for a tenuous plasma. The transition between these two regimes applies if r_p/λ_D is in the range of ~1 to 200. Inside the supersonic jet, the Debye length was ~2 x 10^{-4} cm (11), assuming T_e = 10,000 K and n_e = 1 x 10^{13} cm^{-3}. The magnitude of r_p/λ_D was estimated to be about 190. Thus, the present experiment was approximately in the transition regime as described by Kirchoff et al. (19) and Fraser et al. (20), who considered the combined sheath and diffusion layer structures for a Langmuir probe in a supersonic jet plasma.

A detailed review of probe regimes by Smy is also useful for plasmas at moderate or high pressure (25). Smy defined three regimes of probe measurement in flowing plasmas: $R_e\alpha^2\chi^2 << 1$ for the diffusion-

convection regime, $R_e\alpha^2\chi^2 >> 1$ and $R_e\alpha^2 < 1$ for the sheath-convection regime, and $R_e\alpha^2 > 1$ for the E-field convection regime. The dimensionless quantities, R_e (electric Reynolds number), α and χ are defined in Table 1, reference (13). In the present work, $R_e\alpha^2\chi^2 \sim 0.6$ and $R_e\alpha^2 \sim 0.02$. Thus, Smy's criteria indicate that a Langmuir probe measurement inside a supersonic jet is in the transition between the diffusion-convection and sheath-convection regimes, in general agreement with the considerations discussed above based on references 19 and 20.

As electrons approach a Langmuir probe, collisions can render them vulnerable to cooling or recombination with ions. The resulting values for T_e and n_e would be artificially low if these processes were significant. Smy also describes criteria for evaluating the severity of these effects (25). Cooling of electrons at the probe is negligible if the ratio of the flow velocity (v_f) to r_p is larger than 10^4 sec^{-1}. Because the flow velocity in the supersonic jet is very fast ($\sim 2 \times 10^5$ cm sec^{-1}) (11), $v_f/r_p \sim 10^7$ sec^{-1}, and there should be no electron cooling at the probe. For ion-electron recombination to be negligible at the probe, the Damkohler (D) number should be less than R_e (25). In the present work, $D \sim 0.2$ and $R_e \sim 500$, and this criterion is satisfied easily. Therefore, it is considered that the measured T_e was not greatly affected by cooling and there was little ion-electron recombination in the single probe measurement. These estimates also agree with the experience of French in Langmuir probe measurements in supersonic jets (26).

Electron temperature measurements

Calculation of T_e from a plot of probe current (I) as a function of applied voltage (V) was described in ref. (17). The ion current (I_i) was measured at each value of V by extrapolating the saturation part of the characteristic curve, i.e., the part at low V at the far left of Figure 1. A data point was taken every ~0.3 V, so there are approximately 60 points for each characteristic curve shown here and below. The electron current (I_e) was related to T_e as follows:

$$I_e(V) = I(V) - I_i(V) \qquad (1)$$

$$\frac{d(\ln I_e)}{dV} = \frac{e}{kT_e} \qquad (2)$$

where e = electron charge and k = Boltzmann constant. A typical plot of ln I_e as a function of V is shown in Figure 2. Ideally, this plot should have been a straight line, but curvature was observed at high values of V. Similar curvature was seen when double Langmuir probes were used to measure T_e in the ICP and could have been due to a lack of a Maxwellian velocity distribution at a single value of T_e (13). The points at high V values were also suspect because the current did not saturate but continued to increase as V increased (Figure 1). For these reasons, only the 5 or 6 points at low V were used to calculate the T_e values reported below, as was done for T_e measurements in the ICP (13). For example, the slope of the dotted line in Figure 2 was determined and used with equation 2 to calculate T_e; the curvature of $\ln(I_e)$ at high V values was neglected.

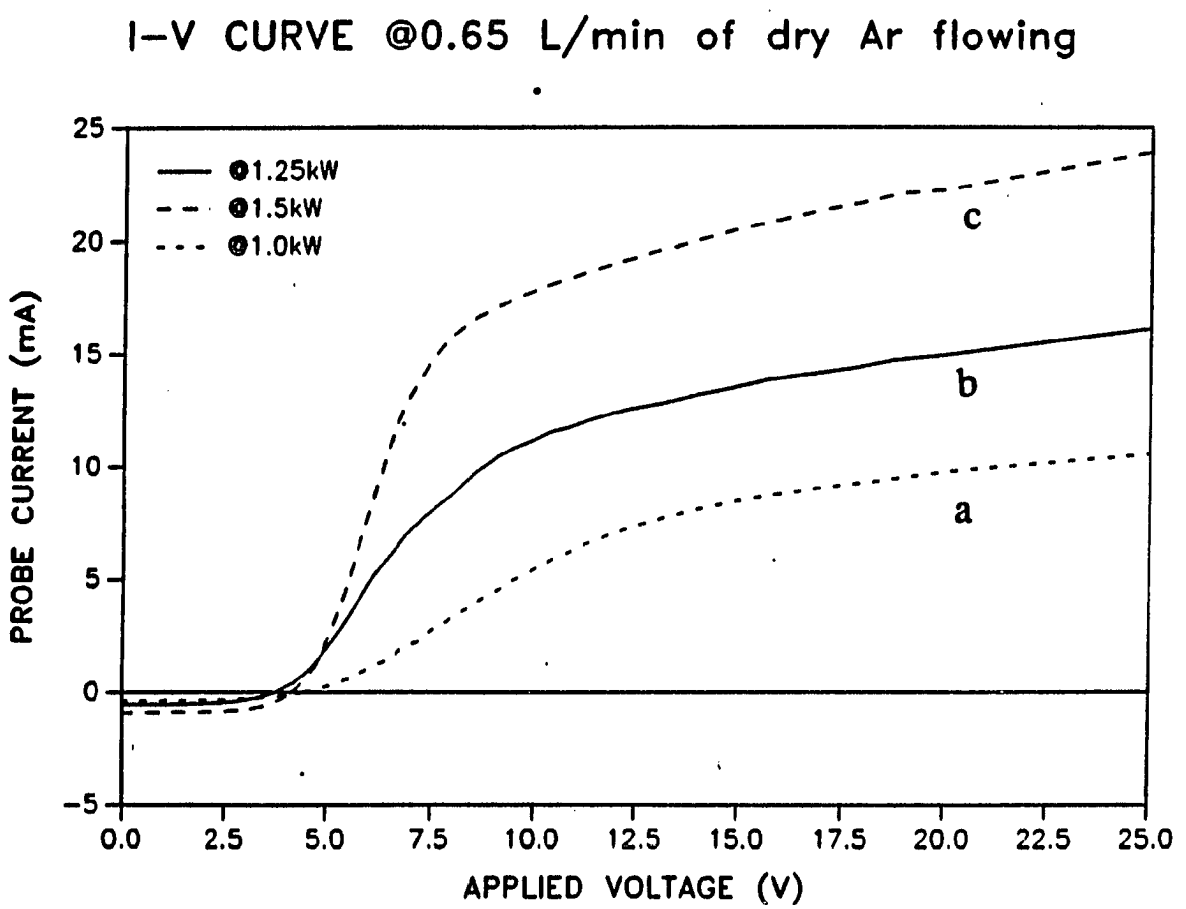

Figure 1. Single probe characteristic curves for dry plasma, "aerosol" gas flow rate = 0.65 L min^{-1} at various powers: a) 1.0 kW, b) 1.25 kW, c) 1.5 kW

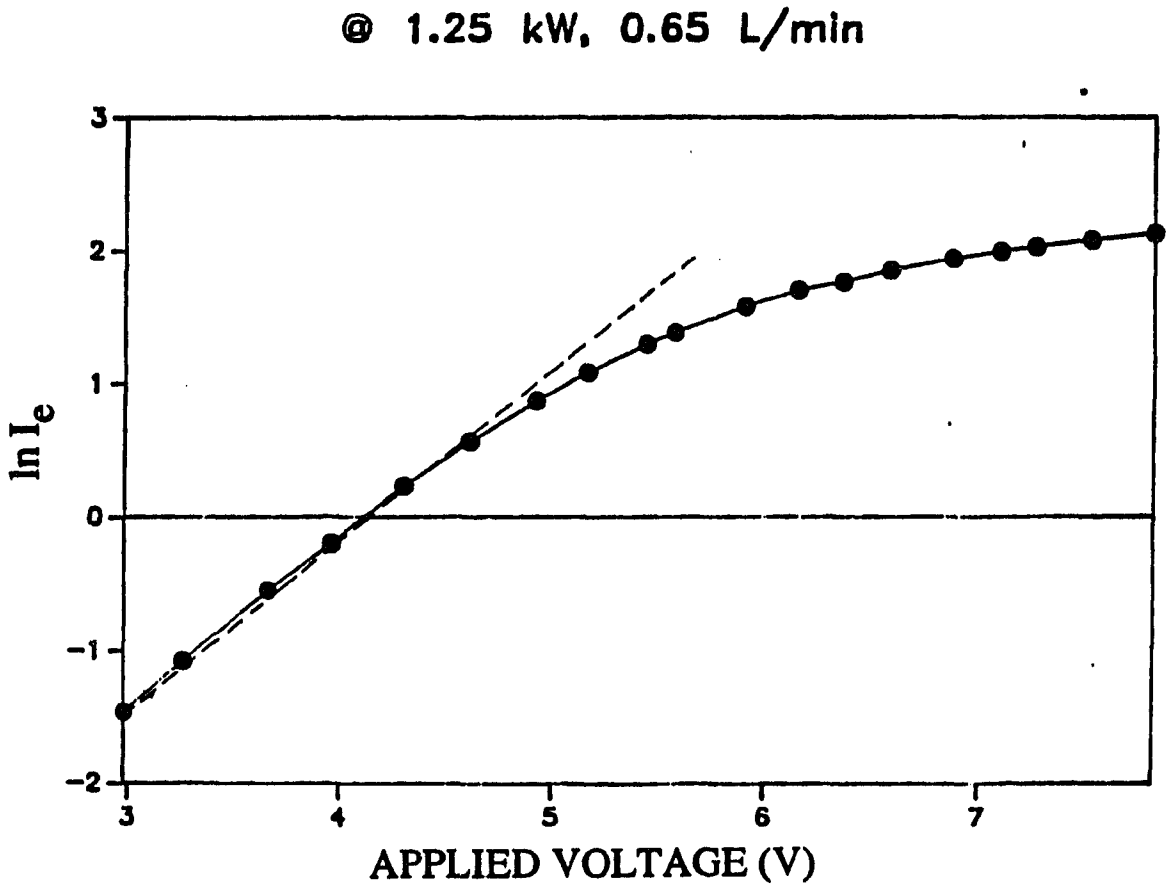

Figure 2. Typical plot used to determine T_e from probe characteristic curve. Conditions: dry plasma, power = 1.25 kW, "aerosol" gas flow rate = 0.65 L min^{-1}. The dotted line fit to only the points at low voltage was used

Electron density measurements

The equation given by Kirchoff et al. for a supersonic jet plasma in the transition regime was used here (19). First, T_e was calculated as described above. Next, the ion current I_i was measured at saturation, i.e., at V = 0 in Figure 1. These quantities were used to calculate n_e from the following equations:

$$I_i = I_s e n_e 2\pi r_p l (kT_e/2\pi m_i)^{1/2} \quad (3)$$

where I_s is the normalized ion-saturation current to a cylindrical probe, including an approximation to the collisionless ion-saturation calculations of Laframboise (27), l is the probe length, and m_i is the ion mass (g $atom^{-1}$). The magnitude of I_s, assuming T_e/T_i = ~10 and R_p/λ_d = ~100, is about 0.054. Therefore, the following simple equation is obtained for calculating n_e:

$$n_e(cm^{-3}) = 5.2 \times 10^{29} I_i (m_i/T_e)^{1/2} \quad (4)$$

The ion mass was assumed to equal 6.6×10^{-23} g (i.e., 40 g $mole^{-1}$, the atomic weight of Ar) except where noted below.

V_f measurements

The floating voltage was estimated to be the intercept of the probe characteristic curve, i.e., the voltage at which the current equalled zero in Figure 1. The earlier estimate that electron cooling and ion-electron recombination were negligible at the probe helped validate this assumption, because these effects can also cause errors in V_f measurements (24).

RESULTS AND DISCUSSION

Characteristic curves

The Langmuir probe method was evaluated first using a "dry" ICP without water vapor or water aerosol. Probe characteristic curves from the jet extracted from such a dry plasma are shown in Figure 1. These curves can be divided into three regions: a) the region of ion current saturation (V ~ 0 to 3 V) used mainly to calculate n_e, b) the electron retarding region (V ~ 3 to 10 V) used to calculate T_e, and c) the electron "saturation" region (V > 10 V). The lack of saturation of the electron current agreed with the observations of Smy for probe measurements in a regime between diffusion-convection and sheath-convection (25). This further validated the applicability of the transition regime model described by Talbot for the present work.

Electron temperature measurements with a dry plasma

Determined values of T_e are presented in Table 1. The overall magnitude of these T_e values (7400 K to 16000 K) was high enough to show that electron cooling at the probe was negligible, as described in experimental section. The magnitude of these T_e values also indicated that the electrons were not cooled greatly during the extraction process, as described by Douglas and French (11). In fact, at 1.0 kW, the measured T_es in the jet were 11000 K to 16000 K, rather higher than the range of 7000 K to 8500 K reported previously in the ICP itself at comparable power levels (13,28-32).

Table 1. Electron temperature measurements in the jet extracted from a dry plasma

"Aerosol" gas flow rate (L min^{-1})	T_e (K) in jet at indicated power 1.0 kW	1.25 kW	1.5 kW
0	11000[a]	8500	7400
0.45	13000	9200	8400
0.65	14000	12000	9400
0.90	16000	13000	10000

[a]Reproducibility typically ±100 K for duplicate measurements on different days.

Table 1 also shows that T_e in the jet decreased as power increased and as aerosol gas flow rate decreased. Measuring T_e in the plasma is difficult, hence this parameter has not been characterized extensively over a wide range of plasma operating conditions. However, T_e in the ICP would be expected to show precisely the opposite trends with power and aerosol gas flow rate as those indicated in Table 1 for T_e in the jet. The load coil geometry used with this plasma caused a mild secondary discharge between the plasma and the sampling orifice. This discharge has been shown to be most severe at low power and high aerosol gas flow rate (5,33,34). It is likely that the strength of the discharge affected the kinetic energies of electrons as they were extracted, hence the trends in T_e in the jet followed those expected for the discharge rather than for the plasma.

Electron density measurements with a dry plasma

The determined values of n_e in the jet (Table 2) were of the order of 10^{13} cm^{-3}. Electron density in the jet increased as power increased and as aerosol gas flow rate decreased, which were the same trends as expected for n_e in the ICP. It is instructive to compare these n_e values with those calculated from the work of Douglas and French. The electron density at axial position x in the jet should be given by (11):

$$n_e\ (x) = 0.161 \left(\frac{D_o}{x}\right)^2 n_{e,ICP} \qquad (5)$$

where D_o = orifice diameter (0.76 mm), $n_{e,ICP}$ = electron density in the ICP region sampled, and x is the probe position measured relative to the sampling orifice. In the present work, x = 4 mm (i.e., the separation

Table 2. Electron densities in the jet extracted from a dry plasma

"Aerosol" gas flow rate (L min^{-1})	n_e (cm^{-3}) at indicated power 1.0 kW	1.25 kW	1.5 kW
0	2.3×10^{13} [a]	4.2×10^{13}	7.3×10^{13}
0.45	1.8	3.3	5.9
0.65	1.5	2.2	4.1
0.9	1.5	1.8	3.5

[a]Reproducibility typically $\pm 0.1 \times 10^{13}$ cm^{-3} for duplicate measurements on different days.

between :ifice and the tip of the probe), and equation 5 simplifi

$$n_{e,jet} \sim 0.006\ n_{e,ICP} \qquad (6)$$

If $n_{e,IC}$ pproximately 1 x 10^{15} cm^{-3} to 3 x 10^{15} cm^{-3}, $n_{e,jet}$ sy 6 x 10^{12} cm^{-3} to 2 x 10^{13} cm^{-3}; these values for $n_{e,}$ ple to or a bit lower than the measured n_e values in Tabl in the jet is at least as high as that calculated from thdas and French, the present work clearly indicates that thon-electron recombination in the jet, as they contend

The between the measured n_e values and those anticipculations of Douglas and French were likely caused by some of probe behavior that causes the measured n_e to be a lit For example, the T_e value used in equation 4 was itself se of the curvature in Figure 2. Use of a higher value o included contributions from the points to the right ild have yielded a lower value of n_e than those shown ithis vein, it is interesting to note that previous measureP with a double Langmuir probe also yielded high values

Effects ater and matrix elements

Th of aqueous aerosol and matrix elements into the ICP pro changes in the characteristic curves, as shown in Figure uration current (in the lower left part of the curves): much when either dry Ar, aqueous aerosol, or

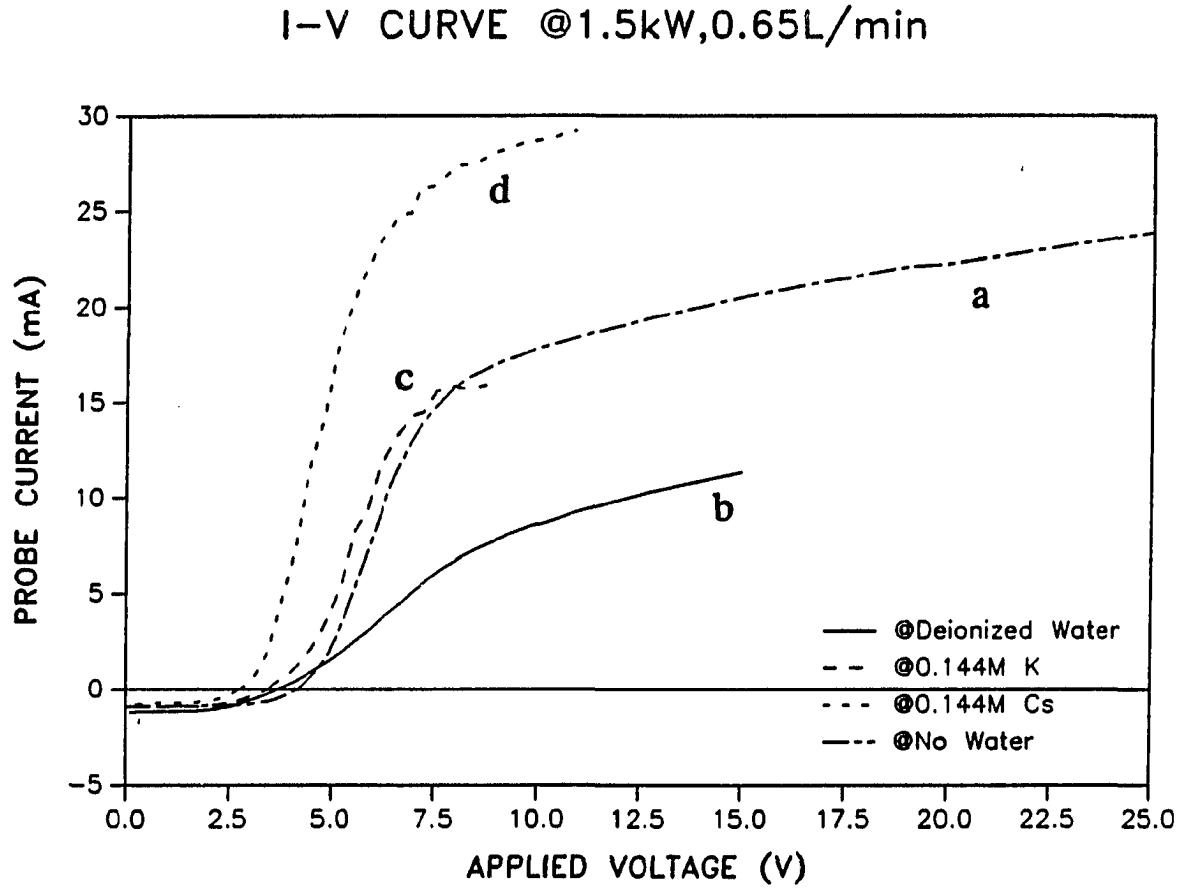

Figure 3. Probe characteristic curves at 1.5 kW, aerosol gas flow rate = 0.65 L min^{-1} during introduction of a) dry Ar, b) deionized water, c) water + 0.144 M K, d) water + 0.144 M Cs

aerosol containing a matrix element was added. However, the slope of the electron retarding region and the current in the electron "saturation" region were very sensitive to the nature of the injected sample. Also, probe characteristic curves obtained with either K or Cs present tended to be noisier and less smooth than the other curves.

Measured electron temperatures are reported in Table 3. The three values listed for dry Ar agreed well with those listed in Table 1, which were obtained on a different day. At all three power levels, introduction of nebulized water caused a large increase (of 4000 K to 6000 K) in T_e. With the load coil geometry employed in this work, introduction of water caused a substantial increase in plasma potential and in the severity of the secondary discharge (5). These observations provided further evidence that the T_e values in the jet were apparently quite sensitive to the secondary discharge, as if a higher plasma potential and a stronger discharge accelerated electrons during the extraction process and displaced T_e in the jet to higher values.

Table 3 also shows that a) introduction of a matrix element depressed T_e, and b) Cs induced a greater depression than an equimolar solution of K. With Cs present, T_e was less than half that for deionized water. The extent to which both T_e in the plasma and the intensity of the secondary discharge depended on the sample matrix was not well known. Previous work showed that alkali metal concomitants (particularly Cs) induced a substantial change in the potential in the jet (14). These effects could be related to matrix interferences in ICP-MS. For example, either K or Cs at 0.14 M would cause a substantial

Table 3. Effect of nebulized water and matrix elements on T_e at 0.65 L min^{-1} aerosol flow rate

	T_e (K) at indicated power		
Sample	1.0 kW	1.25 kW	1.5 kW
Dry Ar	13000[a]	12000	8800
Deionized H_2O	17000	16000	15000
KNO_3 (0.14 M)	---	---	10000
$CsNO_3$ (0.14 M)	---	7200	6400

[a]Reproducibility typically ±100 K.

suppression of analyte ion signal in ICP-MS (35-40), which could in turn be caused by a change in either T_e or potential with the matrix element present.

Table 4 shows the dependence of n_e in the jet on the sample type. As stated earlier, the saturation ion current did not change much for the different samples. The n_e values also did not depend much on the sample type for dry Ar, H_2O, or K matrix. At 1.0 kW, introduction of H_2O caused an increase in n_e, in agreement with some reports that n_e in ICPs increased when some H_2O was added (41). As illustrated in equation. 4, calculation of n_e depended on m_i. Introduction of H_2O and K should not have charged m_i greatly, so m_i = 40 g mole^{-1} was used in these cases. With Cs, however, m_i could have increased if Cs^+ were substantial relative to the normal ambient ions, so a range of n_e values was calculated to compensate for this effect. Table 4 shows that n_e was at least as high in the presence of Cs as with a blank solution, but the ambiguity in m_i precluded a more definite statement about the effect of Cs concomitant on n_e.

V_f measurements

In the present work, V_f was determined from the intercept of the characteristic curve using a biased probe. These V_f values are shown in Figure 4 and are compared with potential values measured using a floating probe at the same position in the jet (14). The trends of potential with power and aerosol gas flow rate are similar for the two methods of measuring potential. The potentials measured with the biased probe are consistently above those measured with the floating probe by

Table 4. Effect of nebulized water and matrix elements on n_e in jet, aerosol gas flow rate = 0.65 L min^{-1}

	n_e (cm^{-3}) at indicated power		
Sample	1.0 kW	1.25 kW	1.5 kW
Dry Ar	1.5×10^{13}[a]	2.2×10^{13}	4.1×10^{13}
Deionized H_2O	2.2	2.3	4.1
KNO_3 (0.14 M)	--	--	3.9
$CsNO_3$ (0.14 M)	--	2.4[b]-3.8[c]	4.3[b]-6.8[c]

[a]Reproducibility typically $\pm 0.1 \times 10^{13}$ cm^{-3}.

[b]Lower limit calculated assuming m_i = 40 g $mole^{-1}$.

[c]Upper limit calculated assuming addition of Cs causes average ion mass to increase to m_i = 100 g $mole^{-1}$.

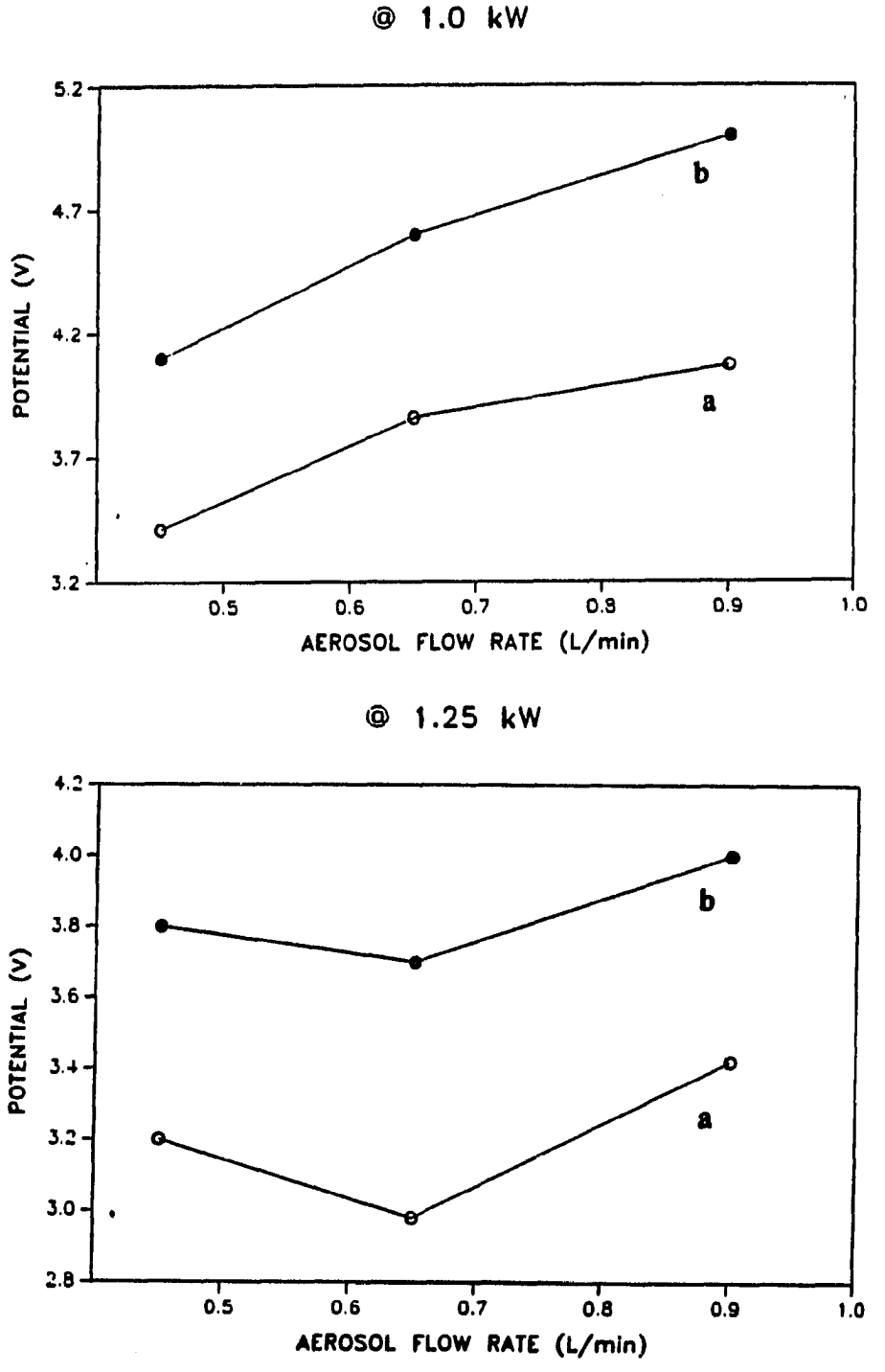

Figure 4. Comparison of potentials measured in jet by a) floating probe, and b) biased probe (14). A dry plasma was used

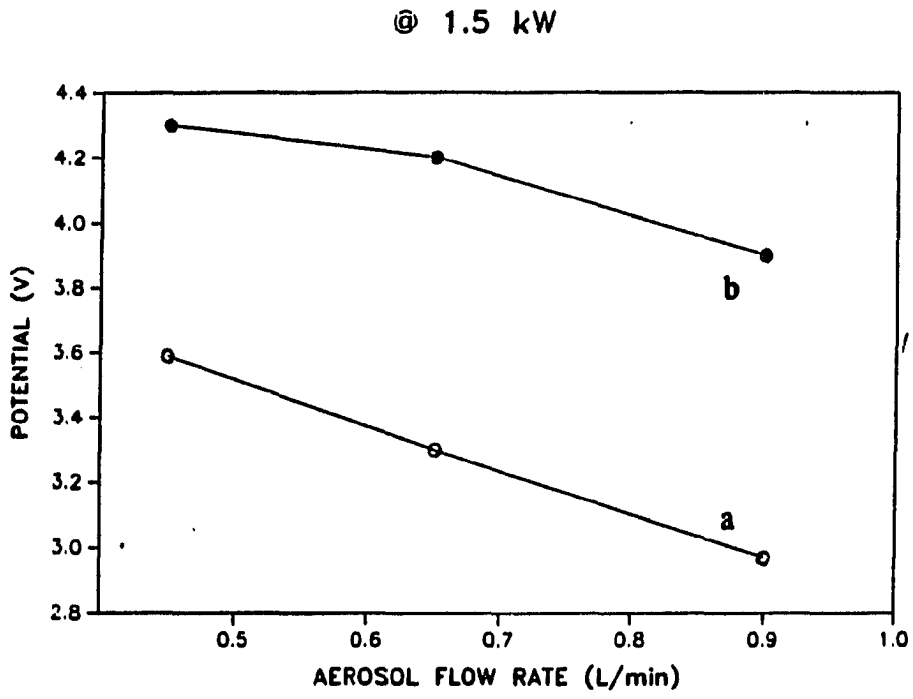

Figure 4. (continued)

0.8 V to 1.0 V. At low power (1.0 kW) the potential measured by either method increases with aerosol gas flow rate. At high power (1.5 kW), the measured potential decreased as aerosol gas flow rate increased. Intermediate behavior was seen at 1.25 kW. Finally, Figure 3 shows that $V_f(Cs) < V_f(K) < V_f(H_2O)$, in qualitative agreement with floating probe measurements with matrix elements present (14).

These data indicate that either method (floating probe or biased probe) is adequate for determining whether changing a plasma parameter causes potential in the jet to increase or decrease. Determination of the true potential of a plasma is not an easy task (24), and it is hard to say which of the two methods comes closer to this goal.

CONCLUSION

The present work essentially demonstrates the feasibility of Langmuir probe measurements for estimating T_e in the supersonic jet extracted from an analytical ICP. The measured values of T_e indicate that electrons are not cooled greatly during the extraction process, in agreement with the model of Douglas and French (11). Some interesting effects of water loading and matrix elements on T_e are apparent; these should be studied further because of their possible implications in ICP-MS. The secondary discharge apparently influences T_e substantially, which suggests that the discharge accelerates electrons effectively. Further T_e measurements using a plasma formed with a center-tapped load coil, which greatly attenuates the discharge (4), should also prove valuable.

LITERATURE CITED

1. Houk, R. S.; Thompson, J. J. Mass Spectrom. Rev. 1988, 7, 425.
2. Date, A. R.; Gray, A. L. Applications of Inductively Coupled Plasma Mass Spectrometry; Blackie and Sons Ltd.: London, 1988.
3. Douglas, D. J. Canad. J. Spectrosc. 1989, 34, 38.
4. Douglas, D. J.; French, J. B. Spectrochim. Acta, Part B 1986, 41B, 197.
5. Gray, A. L.; Houk, R. S.; Williams, J. G. J. Anal. At. Spectrom. 1987, 2, 13.
6. Houk, R. S.; Schoer, J. K.; Crain, J. S. J. Anal. At. Spectrom 1987, .2, 283.
7. Houk, R. S.; Lim, H. B. Anal. Chem. 1986, 58, 3244.
8. Lim, H. B.; Houk, R. S.; Edelson, M. C.; Carney, K. P. J. Anal. At. Spectrom. 1989, 4, 365.
9. Kawaguchi, H.; Asada, K.; Mizuike, A. Mikrochim. Acta 1988, 3, 143.
10. Gray, A. L. J. Anal. At. Spectrom. 1989, 4, 371.
11. Douglas, D. J.; French, J. B. J. Anal. At. Spectrom. 1988, 3, 743.
12. Douglas, D. J.; Kerr, L. A. J. Anal. At. Spectrom. 1988, 3, 749.
13. Pei-qi, L.; Pei-Shong, G.; Tie-sheng, L.; Houk, R. S. Spectrochim. Acta, Part B 1988, 43B, 273.
14. Lim, H. B.; Houk, R. S.; Crain, J. S. Spectrochim. Acta, Part B, 1989, in press.
15. Olson, K. W.; Haas, W. J., Jr.; Fassel, V. A. Anal. Chem. 1977, 49, 632.

16. Bear, B. R.; Fassel, V. A. Spectrochim. Acta, Part B, 1986, 41B, 1089.

17. Schoot, L. In Reactions under Plasma Conditions; Venugopalan, M. Ed.; Wiley Interscience: New York, 1971; Chapter 5.

18. Chung, R. M.; Talbot, L.; Touryan, K. J. Electrical Probes in Stationary and Flowing Plasmas; Springer, New York, 1975.

19. Kirchoff, R. H.; Peterson, E. W.; Talbot, L. AIAA J. 1971, 9, 1686.

20. Fraser, R. B.; Robben, F. Talbot, L. Phys. Fluids 1971, 14, 2317.

21. Smith, D.; Adams, N. G.; Dean, A. G. Church, M. J. J. Phys. D: Appl. Phys. 1975, 8, 141.

22. Smith, D.; Plumb, I. C. J. Phys. D: Appl. Phys. 1972, 5, 1226.

23. Swift, J. D.; Schwar, M. J. R. Electriacl Probes for Plasma Diagnostics: Iliffe Books: London, 1969.

24. Clements, R. M.; Smy, P. R. J. Phys. D: Appl. Phys. 7, 551.

25. Smy, P. R. Adv. Phys. 1976, 5, 517.

26. French, J. B. University of Toronto, Canada; personal communication 1989.

27. Laframboise, J. G. "Theory of Spherical and Cylindrical Langmuir Probes in a Collisionless Maxwellian Plasma at Rest"; Report No. 100; Institute for Aerospace Studies; University of Toronto, 1966.

28. Batal, A.; Jarosz, J.; Mermet, J. M. Spectrochim. Acta, Part B 1981, 36B, 983.

29. Bastiaans, G. J.; Mangold, R. A. Spectrochim. Acta, Part B 1985, 40B, 885.

30. Huang, M.; Hieftje, G. M. Spectrochim. Acta, Part B 1985, 40B, 1387.

31. Huang, M.; Marshall, K. A.; Hieftje, G. M. Anal. Chem. 1986, 58, 207.

32. Hieftje, G. M.; Marshall, K. A.; Huang, M.; Wilson, D. A.; Vickers, G. H.; Monnig, C. A.; Gebhart, B. G.; Hsu, W.-H. Meeting of Fedration of Analytical Chemistry and Spectroscopy Societies; Detroit, MI, October 1987; Paper No. 500.

33. Olivares, J. A.; Houk, R. S. Appl. Spectrosc. 1985, 39, 1070.

34. Gray, A. L.; Williams, J. G. J. Anal. At. Spectrom. 1987, 2, 599.

35. Olivares, J. A.; Houk, R. S. Anal. Chem. 1986, 58, 20.

36. Thompson, J. J.; Houk, R. S. Appl. Spectrosc. 1987, 41, 801.

37. Crain, J. S.; Houk, R. S.; Smith, F. G. Spectrochim. Acta, Part B 1988, 43B, 1355.

38. Tan, S. H.; Horlick, G. J. Anal. At. Spectrom. 1987, 2, 745.

39. Gregoire, D. C. Spectrochim. Acta, Part B 1987, 42B, 895.; Appl. Spectrosc. 1987, 41, 897.

40. Kawaguchi, H.; Tanaka, T.; Nakamura, T.; Morishita, M.; Mizuike, A. Anal. Sci.(Japan) 1987, 3, 305.

41. Alder, J. F.; Bombelka, R. M.; Kirkbright, G. F. Spectrochim. Acta, Part B 1980, 35B, 163.

SECTION V. EXTRACTION DISCHARGE SOURCE FOR INDUCTIVELY COUPLED PLASMA ATOMIC EMISSION SPECTROMETRY: A STUDY OF LINEWIDTHS, INTERFERENCES AND MEMORY EFFECT

INTRODUCTION

The jet formed between the sampler and skimmer in ICP-MS has been one of the main subjects for the fundamental study of the extraction process (1-3). Another important characteristic of the extraction process is the formation of the secondary discharge outside the sampling orifice. This supplementary discharge is attributable to the interaction of the plasma potential with the sampling orifice plate. The general shape and explanation of this discharge were discussed in many ICP-MS papers (4-7). The secondary discharge has been named as pinch discharge, but Hieftje and Vickers recently introduced an interesting acronym, OLD, i.e., orifice-linked discharge (8). The effect of the discharge was very severe in the boundary layer extraction of early ICP-MS, for instance, the discharge caused erosion of the sampling orifice and the formation of doubly charged ions. This discharge affected the physical properties of extracted ions, i.e., potential and temperature as well (9,10).

Because of the intense emission from the supplementary discharge, its application as an emission source could be successful. It was reported that the discharge induced supplementary excitation and signal enhancement relative to ICP alone (6). The signal enhancement and suppression induced by the secondary discharge depend on the experimental conditions. For instance, the noticeably weaker discharge was reported at an ICP generator frequency of 27.12 MHz compared to 40.68 MHz, and a stronger discharge was observed at higher aerosol flow rate and lower ICP power (6).

The enhancement or suppression of analyte lines induced by the discharge is discussed in this section. The matrix effect is a main concern in this experiment for the analytical application of the discharge. The rinse-out time is tested to check the memory effect due to the presence of the sampling orifice. The widths of analyte lines in the discharge are presented as well.

EXPERIMENTAL

Figure 1 shows the ICP and the extraction apparatus used to generate the secondary discharge. Details of the instrumental components and operating conditions are listed in Table I.

A high frequency ICP generator, 40.68 MHz, was used to produce the stronger discharge. The load coil, torch and extraction cone are located inside the same shielding box. A conventional type of load coil was employed because this configuration brought about a more intense discharge than did the reversed or center-tapped geometries (11).

The fabrication procedure for the extraction apparatus was described in reference 6. A solid piece of copper, ~2 cm diameter and 6.3 cm length, was machined to make a sampling cone with 5/8 inch drill bit. The tip angle of the cone was 45 degree, and the wall thickness of the sampling cone was about 1.6 mm. After the cone was soldered into the copper tube, which will be connected to the mechanical pump, the cooling copper coil was soldered to the outside of cone and tube. The sampling cone tip was blunt to protect the cone tip from erosion. The orifice was drilled into its center and was deliberately made longer than its diameter of 0.53 mm to facilitate cooling and to prevent erosion by the intense discharge.

A quartz lens (focal length 15 cm, f/5.9) was used for the image transfer system. A 1:1 image of the discharge and plasma was formed on the entrance slit of the monochromator (f/5.0). The height of the optical region, slit height, was fixed at 5 mm by adjusting the height

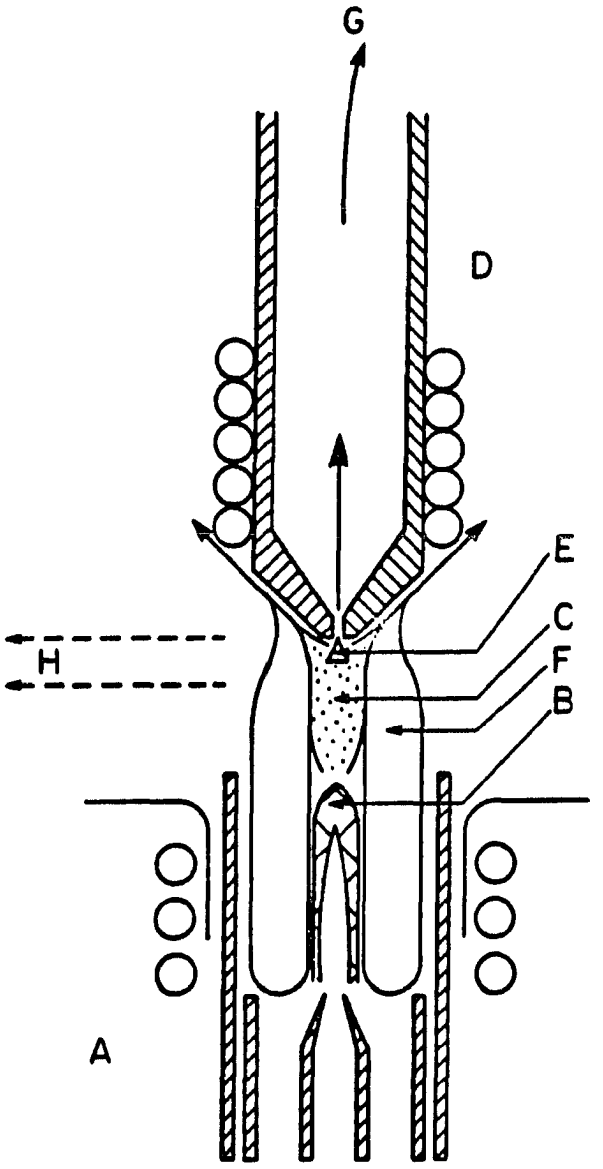

Figure 1. ICP and supplementary discharge. A: ICP torch, load coil, and bonnet; B: initial radiation zone of ICP; C: normal analytical zone; D: vacuum apparatus for generating discharge; D: supplementary discharge flowing into extraction orifice; F: outer Ar envelope of ICP; G: to rotary vacuum pump; H: region observed when discharge and ICP were viewed

Table 1. General instrumental facilities

Component	Operating conditions, materials or dimensions
ICP generator Type HFP 2500 with AMNPS-1 impedance matching network RF Plasma Products, Kresson, NJ, USA	forward power 1.25 kW 0.8 kW for discharge reflected power < 50 W frequency 40.68 MHz
ICP torch: Ames Laboratory construction extended torch: 5 mm longer than standard torch standard torch for matrix study and linewidth	argon flow rate outer gas : 20 L min^{-1} aerosol gas: 1.0 L min^{-1} 1.2 L min^{-1} (discharge) auxiliary gas : 1.0 L min^{-1}
nebulizer: concentric pneumatic type C, size 1.0	uptake rate 1.0 ml min^{-1}
extraction system for generating discharge	0.53 mm diameter circular orifice in copper cone orifice length = 2 x orifice diameter orifice centered on ICP 33 mm from the top of load coil
monochromator Model HR-320 Instrument, SA	Czerny-Turner configuration, focal length 0.32 m, 2,400 grooves mm^{-1}, slit width: 20 µm, slit height: 5 mm

of a mask between the lens and the entrance slit.

Both the discharge and the adjacent section of the ICP, i.e., toward the load coil, were observed as shown in Figure 1. Naturally, the central regions of the plasma and discharge were viewed through the outer Ar envelope of the ICP. For the comparison between the signal to noise ratios (S/N) of the discharge and ICP with those from the ICP alone, the plasma was lowered to view the optimized analytical zone and obtain the maximum S/N at 22 mm from the load coil without the extraction apparatus.

The optimum discharge was formed at 33 mm from the load coil by adjusting the extraction apparatus. Both the width and the height of discharge were about 1.0 mm, and the discharge was weaker and smaller than that of previous experiments (6).

A single quartz optical fiber, 7 m long and 600 μm diameter, and high resolution monochromator (Jobin Yvon, 3600 groove mm^{-1}, double pass) were used to measure the linewidth from the discharge. The slit width of monochromator was 10 μm at this time.

Sometimes the arcing was produced from the load coil toward the bottom of the torch through the auxiliary or outer argon gas stream. This arcing could heat the torch and make the plasma unstable. Since most of the arcing was produced through the auxiliary gas stream, it can be eliminated by running the ICP without any auxiliary gas flow. Also, a closer distance between the load coil and sample injection tube of the torch and good grounding of the extraction apparatus reduced this problem. However, the good grounding could reduce the secondary discharge when the vacuum pump was activated. The standard torch, 20 mm

long of outer tube above the tip of injection tube, was employed for the study of matrix effect and linewidth measurement. The extended torch, of which the outer tube was 15 mm longer than for the standard torch, was used for the signal to noise ratio enhancement study. The ICP generator, vacuum pump, and other detection devices are the same as used for the rotational temperature measurement in section II.

All the chemicals used were reagent grade and all the solutions were prepared in distilled de-ionized water with 1% HNO_3.

RESULTS AND DISCUSSION

Enhancement study

Unlike the results in reference 6, the enhancement factors in this experiment are not so large, as shown in Table II. The signal to noise ratio reported in this experiment is derived from net, i.e., background subtracted, signal intensity versus noise. From the table, the enhancement of Ca (II) line is superior to those of Zn (II) and Cd (II), for which the excitation energies are higher than that of Ca (II). The Zn (II) line with the more energetic upper level is enhanced by a slightly greater factor than was the Zn (II) line with the less energetic upper level. This behavior is also observed for the Cd (II) line, the excitation energy of which is close to that of Zn (II). These results are consistent with the observation of Cu (II) lines, reported in the previous experiment.

It is observed that the atom lines of Zn and Cd were suppressed by the supplementary discharge, instead of being enhanced. This improvement of signal to noise ratio for at least one ion line from each element by the supplementary discharge could improve the detection limits for those elements.

Memory effect

Copper lines from the sampler was not observed, as shown in Figure 2. There was still the possibility of a memory effect in this discharge experiment. This memory effect due to the presence of the extraction

Table II. Signal to noise ratio from ICP and supplementary discharge compared to viewing ICP alone

line, nm	signal to noise ratio	
	from discharge + ICP	discharge + ICP / ICP
Ca II 393.4	64[a]	2.5
Zn II 202.6	55[b]	1.4
II 206.2	45	1.2
I 213.9	61	0.4
Cd II 214.4	97[b]	1.5
II 226.5	168	1.5
I 228.8	148	0.9

[a]The analyte concentration was 0.5 mg L^{-1}.
[b]The analyte concentration was 5 mg L^{-1}.

apparatus could be tested by the determination of rinse-out time.

The typical rinse-out time is shown in Figure 3. While monitoring at Y (II) 242.2 nm, an yttrium solution (1500 ppm) was injected into the ICP for about 35 seconds. This sample was then cleaned out of the ICP torch and extraction apparatus by introducing deionized water. From Figure 3, the data points with * were collected with the speed of 3 data per second. The relative standard deviation for Y (II) signal on the left is 1.5%. The times required to reduce the Y (II) signal to 1% and 0.1% of the initial intensity were 7 seconds and 17 seconds, respectively. These times are comparable to those observed from the ICP alone. Therefore, the presence of the extraction orifice in the ICP did not introduce additional memory effects.

Matrix effect

Matrix effects in the presence of sampling orifice are shown in Figure 4. From the figure, all ionic signals in this experiment were suppressed in the presence of high concentration of matrix element, as reported in ICP-MS (12-14) and ICP-AES (15,16). At this time, the onset concentration of NaCl to suppress the analyte signal was about 100 ppm of Na.

It was observed that all atomic signals, i.e., Cd (I), Cu (I) and Zn (I), were also suppressed with increasing the concentration of NaCl. In ICP-AES, the ionic lines were suppressed to a greater extent than the atomic lines. The magnitudes of atomic signal suppression or enhancement depended on the elements and the observation height. For

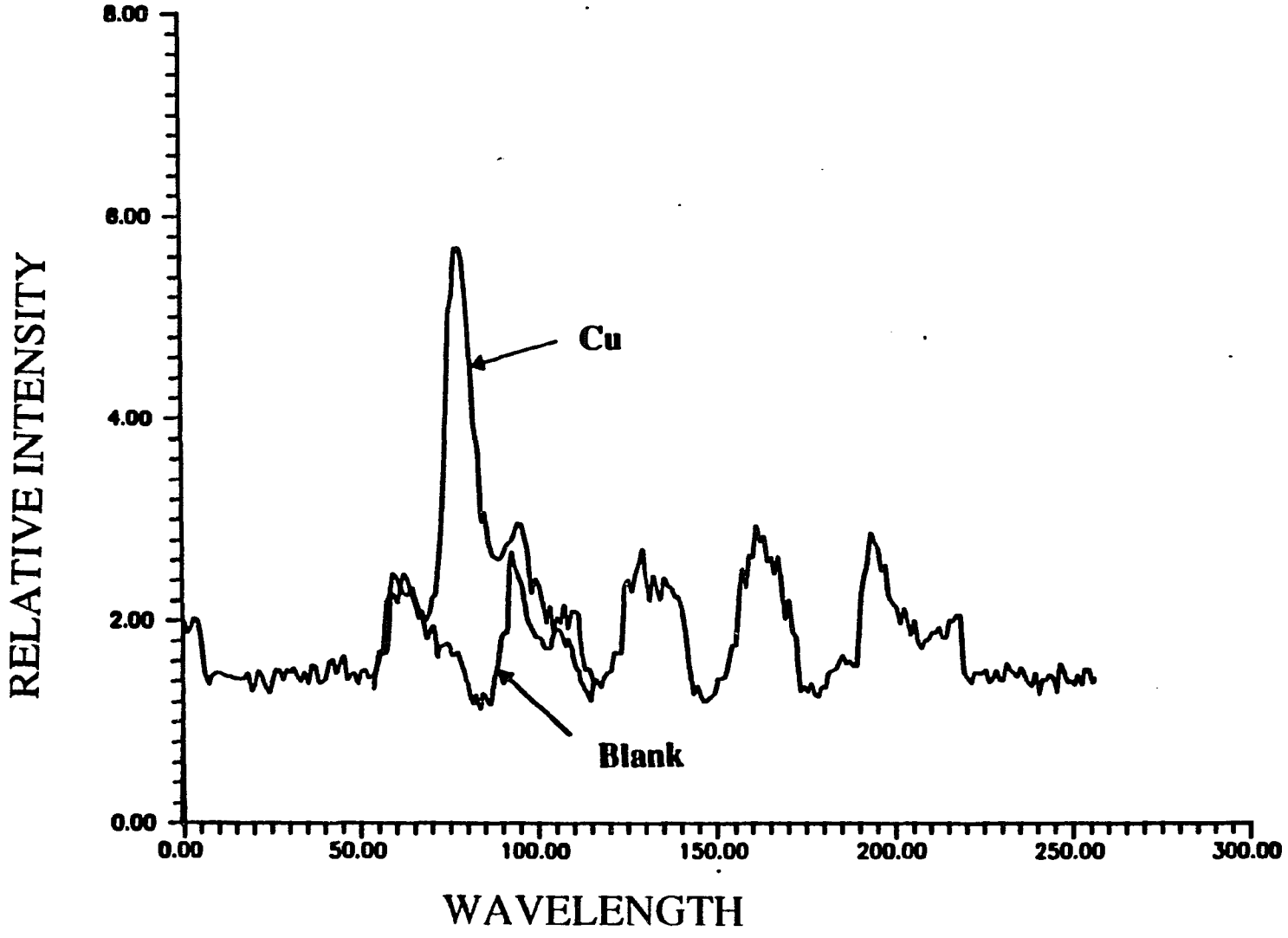

Figure 2. Spectra of 10 mg L^{-1} Cu, Cu (II) 224.7 nm, and blank (de-ionized water) in the presence of extraction orifice (scan rate = 2 ≈ min^{-1}, 3 data points = 1 second)

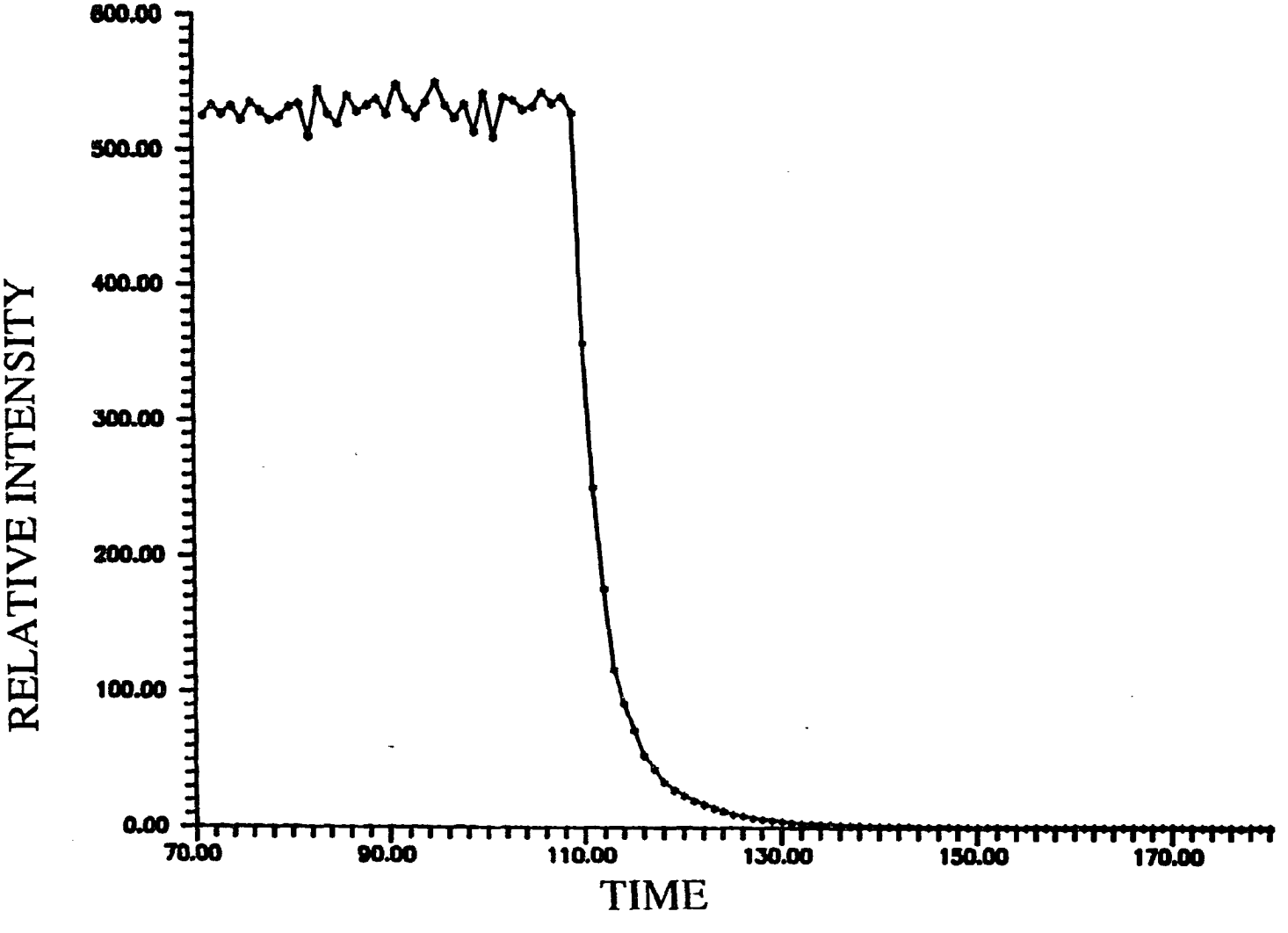

Figure 3. Rinse-out time with the presence of extraction orifice into ICP; 1500 mg L^{-1} of Y, Y (II) 242.2 nm, 3 data points = 1 second

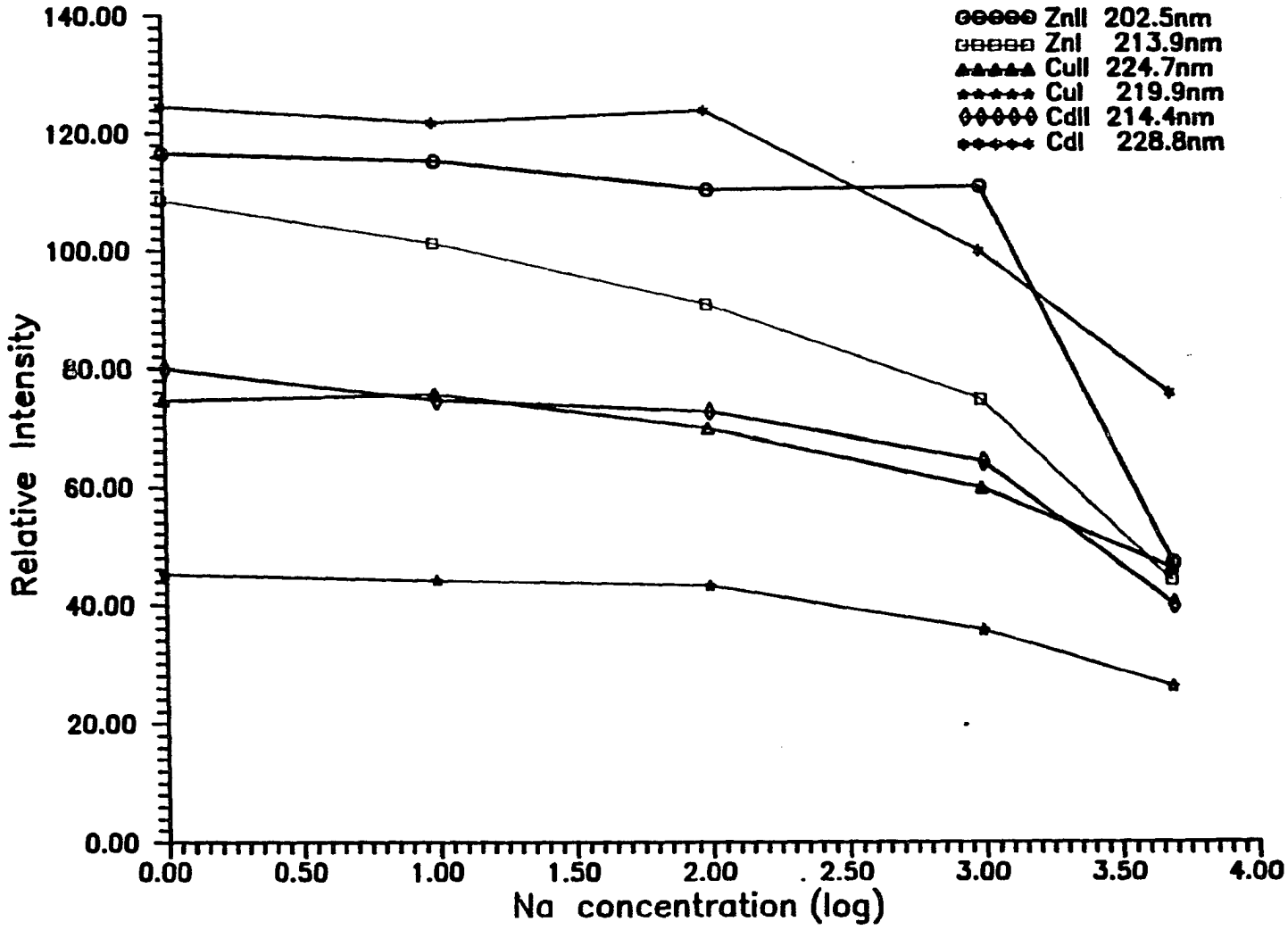

Figure 4. Effect of Na on Zn, Cu and Cd emission intensity with the presence of extraction orifice into ICP; the analyte concentration was 5 mg L^{-1}. The unit of Na concentration was ppm (mg L^{-1})

example, it was reported that the atomic signal for low ionization energy elements, e.g., Ca (6.11 eV) and Sr (5.70 eV), rose as the matrix concentration and the observation height increased, but the atomic signal from Cd was suppressed at 25 mm above the load coil because of the higher ionization energy of Cd (8.99 eV) (15). In this experiment, the observation height above the load coil for the secondary discharge was high (33 mm) and the ionization energies of elements tested (7.73 eV for Cu and 9.39 eV for Zn) are close to that of Cd.

Linewidth measurement

The linewidth was measured in order to estimate the gas temperature of discharge. The line profiles of Ca II emission from the discharge and ICP and the ICP alone, were shown in Figure 5. The full width at half maximum of the line emitted by the discharge was nearly equal to that from the ICP. Even though the linewidth measurement employed in this experiment is not very sensitive to the temperature of discharge because the discharge area is relatively small compared to the total viewing field, the gas temperature of the supplementary discharge is almost equal to that of the ICP. This result also shows that spectral overlap interferences will be no worse when the supplementary discharge is used.

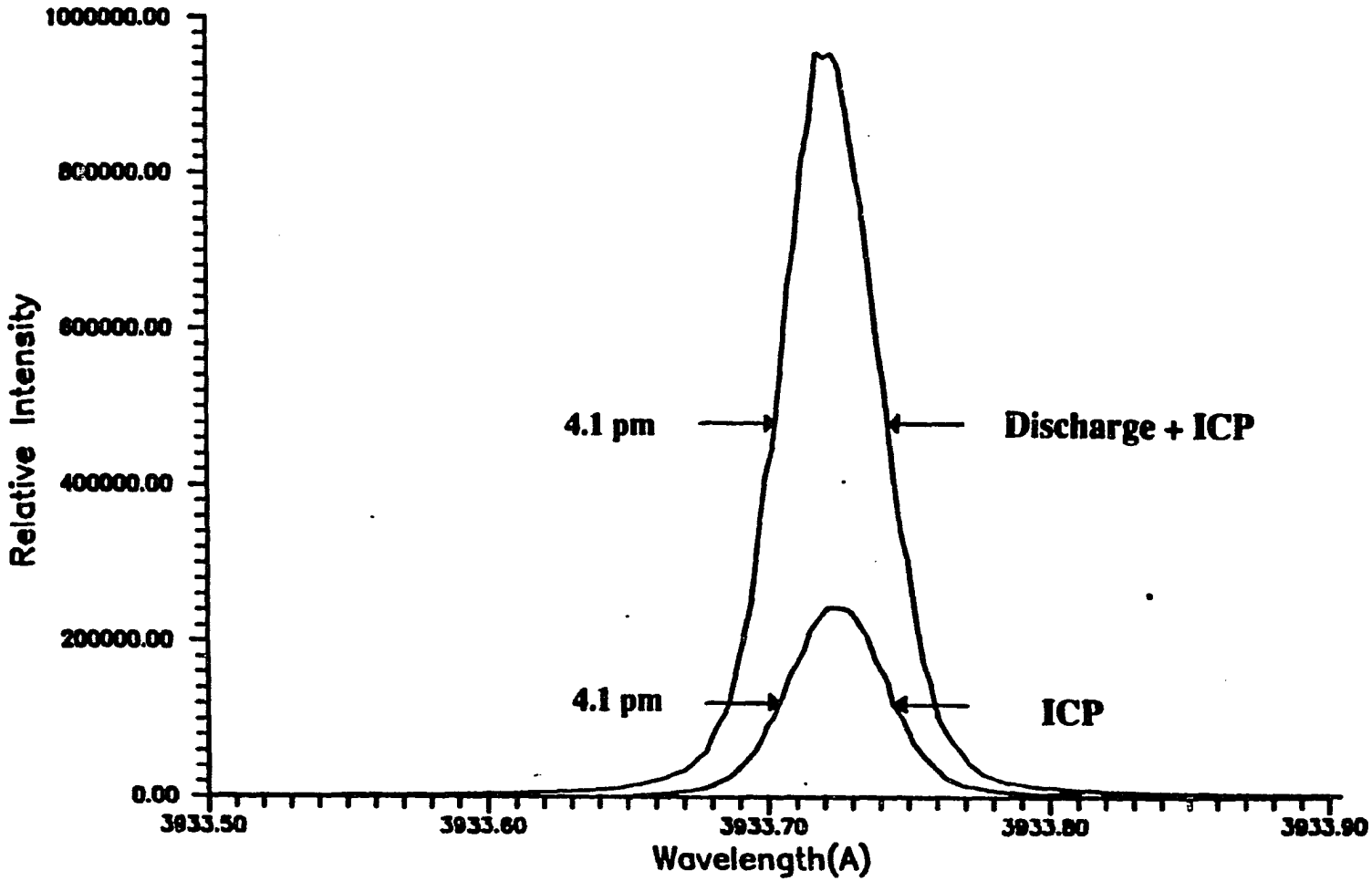

Figure 5. Ca emission line at 393.4 nm. The analyte concentration was 5 mg L^{-1}. The spectra are plotted on the same wavelength scale. The unit of intensity is arbitrary

LITERATURE CITED

1. Houk, R. S.; Lim, H. B. Anal. Chem. 1986, 58, 3244.
2. Kawaguchi, H.; Asada, K.; Misuike, A. Mikrochim. Acta 1988, 3, 143.
3. Gray, A. Spectrochim. Acta, Part B 1989, in press.
4. Houk, R. S.; Fassel, V. A.; Svec, H. J. Dynamic Mass Spectrom. 1981, 6, 234.
5. Douglas, D. J. Canadian J. Spectrosc. 1989, 34, 38.
6. Houk, R. S.; Lafreniere, B. R.; Lim, H. B.; Fassel, V. A. Appl. Spectrosc. 1987, 41, 391.
7. Gray, A. L. J. Anal. Atomic Spectrom. 1986, 1, 247.
8. Hieftje, G. M.; Vickers, G. H. Analytica Chimica Acta 1989, 216, 1.
9. Lim, H. B.; Houk, R. S.; Crain, J. S. Spectrochim. Acta, Part B 1989, in press.
10. Lim, H. B.; Houk, R. S. submitted for publication in Spectrochim. Acta, Part B 1989.
11. Douglas, D. J.; French, J. B. Spectrochim. Acta, Part B 1986, 41B, 197.
12. Olivares, J. A.; Houk, R. S. Anal. Chem. 1986, 58, 20.
13. Kawaguchi, H.; Tanaka, T.; Nakamura, T.; Morishita, M.; Mizuike, A. Analytical Sciences 1987, 3, 305.
14. Crain, J. S.; Houk, R. S.; Smith, F. G. Spectrochim. Acta, Part B 1988, 43B, 1355.

15. Larson, G. F.; Fassel, V. A.; Scott, R. H.; Kniseley, R. N. Anal. Chem. 1975, 47, 238.

16. Blades, M. W.; Horlick, G. Spectrochim. Acta, Part B 1981, 36B, 881.

SUMMARY AND CONCLUSION

In addition to application of jet and secondary discharge to analytical atomic spectrometry, a purpose of this dissertation was the fundamental study of extraction process to improve the analytical performance of inductively coupled plasma mass spectrometry (ICP-MS).

Although the emission from the jet was very weak and the limits of detection were poor, the lines emitted by the jet were sharper than those from the ICP. Thus, interferences caused by overlapping spectral lines for atomic spectrometry might be reduced. Measurement of gas kinetic temperature and rotational temperature indicated that the collisions in the Mach disk re-heated the sampled gas that had been cooled during supersonic expansion.

Electron temperature inside the jet was at least as hot as that in the ICP, and it was greatly affected by the secondary discharge formed during the extraction process. This effect of secondary discharge on the electron temperature can be confirmed by the measurement of electron temperature in the ICP with center tap load coil, which is known to attenuate the secondary discharge significantly.

In contrast with the electron temperature, electron density inside the jet is not affected by the secondary discharge. The electron density is somewhat higher than expected by Douglas and French. Because electron temperature and electron density are dependent upon the distance from the sampling orifice, determining their spatial distribution inside the jet could be an interesting experiment.

The basic reasons for matrix interferences in ICP-MS are not entirely clear yet, but there are some arguments that these interferences depend upon analyte mass, ionization energy or space charge effect. From this dissertation, the presence of easily ionized concomitant elements influenced the electron temperatures and potentials inside the jet, even though it is not certain that those results are directly related to matrix interferences in ICP-MS.

For future work, the measurement of linewidth in the supersonic jet using laser fluorescence spectrometry would be an interesting experiment. The narrow lines from the jet should be useful for high resolution spectrometry. Finally, analytical applications of the secondary discharge should be useful for elemental analysis because of the signal enhancements observed.

LITERATURE CITED FOR GENERAL INTRODUCTION

1. Reed, T.B. J. Appl. Phys. 1961, 32, 821-824.
2. Greenfield, S.; Jones, I.L.; Berry, C.T.; Spash, D.I. British Patent 1 109 602, 1968; Chem. Abstr.
3. Dickinson, G. W.; Fassel, V. A. Anal. Chem. 1969, 41, 1021-1024.
4. Huang, X.; Lanauze, J.; Winefordner, J. D. Appl. Spectrosc. 1985, 39, 1042-1047.
5. Masamba, W. R.; Smith, B. W.; Krupa, R. J.; Winefordner, J. D. Appl. Spectrosc. 1988, 42, 872.
6. Demers, D. R.; Busch, D. A.; Allemand, C. D. Am. Lab. 1982, 14, 167.
7. Jansen, E. B. M.; Demers, D. R. Analyst 1985, 110, 541.
8. Greenfield, S.; Thomsen, M. Spectrochim. Acta, Part B 1985, 40B, 1369-1377.
9. Krupa, R.J.; Long, G.L.; Winefordner, J. D. Spectrochim. Acta, Part B 1985, 40B, 1485-1494.
10. Hasegawa, T.; Haraguchi, H. Spectrochim. Acta, Part B 1985, 40B, 123-133.
11. Boumans, P. W. J. M.; Vrakking, J. J. A. M. Spectrochim. Acta, Part B 1986, 41B, 1235-1275.
12. Boumans, P. W. J. M.; Vrakking, J. J. A. M. Spectrochim. Acta, Part B 1987, 42B, 553-579.
13. Human, H. G. C.; Scott, R. H. Spectrochim. Acta, Part B 1976, 31B, 459-473.

14. Kawaguchi, H.; Oshio, Y.; Mizuike, A. Spectrochim. Acta, Part B 1982, 37B, 809-816.

15. Stubley, E. A.; Horlick, G. Appl. Spectrosc. 1985, 39, 805-810.

16. Stubley, E. A.; Horlick, G. Appl. Spectrosc. 1985, 39, 811-817.

17. LaFreniere, B. R. Ph.D. Dissertation, Iowa State University, 1987.

18. Houk, R. S.; Fassel, V. A.; Flesch, G. D.; Svec, H. J.; Gray, A. L.; Taylor, C. E. Anal. Chem. 1980, 52, 2283-2289.

19. Houk, R. S. Handbook of Physics & Chemistry of Rare Earth, in press.

20. Houk, R. S. Anal. Chem. 1986, 58, 97A-105A.

21. Date, A. R.; Gray, A. L. Application of Inductively Coupled Plasma Mass Spectrometry; Blackie and Sons Ltd.: London, 1988.

22. Houk, R. S.; Thompson, J. J. Mass Spectrometry Reviews 1988, 7, 929.

23. Gillson, G. R.; Douglas, D. J.; Fulford, J. E.; Halligan, K. W.; Tanner, S. D. Anal. Chem. 1988, 60, 1472.

24. Crain, J. S.; Houk, R. S.; Eckels, D. E. Anal. Chem. 1989, 61, 606-612.

25. Houk, R. S.; Fassel, V. A.; Svec, H. J. Dynamic Mass Spectrom. 1981, 6. 234.

26. Douglas, D. J.; French, J. B. Spectrochim. Acta, Part B 1986, 41B, 197.

27. Anderson, J. B. In Molecular Beam and Low Density Gas Dynamics; Wegener, G. Ed.; New York, 1974; chapter 1.

28. Stearns, C. A.; Kohl, F. J.; Fryburg, G. C.; Miller, R. A. Proceedings of the 10th Materials Research Symposium; NBS Special Publication 561; 1979; page 303.

29. Campargue, R. J. Phys. Chem. 1984, 88, 4466.

30. Bajaj, P. N.; Chakraborti, P. K. Chem. Phys. 1986, 104, 41-48.

31. Smalley, R. E.; Wharton, L.; Levy, D.H. Acc. Chem. Res. 1977, 10, 139-145.

32. Hayes, J. M. Chem. Rev. 1987, 87, 745-760.

33. Hayes, J. M.; Small, G. J. Anal. Chem. 1983, 55, 566A.

34. Vaida, V. Acc. Chem. Res. 1986, 19, 114-120.

35. Douglas, D. J.; French, J. B. J. Anal. At. Spectrom. 1988, 3, 743.

36. Ashkenas, H.; Sherman, F. S. 4th Symp. on Rarefied Gas Dynamics. 1966, 2, 84.

37. Hasegawa, T.; Haraguchi, H. In Inductively Coupled Plasmas in Analytical Atomic Spectroscopy; Montaser, A.; Golightly, D. W., Ed.; VCH: New York, 1987; Chapter 8.

38. Mermet, J. M. In Inductively Coupled Plasma Emission Spectroscopy; Boumans, P. W. J. M., Ed.; 1987, 90; Part 2, Chapter 10.

39. Griem, H. R. Plasma Spectroscopy; McGraw-Hill; New York, 1964; 119.

40. Alder, J. F.; Bombelka, R. M.; Kirkbright, G. F. Spectrochim. Acta, Part B 1980, 35B, 163-175.

41. Furuta, N. Spectrochim. Acta, Part B 1985, 40B, 1013-1022.

42. Houk, R. S.; Montaser, A.; Fassel, V. A. Appl. Spectrosc. 1983, 37, 425-428.

43. Houk, R. S.; Svec, H. V.; Fassel, V. A. Appl. Spectrosc. 1981, 35, 380-384.

44. Chan, S.; Montaser, A. Spectrochim. Acta, Part B 1987, 42B, 591-597.

45. Furuta, N.; Horlick, G. Spectrochim. Acta, Part B 1982, 37B, 53-64.

46. Kawaguchi, H.; Ito, T.; Mizuike, A. Spectrochim. Acta, Part B 1981, 36B, 615-623.

47. Kornblum, G. R.; de Galan, L. Spectrochim. Acta, Part B 1977, 32B, 71-96.

48. Kornblum, G. R.; de Galan, L. Spectrochim. Acta, Part B 1974, 29B, 249-261.

49. Abdallah, M. H.; Mermit, J. M. Spectrochim. Acta, Part B 1982, 37B, 391-397.

50. Workman, J. M.; Fleitz, P. A.; Fannin, H. B.; Caruso, J. A.; Seliskar, C. J. Appl. Spectrosc. 1988, 42, 96.

51. Swift, J. D.; Schwar, M. J. R. Electrical Probes for Plasma Diagnostics; Am. els.: New York, 1969.

52. Schott, L. In Reactions under Plasma Conditions; Venugopalan, M., Ed.; John-Wiley & Sons: New York, 1971; vol. 1, Chapter 9.

53. Smy, P. R. Advances in Physics, 1976, 25, 517.

54. Kalnicky, D. J.; Fassel, V. A.; Kniseley, R. N. Appl. Spectrosc. 1977, 31, 137.

55. Goode, S. R.; Deavor, J. P. Spectrochim. Acta, Part B 1984, 39B, 813-818.

56. Caughlin, B. L.; Blades, M. W. Spectrochim. Acta, Part B 1985, 40B, 987-993.

57. Chan, S.; Montaser, A. Spectrochim. Acta, Part B 1989, 44B, 175-184.

ACKNOWLEDGEMENTS

I would like to greatly acknowledge the thoughtful advice and assistant of Dr. R. S. Houk. None of this work could have been completed without his support, tolerance and guidance.

I would like to thank Dr. M. C. Edelson, safety and security program director of Ames Laboratory, for helpful advice and guidance on this work. I wish to express my appreciation to Dr. K. P. Carney for his encouragement and assistance and to thank Art D'Silva, Edward Dekalb and David Eckels for their help and kindness.

I would like to thank the members of Dr. Houk's group for their friendship and assistance: Jeffry Crain, Fred Smith, Daniel Wiederin, Luis Alves, Ke Hu and Sam Shum. Special gratitude is expressed to Dan and his wife, my godparents, for their kindness and friendship.

I am very grateful to my parents, Chunsoon and Kyunim, for their love and support throughout my education.

Above all, I deeply appreciate and love my wonderful wife, Kyoungsook, for her love, encouragement, patience, and particularly the sacrifices over the past several years, and my lovely daughter, Charry (Jessica), for giving me many, many happy times.